Numerical modelling study on the quantification of in-situ leaching (ISL) of copper in porphyry rock.

Pt I – Review on in-situ leaching of copper from porphyry rock.

Pt II – A reactive transport modelling study to assess copper leaching rates in the vicinity of a hydraulic fracture in porphyry rock.

This study was a thesis research project for completion of the master programme 'Earth Structure and Dynamics' at Utrecht University, performed by:

Margot Elise Houwers

Under supervision of:

Majid Hassanizadeh *(Utrecht University)*

Niels Hartog *(Utrecht University)*

Henning Prommer *(CSIRO Land & Water and University of Western Australia)*

Angus McFarlane *(CSIRO Mineral Resources)*

Completed on 10-05-2015

Abstract

This study aims to assess the various aspects of quantifying in-situ leaching (ISL) of copper in porphyry rock through numerical modelling. The first part involves a detailed review of physical and chemical processes that are expected to affect the leaching rate of copper. For this purpose, chalcopyrite was selected as representative leachable copper sulphide. Three alteration phases of hypogene copper deposits and supergene enriched porphyry rock have the highest potential to be economical ore bodies. Various lixiviant systems are discussed of which hydrochloric acid (HCL) was selected to be most suitable leaching agent for the purpose of the initial development of a modelling framework. Transport of the injected lixiviant relies on sufficiently permeable fractures, due the naturally low permeability of crystalline rock. Fracture stimulation is considered essential to establish a connected fracture network which would also develop an increased reaction surface area between the lixiviant and the target mineral.

The second part of the study integrates all relevant hydrodynamic and chemical processes and parameters into a reactive transport modelling framework. A range of conceptual modelling scenarios were developed and translated into illustrative numerical models. The considered cases were guided by the analysis of mineral maps that were developed from high resolution chemical analyses of samples for porphyry rock deposits. Simulations were performed at the cm-scale under consideration of physical and chemical heterogeneity. The impact of a hydraulic fracture was considered in which predominant solute transport occurs through advection. In contrast solute migration in the adjacent matrix was controlled by diffusion. Model variants were defined to investigate the sensitivity of copper extraction rates to selected physical parameters, such as different orientation of the hydraulic fracture in relation to the vein and porosity variations according porosity measurements on similar samples. In other scenarios the reaction network was varied by the addition of secondary minerals and the composition of the lixiviant and/or groundwater solution was varied. The orientation of the hydraulic fracture, the pH of the leaching solution and porosity variations showed to be most important factors for the copper extraction rate. The study provides a basis for developing suitable upscaling-approaches that will allow realistic reactive transport model simulations at the field scale.

0. Content

Pt I – Review on in-situ leaching of copper from porphyry rock.

Pt II – A reactive transport modelling study to assess copper leaching rates in the vicinity of a hydraulic fracture in porphyry rock.

Pt I – Review on in-situ leaching of Copper from porphyry rock

1. Introduction

The overall decline of ore grades and extensive exploitation of the most accessible ore bodies, drives development of hydrometallurgical processes to process more complex and low-grade deposits (Watling et al. 2014). The conventional process of mineral recovery requires the ore to be mined, hauled, crushed and then leached. The current basic leaching techniques applied in the mining industry are heap leaching and vat (or tank) leaching (van der Lee 2008). These are energy intensive processes which become increasingly unattractive as depth increases, grades decline and yields decrease. In-situ leaching (ISL) is a technique that dissolves minerals directly in the ore deposit. This is also called in-situ recovery (ISR) and has been a viable commercial technology for more than five decades (Dershowitz 2011). The term 'solution mining' is used as well, but consists of three categories; heap leaching, dump leaching, and in-situ leaching (Hiskey 1994). In this review the concept of in-situ leaching, characteristics of copper as the target mineral and the challenges related to ISL will be introduced.

1.1 In-situ leaching

ISL is a mining method in which a leaching agent is used to dissolve minerals from ores that remain in their original environment. A leaching solution (lixiviant) is injected through injection wells and the fluid enriched with dissolved (target) minerals is pumped to the surface via an extraction well where the desired element is recovered (IAEA 2001) (Figure 1: Schematic overview of an in-situ leaching system (Harpalani, 1999)Figure 1). At present, ISL is only commercially used for uranium mining. New projects are being developed for copper leaching in Mopani in the Zambian Copperbelt (BGS 2007), in Arizona (County et al. 2013) (Millenacker, 1989). Research on novel ISL techniques, for example ISL of gold, has started (Martens et al. 2012).

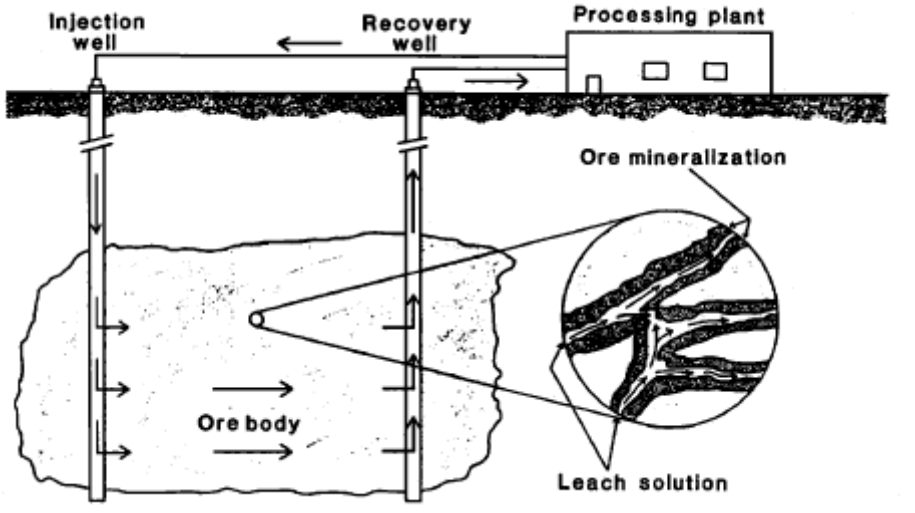

Figure 1: Schematic overview of an in-situ leaching system (Harpalani, 1999)

The advantages of ISL over conventional mining methods are mostly the lack of surface disturbance (e.g. tailings, open pit, etc.) and significantly lower water and energy consumption. Major costs associated with pre-stripping and above ground processing plants are avoided and the cost of any physical post-closure mine rehabilitation are lowered as the valuable components are selectively recovered with the bulk of the rock in place (e.g. Hiskey 1994; Dershowitz 2011).

For ISL to be applicable, some general conditions for mineral dissolution apply. Firstly, favourable dissolution kinetics of the target minerals in contact with the lixiviant is required. Also low buffer capacity of the non-target matrix (gangue) with respect to the leaching agent makes dissolution more effective. For example in the case of protons as a leaching agent, low carbonate content is preferable since carbonates are fast acid-consumers. With respect to the hydrodynamic environment, the mineral enriched grains need to be accessible and the medium must be confined to avoid leakage and to guide the leaching fluid through the permeable ore body (van der Lee 2008).

According to these requirements, conventional heap leaching does not provide the most efficient leaching conditions. Recovery rates are related to flow rates of the lixiviant as this determines the amount of reactive agent available for the mineral to react (Córdoba et al. 2008b; Velásquez Yévenes 2009; Senanayake 2009). In the finely crushed bulk rock, complex flow paths will develop depending on e.g. injection pressure, capillary pressures, micro - and macro - gradients. Consequently major amounts of the lixiviant will be exposed to gangue minerals. ISL however, could be expected to be more effective than heap leaching, as permeability mostly relies on fracture stimulation and induced fractures tend to develop along pre-existing (mineralized) veins due to the difference in mechanical properties of the vein and rock matrix (e.g. Zhang 2013; Rahman 2013). Nonetheless, information on chemical behaviour of the bulk rock composition, comprising both the ore and gangue minerals as a result of decades of experience with heap leaching, will be useful for the exploration of the potential of copper extraction using ISL.

1.2 Copper ore

This review will focus on the application of ISL for the recovery of copper minerals from porphyry rock. This is a suitable target mineral to discuss the feasibility of ISL as it is 1) widely abundant in the crust 2) has many different mineral phases and 3) more than a century of experience of copper mining provides extensive data and knowledge. Other metal ore deposits such as gold, molybdenum, lead, tin and zinc are encountered in similar hard rock deposits and will be discussed to compare the challenges related to the different ore types. Uranium is already actively produced via ISL (e.g. Mudd 2002), showing the feasibility of the mining method. However, uranium generally occurs in sandstone at relatively shallow depth, which implies hydraulic conditions that are dissimilar to those in hard rock systems discussed in this review.

1.3 Permeability of hard rock ore bodies

Application of ISL will initially be cost attractive for recovery of low grade ore bodies at significant depth because of the environmental and economic advantages explained above. However, the porphyry rock type and large depth imply very low permeability (Figure 2). Advective solute transport therefore primarily relies on fracture permeability. A fracture network in porphyry rocks can occur naturally or can be induced by fracture stimulation like hydraulic fracturing. Natural fractures can result of several generations of rock deformation and in turn interact with other fracture generations and induced fractures. As ISL mainly relies on fracture networks for the lixiviant to flow, the structural development and current stress state of the ore body is essential to take into account.

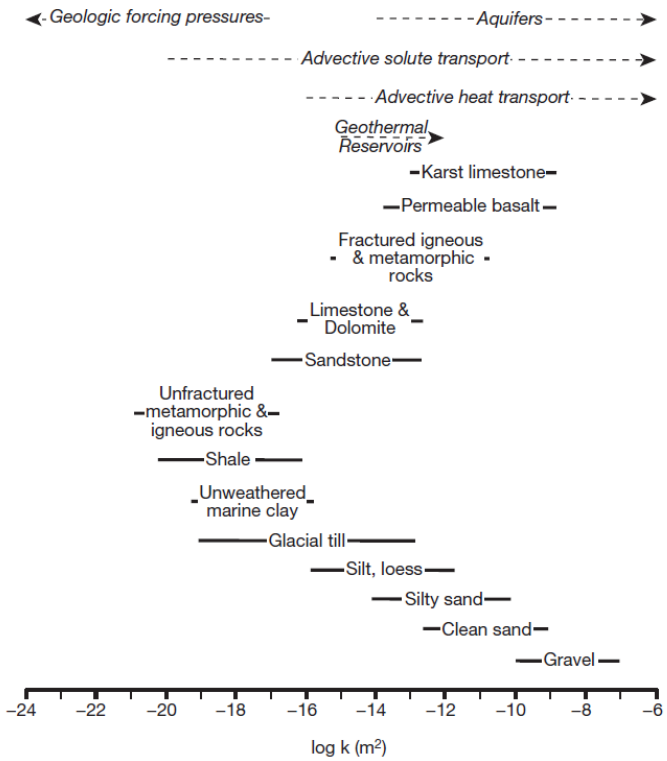

Figure 2: Range of permeability in geological media (Ingebritsen & Appold 2012).

In this review primary predictions on composition and distribution of the ore deposit according to geological setting, geological history and related alteration phases are covered in section 2. Section 3 considers potential leaching methods and section 4 focuses on challenges related to permeability and required fracture stimulation in porphyry rock.

2. Porphyry Copper

Porphyry copper systems are large volumes, 10-100 km^3, of rock that has been hydrothermally altered by the circulation of metal-rich hydrothermal fluids. These fluids are exsolved from acid to intermediate magma bodies emplaced at intermediate depths (1–4 km), based on existing porphyry Cu stocks (Richards 2003; Sillitoe 2010). Slow cooling in the crust allows large (> 2 mm) crystals to grow (Richards 2003; Sillitoe 2010; Li et al. 2008; Meindert et al. 2005). The large size and structural control on their development distinguish porphyry deposits from other granite-related deposits (Sinclair 2007).

The principal ore minerals in porphyry ore deposits are chalcopyrite ($CuFeS_2$), bornite, chalcocite, tennantite, enargite, and other Cu sulphides (Error! Reference source not found.). Associated minerals include pyrite, magnetite, quartz, biotite, k-feldspar, anhydrite, muscovite, clay minerals, epidote and chlorite (Sinclair 2007). The latter non-target minerals are referred to as gangue minerals. The migration of hydrothermal fluids is controlled by pre-existing veins, vein sets, stockworks, fractures and breccias, which can all be related to different conditions of crystallization. As a result, ore and gangue mineralogy vary widely, and can significantly differ locally in a deposit (Richards, 2011). As one of the major issues involved in the leaching of copper is the consumption of lixiviant by gangue minerals, the overall mineralogy requires attention (Jansen 2003).

Two main characterizations are commonly used in literature, referring to the grade and nature of a copper ore body. The grade refers to the weight percentage of copper in 3 classes; high-grade > 0.75 wt % Cu, intermediate-grade 0.75-0.5 wt % Cu and low-grade < 0.5 wt % Cu (Cooke et al. 2005). Deposits are classified as being supergene or hypogene by nature, referring to shallow and deeper crystallization bodies respectively. The composition of the ore deposits is discussed in the first part of this section, followed by differentiating their distribution in hypogene and supergene bodies and finally structural control on the distribution.

2.1 Compositions and alteration phases of porphyry rocks

The crystallization and migration of hydrothermal fluids results in different mineral compositions according to conditions such as temperature, acidity, and host rock composition. Several structures and alteration phases that result in deposits which are potentially suitable for ISL are explained below.

Table 1: Common copper phases found in economic deposits

Mineral name	***Chemical formula***	***Max. Cu content (wt %)***
Native copper	Cu	100
Cuprite	Cu_2O	88.8
Chalcocite	Cu_2S	79.9
Covellite	CuS	66.4
Bornite	Cu_5FeS_4	63.3
Malachite	$Cu_2CO_3(OH)_2$	57.5
Azurite	$2CuCO_3.Cu(OH)_2$	55.3
Antlerite	$Cu_3SO_4(OH)_4$	53.7
Enargite	Cu_3AsS_4	49

Chrysocolla	$CuSiO_3.2H_2O$	36.2
Chalcopyrite	$CuFeS_2$	34.6

2.1.1 Copper phases

Copper occurs in different minerals, with a wide variation in characteristics such as copper content (**Error! Reference source not found.**). Chalcopyrite ($CuFeS_2$) is the most abundant copper sulphide mineral accounting for nearly 70% of the known copper reserves in the world (Olvera et al. 2014) of which the majority occurs in porphyry Cu systems (Sillitoe 2010; Weis et al. 2012; Richards 2003). Therefore this review focuses on the occurrence and behaviour of chalcopyrite.

2.1.2 Alteration-zonation

Porphyry ore bodies occur typically around a core of intense alteration, developing distinct zones of mineralization outwards, each characterised by secondary altered minerals (Figure 3). The zoning of the mineral alteration potentially extends up to several cubic kilometres (Sillitoe 2010). The sequence of alteration-mineralization types is related to paleo depth and system life span. During crystallization of the system, declining temperature of hydrothermal fluids causes decreasing acidity and increasing sulfidation state (Figure 4). In literature, four different stages of mineralization are recognized according to their timing. They involve ore bodies which are emplaced immediately before, during, near the end or after the mineralization events. They are referred to as early, intermineral, lateminerals and postmineral porphyries respectively (Gustafson 1978). This way the early porphyries generally contain the highest grade mineralization, intermineral porphyries are typically less well mineralized as they become progressively younger and late-and post mineral phases are barren (Sillitoe 2010; Li et al. 2008) (Sillitoe, 2010; Li, 2008).

Three alteration types are rich in copper sulphide assemblages and therefore potential economical ore deposits. These porphyry alterations are recognized in a sequence of potassic, sericitic to chloritic alteration from the core towards the surface (Figure 3). Metal zoning of copper (Cu), molybdenum (Mo) and gold (Au) is well defined for the potassic, cholorite-sericite and sericitic cores. Au and Cu are introduced together as components of centrally located potassic zones and therefore correlate closely (Sillitoe 2010). Zonation of these elements typically extends to kilometre-scale and is defined by anomalous Zn, Pb and Ag values reflecting lower temperature and hydrothermal conditions (Meinert et al. 2005).

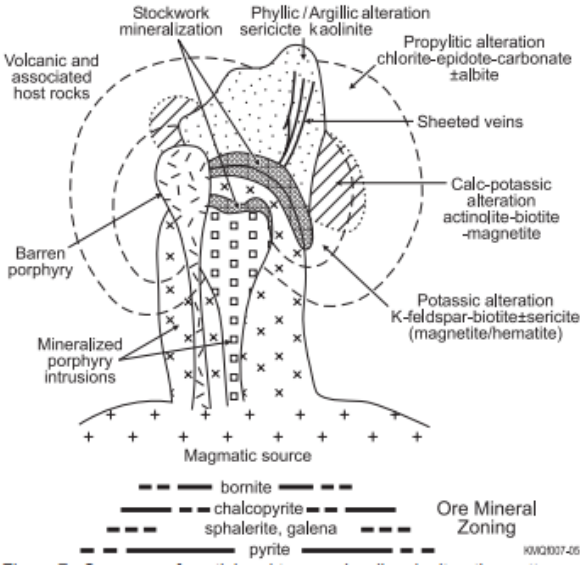

Figure 4: Alteration patterns around porphyry copper systems (McQueen 2005).

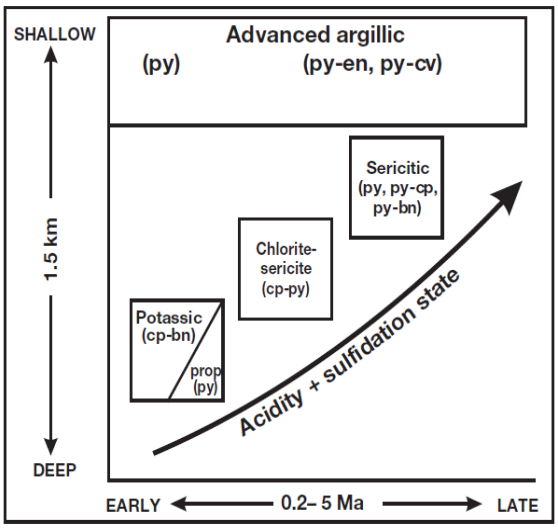

Figure 3: Alteration-mineralization sequence and sulfidation state in porphyry Cu system related to paleodepth and life span (Sillitoe 2010)*, in which py = pyrite, en=enargite, cv=covellite. cp=chalcopyrite, bn=bornite.*

Potassic alteration occurs at the largest depth of core zones and is characterized by biotite and k-feldspar. The major sulphide phases are pyrite, chalcopyrite, bornite, digenite and chalcocite. This alteration zone mainly affects early- and inter-mineral porphyry generations, magmatic-hydrothermal breccias and potentially volumes of wall rock (Einaudi et al. 2003; Sillitoe 2010).

Subsequently, chlorite-sericite alteration occurs in the upper part of a porphyry copper core zone, characterized by chlorite, sericite, illite and hematite. These zones develop when hydrothermal fluids intrude permeable country rock and plagioclase feldspar is converted to mica. Pyrite commonly dominates, implying removal of Cu, but chlorite-sericite alteration also occurs with significant Cu remains (Einaudi et al. 2003).

Thirdly, upper parts of porphyry copper deposits show sericitic (phyllic) alteration, characterized by transformation of mafic mineral to chlorite, plagioclase to sericite (fine-grained muscovite) and magnetite to hematite. This alteration in porphyry Cu deposits normally overprints and (partially) removes the potassic and chlorite-serictic assemblages. They most commonly occur as structurally controlled replacements in the upper parts of the previous alteration zones. Predominant copper sulphides are pyrite, but also assemblages with enargite, tennantite, bornite and chalcocite occur (Sillitoe 2010). These high-sulfidation assemblages commonly have higher Cu contents than the former potassic alteration and overprint quartz veinlet stockworks (Brimhall 1979). They are referred to as supergene copper sulphide enrichments.

Independent of the general alteration zones, magmatic-hydrothermal breccias commonly develop during mineralization of an ore body and hence relate to intermineral porphyry phases. Early breccias contain potassic alteration rich in biotite, magnetite and chalcopyrite cements. Later ones are commonly sericitized and contain abundant specularite, chalcopyrite, pyrite cements. Metal content in cements resulting of magmatic-hydrothermal alteration may be higher than the surrounding host rock (Sillitoe 2010).

2.2 Distribution of copper phases

The scale, structure and copper content of a copper deposit, depend on the process that drives the intrusive activity of which most common variations will be discussed here. Understanding these processes, settings and structures gives insight in the distribution of copper mineralization which is required to locate potential ISL systems. As development of ore bodies is closely related to crystallization of gold, molybdebum and silver (Sillitoe 2010), studies on these minerals are useful for this purpose. Characteristics of commonly occurring hypogene and supergene porphyry rock deposits potentially high in chalcopyrite are discussed.

Hypogene deposits

Large, high-grade hypogene copper systems are generated mainly in magmatic (back arc) environments, often related to (partially) contractional settings which are marked by crustal thickening, surface uplift and rapid exhumation (Figure 6) (Richards 2003). The shape of porphyry orebodies often resembles those of their host intrusions (Khashgerel 2006). Hence, resulting ore bodies are large stratiform lenses and sheets formed on the seafloor through the discharge of metal-rich hydrothermal fluids and mound-shaped stratabound massive sulphide bodies are typically underlain by a stockwork feeder zone. The top of the ore body commonly coincides with the level up to which hydrothermal fluid pressure was sufficient to cause hydrofractures, recognized by high vein intensity. The copper enrichment in these veins decreases with the size of the source pluton and their distribution becomes more concentrated with increasing host rock permeability (Figure 5). Shallow,

lower temperature deposits are associated with plate boundaries and occur as veins, stockworks or breccias (Sillitoe 2010; Seedorff & Einaudi 2004; Richards 2011; Tosdal & Richards 2001).

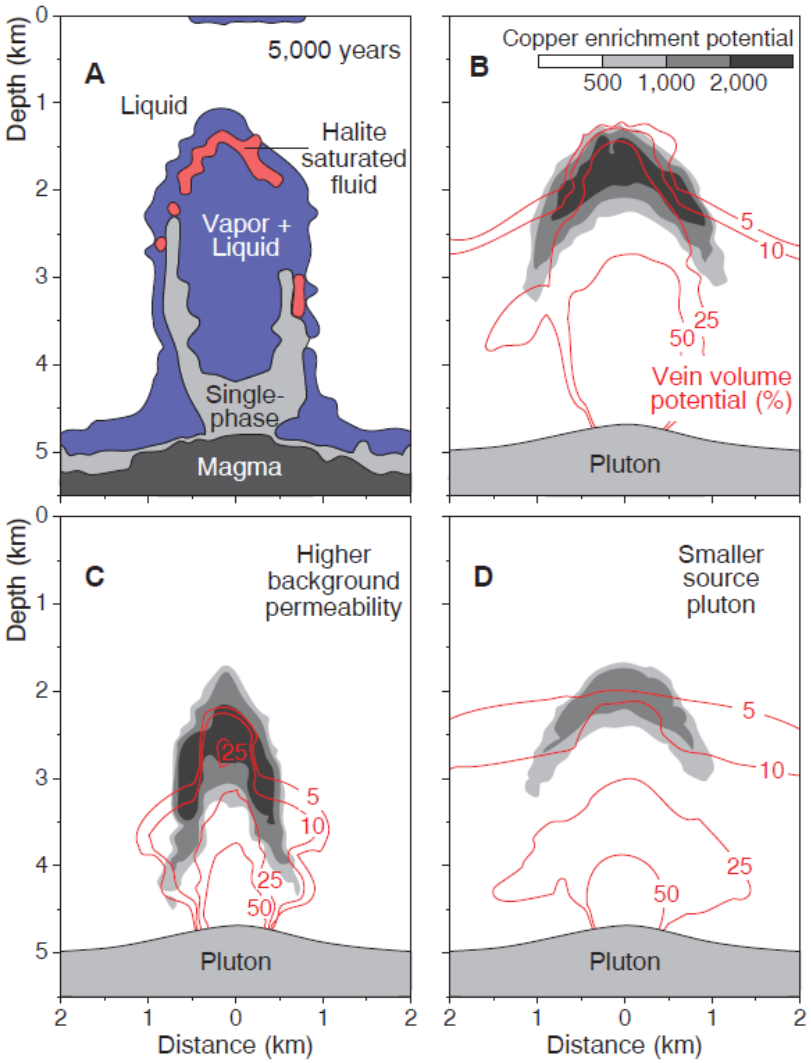

Figure 5: Copper enrichment and vein density related to background permeability and source pluton (Weis, 2012).

Supergene deposits

Supergene enriched zones in porphyry Cu deposits develop by weathering and upward migration of primary sulphides, in some cases resulting in higher Cu grades than early mineralisation (Sinclair 2007). Primary (hypogene) ore minerals are oxidized and re-precipitated after reduction (Richards 2003). The formation of supergene deposits is enhanced by permeability of the hostrock to meteoric water and richness in pyrite and chalcopyrite which allow formation of oxidizing agents. This way, pyrite and chalcopyrite weather and form hematite or chalcocite (Ingebritsen & Appold 2012). Many porphyry copper systems are economically viable due to supergene enrichment. Some of the major copper deposits in northern Chile that occur relatively shallow, are supergene enrichments in chalcocite (Richards 2011).

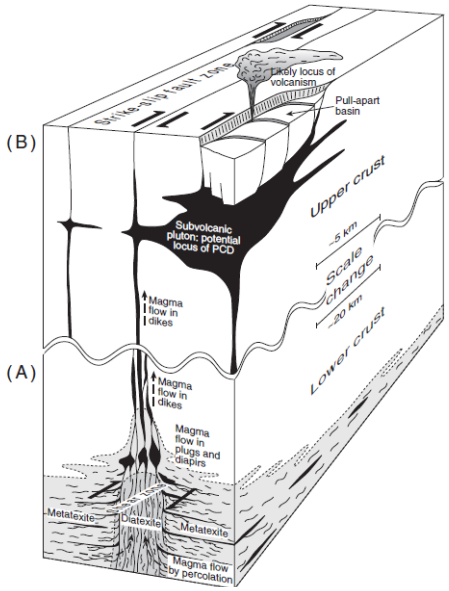

Figure 6: Structural control on development of porphyry copper deposits (PCD) (Richards 2003).

2.3 Intrusive processes

The core of porphyry intrusions can range from vertical stocks, circular to elongate, dike arrays and small, irregular bodies. Stocks and dikes commonly have diameters and lengths varying from 1 – 14 km (Sillitoe 2010; Khashgerel 2006). Vertical stocks have lengths of a few kilometres, e.g. in Northern Chile (Seedorff et al. 2008). No relation appears between the size of the porphyry deposit and the copper contents (Seedorff & Einaudi 2004).

Diatremes are volcanic vents generated mainly by phreato-magmatic eruptive activity. Their maximum (shallow) diameter is ≥ 1 km and their vertical extent is over 2 km (Camus 2003). Diatreme breccias have a distinctive texture with centimetre-sized clasts in a poorly lithified, friable matrix, containing an andesistic to dacitic tuffaceous component (Garwin 2002; Sillitoe 2010).

Breccias can be of meteoric- and magmatic-hydrothermal nature. The latter is the most common type and contains products of release of over pressured magmatic fluids. Magmatic hydrothermal breccias generally occur as pipelike to irregular bodies and of inter-mineral timing. Many porphyry Cu deposits contain minor volumes (5-10%) of this breccia type. The variety of breccia textures depends on clast form and composition, alteration type and clast, matrix and cement- ratio. The matrix is characterized by rock-flour, hydrothermal cement and fine-grained igneous material (Sillitoe 2010). Due to their high intrinsic permeability their final mineral content may be higher than surrounding porphyry stockwork. Meteoric-hydrothermal (phreatic) breccias are subdivided into (late-mineral) pebble dikes or steep, tabular to irregular bodies triggered by vapour-pressure build-up beneath impermeable layers (Sillitoe 2010). Dikes contain polymict clasts and a muddy, rock-flour matrix. They are typically late stage features and hence unaltered and barren (Hedenquist & Henley 2001).

2.3.1 Structural control

Fractures and faults form preferential fluid pathways for mineralized fluids to move upwards through the crust. Due to building pressures, (re-)activated fractures accommodate the ascent of hydrothermal fluids by advective flow which is primarily driven by buoyancy forces (Fournier 1999; Richards 2003; Bierlein et al. 2006; Riveros et al. 2014). Mineralization in fracture controlled deposits is in turn related to the different phases of mineralization alteration (Cooke et al. 2006; Faleiros et al. 2014; Richards 2003).

Crustal stress and strain patterns cause (predictable) fault and fracture orientations (Groves 1993; Cox et al. 2001). A feedback mechanism operates, whereby pre-existing faults facilitate magma ascent, the heat from which further weakens the crust and focuses strain (Richards 2003; Faleiros et al. 2014). Translithospheric, orogen-parallel, strike-slip structures serve as a primary control on magma emplacement in many volcanic arcs worldwide (Corbett 2009; Cooke et al. 2005; Richards 2003). During transpressional strain, geometries such as fault jogs, step-overs and fault intersections could form pathways of relatively high permeability (Rabeau et al. 2013; Sibson 2000). Mineralization, fractionation and recharge result in development of ore-forming magmatic-hydrothermal systems, hence, these structures can be used to localize intrusive ore complexes.

2.3.2 Local scale structures

Ore distribution on local scale, is related to quartz veins and subsidiary faults to which major faults supply mineral bearing fluids and are related in terms of orientation and development (Sinclair 2007; Zhang et al. 2011). The precipitation of (ore) minerals from fluids forms hydrothermal veins (Seedorff & Einaudi 2004). The content, volume and density of these veins is therefore of interest for localization of copper enriched zones. Vein density and patterns develop independent of the type of host rock and fracture patterns were found to extend smoothly across geologic contacts in the Pebble deposit in Alaska, contrarily, vein density can be related to alteration phase (Lang et al. 2014).

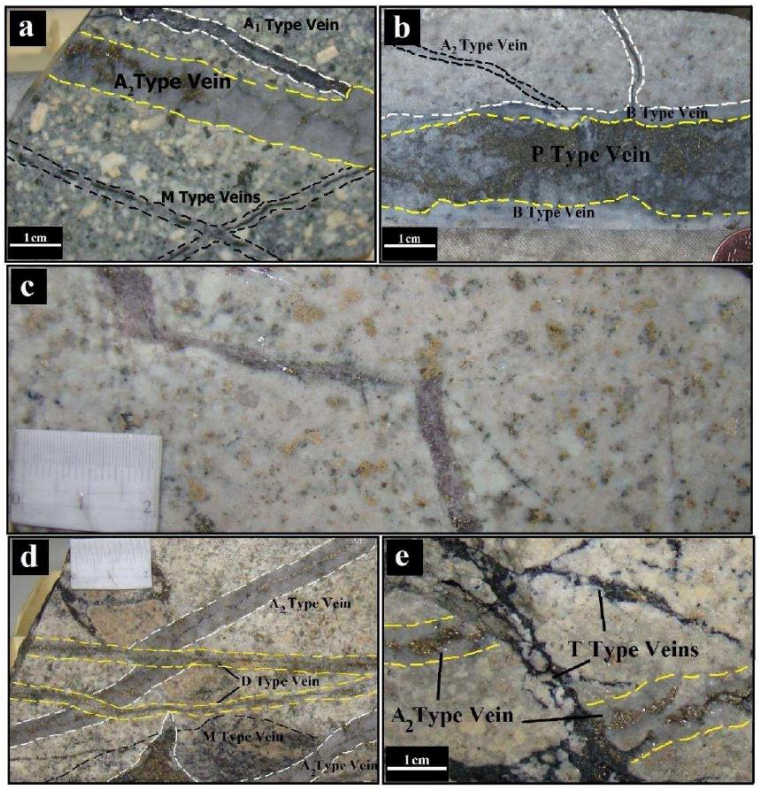

Figure 7: a: Crosscutting sequences between M, A1 and A2 veins; b: A2 veins have been crosscut by B- type and re-opened by a P-type vein; c: P-type vein in quartz diorite, altered by late dacite suite; d: Crosscutting sequences between M-, A2- and D -type veins; e: An A2 vein crosscut by tourmaline breccia (Azadi et al. 2014).

The progressive formation of the chlorite-sericite and sericitic alteration discussed above, is controlled by pre-existing quartz veinlet stockworks, synmineral faults, and permeability contrasts provided by steep intrusive contacts (Hedenquist & Henley 1985; Richards 2003; Rusk et al. 2008). These veins are classified throughout literature as types A, B, M and C and are increasingly younger and with related lower sulphide content (Lang et al. 2014; Gustafson 1978; Clark 1993). These vein types can be recognized by for example cut-through relationships and mineral content. For example, Azadi et al. (2014) recognizes biotite-, M-magnitite- and A-quartz-veins as a result of potassic alteration in the Kahang porphyry copper deposit. Subsequently, B-veins, P-pinkish anhydrite-chalcopyrite veins, D-quartz-sericite-pyrite, T-tourmaline and L-late polymineral veins cross cut all former veins (Figure 7).

For application of ISL, ancient fluid pathways filled by mineralization can result in preferential accessibility for a lixiviant along vein. These could relate to copper recovery in 4 categories:
A. Major veins and high concentration copper sulphides (high recovery).
B. Minor veins with some copper mineralisation (moderate recovery).
C. Veins with no copper mineralisation (reagent consumption).
D. Mineralisation away from vein surfaces (potential recovery via diffusion)

For ISL, an ore deposit with relatively high concentrations of copper is required at operational scale (up to a few tens of meters). Potentially suitable mineralization structures include veins, veinsets, stock works, fractures, breccia pipes. Veins generally have a thickness of mms to cms and generally occur in high density networks. Most veinlets record multiple fracture and vein-filling events to produce veinlets that are 1 mm to 2 cm wide (Zhang & Jeffrey 2013; Azadi et al. 2014; Sillitoe 2010; Geiger et al. 2002). Magmatic-hydrothermal breccias form irregular pipe like bodies varying from 10s-100s of m (Faleiros et al. 2014; Redmond & Einaudi 2010; Sinclair 2007).

3. Copper Leaching

The solubility of different copper phases is illustrated in a Pourbaix diagram (**Figure 8**), which shows the predominant species as a function of pH and redox potential (Eh). From this diagram, it can be seen that the oxidative dissolution of chalcopyrite in an acid medium takes place through a solid transformation in different intermediate sulphides (Cu_5FeS_4, CuS, Cu_2S), increasingly richer in copper.

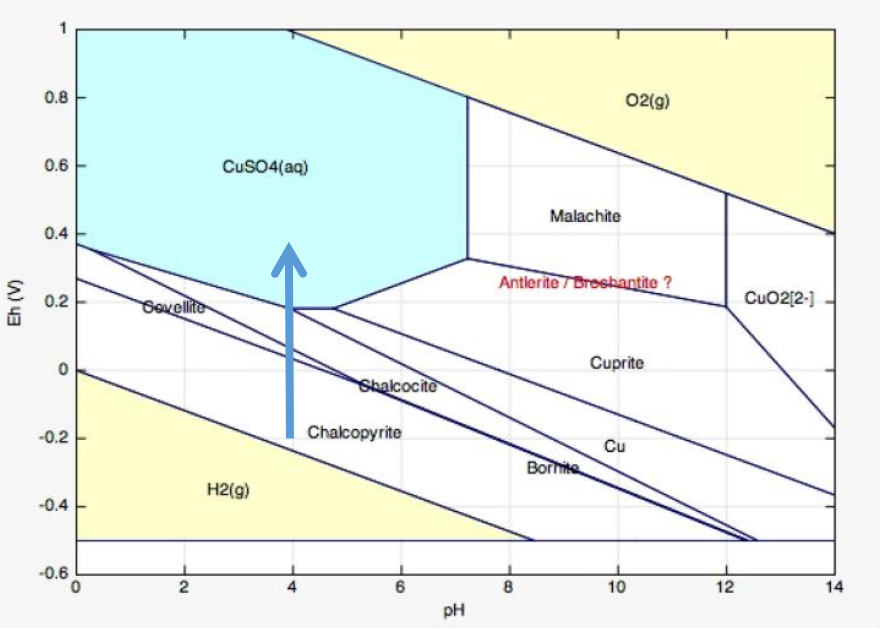

Figure 8: Pourbaix diagram for Cu in presence of Fe, S and Si (Van der Lee, 2008). Blue arrow indicates the transformations that occur for chalcopyrite to dissolve.

According to the Pourbaix diagram a pH<4 and oxidizing redox potential > +0.4 V is required to dissolve copper from chalcopyrite (blue area **Figure 8**). It should be taken into account that the diagram uses a simplified background geochemistry and an instantaneous thermodynamic equilibrium is assumed for calculation of the diagram (van der Lee 2008). Additionally, leaching conditions should not just be favourable for the dissolution of copper but should also minimize dissolution of gangue minerals, precipitation of secondary minerals and possible passivation of the sulphide mineral (e.g. Nicol et al. 2010; Senanayake 2009).

Various aqueous lixiviants are used for solution mining, including heap leaching, dump leaching, and in-situ leaching (Hiskey 1994). The most common types are grouped as acid, alkaline, salts or microbially mediated solutions (Wang 2009; Sparrow & Woodcock 1995). The type of lixiviant applied depends on factors such as the target mineral, bulk rock composition and temperature. It will be harder to control and predict the conditions to which chemicals are exposed in in-situ conditions, compared to conditions in a processing plant used for e.g. tank leaching. For illustration, in-situ conditions are considered to be 100 ˚C and 6700 kPa at about 2 km depth (Bell et al. 1995), compared to 25 ˚C and no lithostatic pressure at the surface.

Hydrochloric acid (HCl) seems the most suitable lixiviant for the dissolution of chalcopyrite in this stage of studying the potential of ISL of copper. Among other reasons; it is one of the more aggressive and general types of lixiviants (Wang 2009; Habache et al. 2005; Watling 2013a). Also, for HCl most data is available on dissolution of chalcopyrite. In the following section several leaching systems will be discussed, followed by a more detailed discussion on properties and (dis-) advantages of HCl as a leaching solution.

3.1 Lixiviants

Leaching agents that are used in conventional leach systems and batch experiments provide insight in dissolution of copper sulphides which can be used to investigate the (rate controlling) reaction steps for ISL (Senanayake 2009). Most naturally occurring minerals require oxidation, for this reason solutions containing the oxidants Fe^{2+}/Fe^{3+}, oxygen and hydrogen peroxide (H_2O_2) are most effective (Wang 2007). However, in-situ conditions are naturally anoxic and the solubility of oxygen in aqueous media is much smaller than the required amount of oxygen to drive chemical reactions (Bell 1995; Cordoba 2009). Therefore, mostly reactions in anoxic conditions will need to be considered for in-situ conditions. Some leaching solutions that have already been applied for ISL will be described first next.

Cyanide

The cyanidation process has been used for gold leaching for over 100 years and is known for its ability to effectively and economically treat ores with low metal concentrations by complexation reactions, e.g. 1-3 ppm Au (Sparrow 1995) or copper from waste containing less than 0.2 % Cu (Hiskey 1994). Application of cyanide loses popularity has severe environmental- and safety issues (e.g. Senanayake 2004; Sparrow 1995). Injection of cyanide into a fractured hard rock reservoir, as required for ISL, is not preferable for these reasons.

Ferric sulphate

Ferric sulphate solutions are dissolve the target mineral by oxidation reactions. This is currently the most widely used lixiviant for copper and uranium dissolution because of the simplicity of the chemistry, low capital and operational cost, and the ease at which copper is subsequently recovered by solvent extraction and electrowinning (Hiroyoshi 2001; Mudd 1998). In spite of the advantages, leaching with ferric sulphate results in low copper recovery, due to passivating layers on the mineral surface that slow down the rate of reaction (Dutrizac 1990; Nazari & Asselin 2009; Olvera et al. 2014). The passivating layer consists of (natro-) jarosite formed by oxidation of ferric iron (Fe^{3+}). Ferric iron both oxidizes and passivates chalcopyrite (Córdoba, 2008). The layer grows by solid state diffusion in chalcopyrite and dissolves simultaneously, resulting in a porous sulphur layer. The porous outer layer of elemental sulphide is concluded not to affect the Cu dissolution rate from chalcopyrite (Córdoba 2008). The formation of sulphur occurs in the presence of ferric iron in the leaching solution (Dutrizac 1974):

$$CuFeS_2 + 4Fe^{3+} \rightarrow Cu^{2+} + 5Fe^{2+} + 2S^0$$

The presence of chloride increases the oxidizing power of ferric sulphate for temperatures higher than 50 ˚ C (Velásquez Yévenes 2009). This effect is ascribed to the higher porosity of the sulphur layer developing on the chalcopyrite surface in presence of chloride(Figure 9).

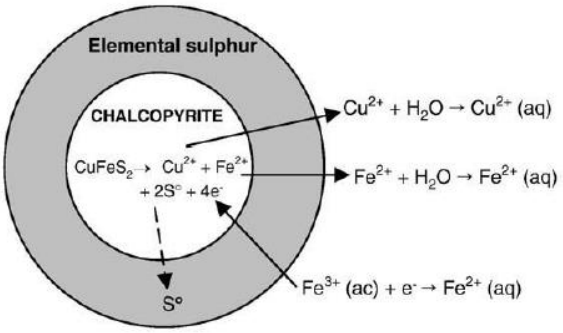

Figure 9: Formation of a low porosity layer of elemental sulphur for chalcopyrite oxidation by Fe^{3+} (Córdoba et al. 2009).

Alternatives for ISL

Acid leaching solutions are effective as they are non-selective and aggressive. The non-selectivity is a disadvantage as it is harmful for the environment, causes corrosion and a major part of the acid will be consumed by species other than copper (Ehrig 2014; Wang 2009; Senanayake 2009). Most commonly used are sulphuric acid (H_2SO_4), nitric acid (HNO_3), hydrochloric acid (HCl) and Agua Regia (HNO_3 + HCl). Of these acids, HCl is the fastest (Flett 2002; Dreisinger 2006), most simple and extensively studied system and is therefore found to be most suitable for ISL as dissolution is already expected to be complex and slow. This lixiviant system will be described in more detail in section 3.2.

A second lixiviant system that is potentially interesting for industrial use is a basic/oxygen system including the reagents NaOH and NH_4OH (Wang 2007). The use of NH_4OH solutions are discussed to be beneficial as corrosive problems are avoided due the basic conditions, gangue minerals will consume only minimal amounts of reagent and cleaner leach solutions are produced (Bell 1995). The supply of oxygen and the build-up of a ferric oxide layer will be problematic using these solutions (Dutrizac 1974).

Oraby & Eksteen (2014) tested the aminoacid glycine as a lixiviant at pH 10-11. However, reagent-copper ratios are relatively very high and thus require large volumes of lixiviant to dissolve sufficient amounts of copper and will thus not be cost effective.

Bioleaching of chalcopyrite requires an acidic medium and often the presence of ferric iron for (electro)chemical reactions to occur (Watling 2006). Interaction with a sulphide mineral occurs via three mechanisms, 1) indirect when bacteria oxidize Fe^{2+} and the resulting Fe^{3+} leaches the mineral; 2) the same as the first reaction but the bacteria occur in a layer attached to the mineral and not in the bulk solution; 3) direct oxidation of the mineral by bacteria on its surface. The main disadvantage of bioleaching is the very slow reaction kinetics (Watling 2006). The most successful copper sulphide that has been mined by bioleaching is chalcocite, due to the faster dissolution rates of days-months compared to chalcopyrite (months-years).

3.2 Hydrochloride system - controlling factors

In this study HCl will be considered, as it results in higher dissolution rates (Flett 2002; Dreisinger 2006) and reduced formation of the passivation sulphur layer as described above (Cordoba, 2008) (Figure 9). The leaching with a hydrochloride (HCl) system on chalcopyrite and secondary copper sulphides using chloride has been studied intensively. The dissolution reaction in non-oxidative conditions is as follows:

$$CuFeS_2 + 2H^+ = CuS + Fe^{2+} + H_2S$$

Favourable characteristics of HCl as a leaching agent for chalcopyrite are the following (Dreisinger 2006; Klauber 2003; Córdoba et al. 2008a; Senanayake 2009; Watling et al. 2014; Velásquez Yévenes 2009):

- HCl is a strong acid which is required for the slow reaction kinetics of chalcopyrite.
- The solubility of metal ions can be significantly increased by the addition of chloride ions due to the formation of metal- chloride complexes.
- Enhanced redox properties as cupric and cuprous ions are stabilised as chloride complexes and the Cu(I)/Cu(II) redox couple could contribute to sulfide oxidation reactions;
- Generation of elemental sulphur rather than sulphur dioxide which make reaction routes become energetically favourable
- Low pyrite reactivity (Velásquez Yévenes 2009; Hiroyoshi et al. 2001; Lu et al. 2000; Aylmore & Muir 2001; Dutrizac 1990; Watling 2013a)

- effective under a wide range of pressure conditions,
- Viability at small and large scale due to potentially lower capital and operational costs, ease of instrumentation and control (Lu et al. 2000).

Disadvantages are (Watling 2014; Lu et al. 2000);

- The corrosive action of chloride;
- Reactions with gangue minerals are triggered by its aggressive and general nature
- The risk of environmental pollution due to its acidity.

The dissolution rate of chalcopyrite depends mostly on the particle diameter, the solid to liquid ratio, the stirring speed, the activation energy and reaction temperature (Yevenes 2010; Emekyapar 2009; Dreisinger 2006). These factors are not straightforward to compare, as different setups are used throughout literature with regards to competing factors as mineralogy, temperature, grain size and structural characteristics. Some of these factors will be explained below.

3.2.1 Rate controlling factors

pH

The effect of pH on the dissolution of chalcopyrite is most favourable in the range of 0.5-2 (e.g. Cordoba 2009; Yevenes 2010). Higher pH favours the dissolution rate of copper. Experiments show that at a pH below 2, the copper extraction increases quickly with increasing pH while at a pH above 2 the rate still increases, although more slowly as a further increased pH favours hydrolysis and precipitation of ferric iron. A maximum pH of 2 is considered in most studies as at higher levels ferric iron will precipitate in the form of ferrihydrites which could decrease the effectivity of leaching (Lu, 2000; Cordoba, 2009; Yevenes, 2010) (Figure 10). Yevenes (2009) observed visible precipitation at pH 2.1 and dissolution of iron was considerably lower than that of copper. The precipitation of (natro-) jarosite (hydrous sulfate) is concluded to cause a slight decrease in pH and related decrease of copper extraction (Lu et al. 2000).

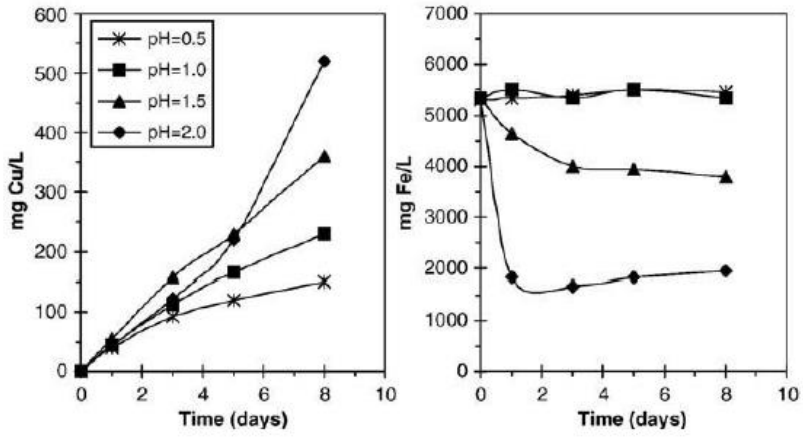

Figure 10: Influence of pH on chalcopyrite dissolution at 68 C (Córdoba et al. 2008a).

Temperature

Higher temperature cause chalcopyrite dissolution rates to increase with activation energies consistent at about 72 kJ mol^{-1} throughout literature (Yevenes 2010; Dutrizac 1987), (Figure 11). These high values of the activation energy are explained by the very slow rates of dissolution due to slow chemical or electrochemical processes occurring on the surface of the mineral

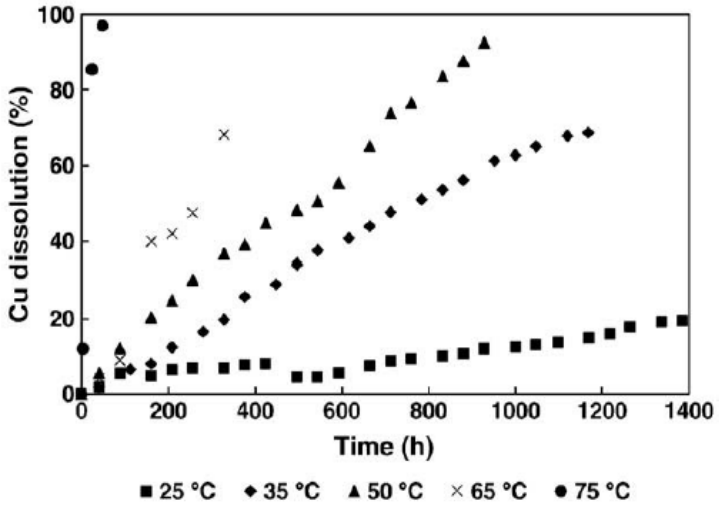

Figure 11: Effect of temperature on the dissolution of copper (Yevenes 2010).

Chloride concentration

The effectiveness of HCl increases upon adding NaCl or $CaCl_2$ to the solution, with an increase of the mean ionic activity coefficient of HCl of 3 and 20 times after adding 1M NaCl and 3 M NaCl respectively. The same molar concentration of $CaCl_2$ is twice as effective (Majima 1985). Similar effects were confirmed by several authors (Hirato 1987; Lu 2000; Yevenes 2010) and might indicate favourable leaching conditions for non-oxidative leaching of chalcopyrite in strongly saline groundwater at a few kilometres depth.

Reactive surface

The reactive surface of minerals to be leached, is mostly considered in terms of grain or particle size, as for conventional processing the ore will be crushed first (e.g. Dutrizac 1981). The grain size can obviously not be controlled in ISL, but should be considered in terms of the surface area of chalcopyrite minerals exposed to the lixiviant. Due to the low permeability of porphyry rock the reactive surface relies on the copper minerals on the surface of hydro fractures. The distribution of chalcopyrite minerals and the tendency of hydro fractures to encounter mineral concentrations, will therefore be key in the effectivity of the lixiviant. The latter phenomena will be further discussed in section 4.

3.2.2 Competing reactions

The use of HCl as a leaching agent not only triggers the dissolution of the target mineral chalcopyrite, but also dissolution of the surrounding, non-target minerals. These parallel or secondary reactions are important to consider as they will consume a significant part of the lixiviant, trigger chemical complexations on the ore surface, but also physical effects as for example newly precipitating solid phases. Mineral precipitation could in turn result in permeability reduction, referred to as clogging. The ratio of lixiviant exposed to reactive gangue and ore determines the speed of Cu dissolution. For heap-leaching processes the amount of reactive gangue minerals could be studied using bulk rock compositions (Helle et al. 2005), as for heap leaching grinding will result in exposure of the entire rock mass.

The most reactive and common gangue minerals include phyllosilicates and iron oxide-hydroxides. Silicate minerals consume acid and release a wide range of products to solution (e.g. K-feldspar, Na-feldspar, Ca-plagioclase and biotite breaks down to ortho-silicic acid, H_4SiO_4, and various metal cations such as Na^{+}, K^{+}, Al^{+3}, Ca^{+2}, Fe^{+2}, Fe^{+3} and Mg^{+2}) (Jansen 2003).

3.3 Effect of groundwater composition

In an ISL system, the leaching agent will be injected at depth and mix with the groundwater in place. The composition of the groundwater could this way affect the chemical behaviour of the leaching agent. With depth, groundwater composition generally increases in salinity, temperature, dissolved solids and gas content. In low permeability porphyry rock, it is mainly density-driven flow that causes minimal groundwater movement. Therefore the groundwater is generally considered to be stagnant (Krásný 2003).

At depths larger than a kilometre the groundwater composition consists mostly of Na, Cl and minor amounts of Ca, the pH ranges from 8-10 and total dissolved solids are maximum 1250 mg/L (Krasny 2003; Nordstrom 1989). HCO_3 occurs in significant amounts at depths between 700-1000 m and carbonate concentrations can be assumed to be minor, for ISL at a depth of > 2 km (Krásný 2003; Nordstrom & Alpers 1998). Dissolution and precipitation of calcite, fluorite and barite, aluminum silicate hydrolysis and additional saline sources are controlling factors for groundwater composition variations at this depth. The basic conditions will buffer the acid leaching solution and this way reduce its effectivity. The low concentration of carbonate is favourable as proton buffering by carbonate is minimal. The high chloride levels are likely to increase reaction rates of chalcopyrite in HCl (section Chloride concentration).

4. Fracture stimulation

The low permeability of porphyry ore (10^{-17}-10^{-19} m^2) requires fracture stimulation to accommodate flow of the leaching solution and increase the reactive surface of the lixiviant with the copper minerals in the ore body (Figure 12). Permeability can be enhanced by several orders of magnitude in naturally fractured reservoirs (Maréchal et al. 2004; Ingebritsen & Appold 2012). Porphyry systems exhibit many different structural features (section 3), which could enhance permeability and potentially be triggered by or interact with induced fractures. The main challenge for ISL is to create a maximum amount of surface area of copper sulphides and minimal amounts of gangue minerals. This section will assess factors that help predict the mechanical behaviour of hydraulic fractures is porphyry ore bodies.

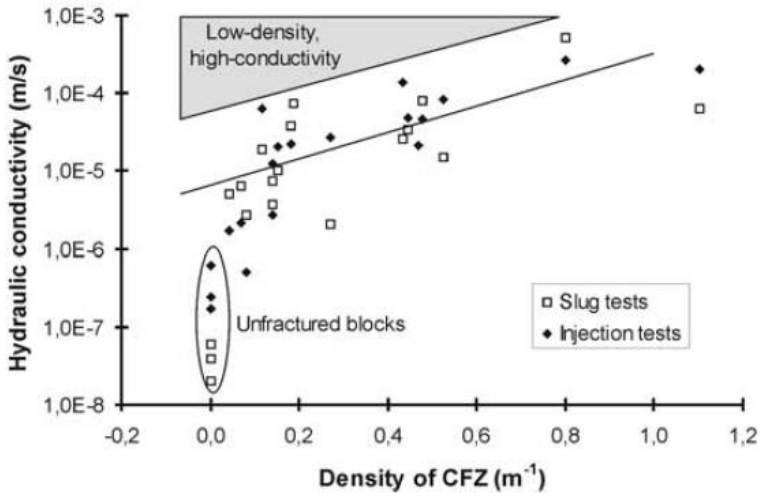

Figure 12: Relation of the density of conductive fracture zones (CFZ) and hydraulic conductivity in a shallow strongly weathered fractured granite (Marechal 2004).

4.1 Hydraulic fracturing

Reservoir rocks can be stimulated using chemical, thermal or hydraulic techniques, hence increasing the accessible reservoir surface. These techniques are applied in the hydrocarbon and mining industry and vital for the exploitation of e.g. tight shale gas reservoirs and hydrothermal systems. Hydraulic fracturing involves injection of fluids along isolated segments of the wellbore into the formation. The hydraulic pressure has to overcome tensile strength of the rock in order for fractures to develop. The in-situ stress field determines the fracture orientation and is described by 3 perpendicular stress components, ea. 2 horizontal and 1 vertical stress components. Fractures will develop in direction of the maximum horizontal stress and opening of the crack will occur in direction of the lowest horizontal stress, commonly modelled as elongated ellipse shaped structures (Chuprakov et al. 2011) (Figure 13). The fracture initiation pressure is higher than the propagation pressure and reopening pressure of the fracture and depend on the in-situ stress conditions (Reinicke et al. 2010; Jeffrey et al. 2009). Consequently pre-existing fractures can be re-acivated or opened at lower hydraulic pressure. Propagation and initiation of hydraulic failure is affected by pre-existing structures like fault zones, bedding planes and intrusions, in particular if differential stress is small (Chuprakov et al. 2011; Reinicke et al. 2010) which is the case a large depth. Accordingly, once pumping stops and the hydraulic pressure drops, the fracture may close and heal, losing the newly created permeability.

Propping agents that are added to the pumped in fluid, usually sand or ceramic spheres, are used to avoid this (Economides & Boney 2000) as further discussed below.

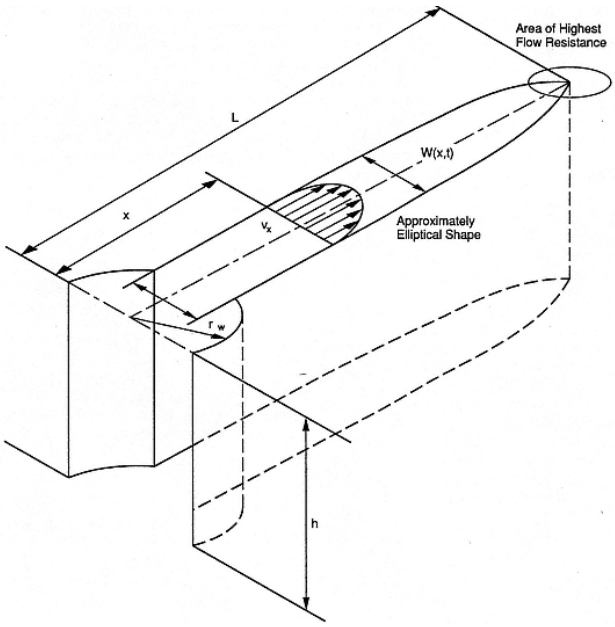

Figure 13: Hydraulic fracture progradation (Mechanics of materials, 2002).

Water fracturing and proppants

Water fracturing is a fracturing method using water with friction reducing elements as a pumping fluid due to its low viscosity compared to gels used in other methods. This method is found to be most suitable for the stimulation of low permeability rock including porphyry rock (Reinicke 2010) current applications are 'Hot Dry Rock' (geothermal) applications to create long and narrow fractures to connect two wells (Baria et al. 1999). Water fracturing is limited to reservoirs with permeability smaller than 1 mDa (Fredd et al. 2000; Britt et al. 2013), which approached the permeability of porphyry copper deposits. The ability of a rock to maintain the fracture width determines the resulting conductivity, this is affected by shear displacement of the fracture faces, their roughness and rock strength (Rushing & Sullivan 2003). Britt et al. (2013) argue that the remaining conductivity will be too small to maintain fluid flow and concluded that creep and pressure solution will cause newly created fractures to close. To prevent closure, low proppant concentrations can be used (Reinicke 2010) such as sieved sand or light weight proppants in concentrations of <0.5 kg /m^2 (Fredd 2000). This type of proppant is not likely to affect the chemical behaviour of the lixiviant as quartz is of very low reactivity. However, the presence of proppants can reduce the exposed surface area of the ore body and hydraulic conductivity of the fracture.

4.2 Porphyry rock stimulation

Naturally, the permeability of porphyry rock is very low and relies on connectivity of porosity which involves vugs, dispersed cracks, tubes developed in and around grains and fractures on the scale of micrometers – meters (Geraud, 1994). Reactivation of initiation of fractures and faults can interconnect natural porosity, creating fluid flow paths which in turn lead to greater fluid flow velocity and greater flow velocity gradients. Rock permeability increases of one to two orders of magnitude due to deformation (Zhang 2000) can lead to an equivalent increase in fluid flow velocity according to Darcy's law (Zhang 2011). Hydraulic fracturing will cause interaction between fluid flow, mineralization and structural mechanisms such as strain localization (shear strain and dilation) and

reactivation or formation of fractures and faults. Other processes that could alter fractures are mineral dissolution, transport and precipitation (Zhang et al. 2011).

4.2.1 Interaction natural fractures

Propagation of the fracture is affected by the heterogeneity of the reservoir rock. The fracture can be diverted or stopped when it runs into a structure of high stiffness and aperture can be wider in softer structure (Brenner & Gudmundsson 2002) (Figure 15). As channelling of the fluid flow may occur in the wider parts of the fracture, and thus result in focus of the lixiviant which directly affects the expected contact with the target mineral, ea. dissolution of copper. This is referred to as Wetted Surface Area (WSA) by (Larsson et al. 2012), who models the effect of heterogeneous fractures on channelling of fluid flow on a scale of 10s of meters.

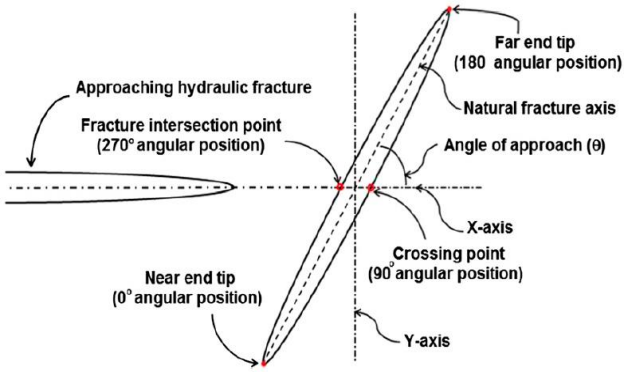

Figure 14: Hydraulic fracture propagation is affected by the angle of approach to a natural fracture and its size (Rahman, 2013).

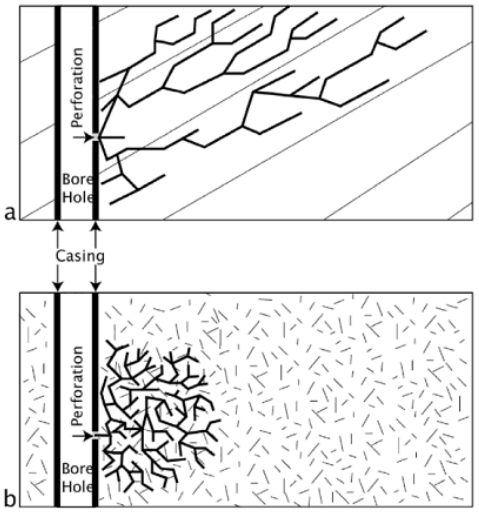

Figure 15: Preferential orientation of fractures according to pre-existing structures in a) layered rock and b) random fracture pattern (Max et al. 2006).

Naturally occurring fracture planes form preferential paths for the injection fluid as re-opening or reactivation of these pre-existing structures requires the least pressure. According to numerical analysis of Chuprakov (2011) the interaction of a pressured hydraulic fracture and a natural fracture depend on four dimensionless parameters: the net pressure in the hydraulic fracture, in-situ differential stress, relative angle between the natural fault and the hydraulic fracture and friction angle of the natural fault (Figure 14) (Jeffrey et al. 2009; Rahman & Rahman 2013). Connecting isolated natural fracture sets depends on the in-situ stress state and fracture arrangement (Dong et al. 2013). Also longer natural fractures (20 m) are more likely to divert the induced fracture than smaller (10 m) natural fractures. At a low angle of approach smaller fractures can still affect the orientation of the induced fracture (Rahman 2013).

The effects of these parameters were tested in experiments by Jeffrey (2009) on volcanic clastic sediments with monzonite porphyry intrusions, sericite-quartz-carbonate faults and quartz-carbonate filled veins. They took into account in-situ stress conditions, Poisson ratios and Young moduli for the different structures. Results show that newly created fractures cut through solid rock, along natural fractures and stepped along inclined shear zones. The propagation of induced fractures along natural fractures at this depth (580 m) is promising for ISL as depths are expected to be larger with related smaller differential stress and hence fracture behaviour will be more strongly affected by natural structural features (Figure 15).

4.2.2 Challenges in prediction of fracture behaviour

Although hydraulic fracturing has been applied for many years, the control on fracture propagation and monitoring is still in development. Monitoring of hydraulic fracturing can be done by micro seismic measurements and tiltmeter data but it is still found to be challenging to get unambiguous results (Jeffrey 2009).

Hydrofracturing of low permeability fractured rock could improve the contact area of the copper minerals with the lixiviant. However, when using ISL in fractured low permeability rock, potential fractures and faults also form a risk in the sense that they could provide escape routes for the leaching solution (Dershowitz 2011).

5. Conclusions

5.1 The potential of copper ISL

- Previous successful ISL projects in uranium mining show the feasibility of ISL. A challenge in leaching from porphyry rock lies in the low permeability, this could be overcome with hydraulic fracturing which has been effectively applied in e.g. hard rock or tight shale stimulation in the geothermal or oil and gas industry.

- Hypogene potassic and supergene alteration zones contain the highest concentration of chalcopyrite and hence expected to have the highest leachable copper content. These zones are distributed in the core of a porphyry system, veinlet stockworks and hydrothermal breccias. As vein deposits might contain locally high concentrations of ore minerals, they are attractive to produce directly from those veins using ISL than conventional heap leaching systems (Dershowitz 2011).

- The injected lixiviant will not only react with the copper sulphide minerals but also with the surrounding (gangue) minerals which requires detailed assessment of the bulk rock composition. The most significant effects on copper dissolution rate when using HCl-based lixiviant are pH increase by the competing proton consumption of clay minerals and clogging due to precipitation of iron sulphates at increased pH.

- Hydrochloric acid is concluded most suitable as a leaching agent in this stage of development of ISL in porphyry rock. Main reasons are its relatively simple chemistry and the abundant data as a result of many applications and studies which enhance the predictability of HCL as a lixiviant. The pH of the lixiviant must be maintained in a range of 0.5-2.0 to optimize the chalcopyrite dissolution rate and to prevent precipitation of iron sulphides and hence reduction of hydraulic conductivity respectively.

- The contact area of the copper sulphide minerals and the injected lixiviant relies on solute transport that will be controlled by advective flow in (stimulated) fractures and diffusion in the rock matrix. The interaction of hydrothermal veins, which could be enriched in copper sulphides, could therefore significantly enhance Cu dissolution rates. Vein stockworks and supergene deposits are there for potentially most prone to opening or reactivation when subjected to mechanical stimulation.

5.2 Key knowledge gaps and research needs towards technology implementation

- For successful ISL of copper, a key challenge is creating contact area for the lixiviant with copper sulphide minerals. Therefor better understanding of copper sulphide distribution and the hydraulic fracture behaviour is required. The presence of fractures and faults in the porphyry deposits forms a risk of losing the lixiviant as these are expected to interact with the induces fractures. High resolution seismic monitoring of structures in the ore body and hydraulic fracture propagation could provide information on these interactions.

- Kinetic rate data on ore mineral dissolution with hydrochloric acid is available from solution mining applications and experiments. However, in-situ conditions will affect chemical processes as high pressure, temperature and salinity change reaction rates, solubility and viscosity. Experiments should be carried out on the effect of these conditions for relevant minerals in porphyry copper. Additional long-term experiments are required to compare the effect of different lixiviants.

-Potential leaching rates from porphyry rock should be assessed taking different scenarios for uncertain parameters into account. Reactive transport models should be developed further to take the interaction of chemical and physical heterogeneity of porphyry copper deposits into account. Currently simulations of flow and transport behaviour in fractured rock most commonly follow dual-domain approach representing flow in fractures and diffusion dominated matrix with a mobile and immobile zone respectively. These models could be improved by considering e.g. heterogeneity in mineral distributions and variations in hydraulic conductivity throughout the matrix.

- Subsequently, the detailed kinetic processes that take local mineralogy into account require upscaling to a scale of industrial use. Upscaling reactive transport models would require high computer process power when high resolution models would be extended. Alternatively, simplified models could be developed in which key parameters would be represented by values that mimic the behaviour obtained by small scale high resolution models.

Pt II – A reactive transport modelling study to assess copper leaching rates in the vicinity of a hydraulic fracture in porphyry rock

1. Background

1.1 ISL in Porphyry rock

The overall decline of ore grades and extensive exploitation of the more easily accessible orebodies drives the development of hydrometallurgical processes that will provide novel options to process more complex and low-grade deposits (Watling 2013b). The conventional process of mineral recovery requires the ore to be mined, hauled, crushed and then leached, which is an energy intensive process. In-situ leaching (ISL) is a technique which dissolves minerals directly within the ore deposit by injecting a lixiviant. ISL is routinely applied for the recovery of uranium, but rarely for any other elements, such as copper (Cu). The world's biggest copper reserves are porphyry copper deposits of which 70% of the copper occurs in chalcopyrite (Olvera et al. 2014; Sillitoe 2010). Structures and compositions exhibit strong variations due to chemical alteration and structural deformation phases to which the porphyry rock is exposed, during and after its formation. In general, magmatic rock is known to have very low permeability (e.g. Geiger et al. 2002; Ingebritsen & Appold 2012; Ranjram et al. 2015) (Figure 1). Enhancing permeability, and making metal recovery economically viable may be achieved by the application of hydraulic fracturing. This provides new and sufficiently permeable flow pathways for the lixiviant (leaching solution) to reach the chalcopyrite minerals. Chalcopyrite has a low kinetic dissolution rate, which is therefore expected to be the rate controlling factor for Cu extraction in hydraulically fractured ore bodies. In contrast to the rock matrix, where solute transport is generally expected to be diffusion controlled. This is a much slower transport process and therefore possibly the rate determining factor in the matrix. It is therefore expected that the grade and availability of the target mineral along newly formed hydraulic fractures will ultimately determine the feasibility and efficiency of ISL. The main challenges for ISL in such systems are the currently still significant uncertainties that are introduced by the complex interactions within the chemically and

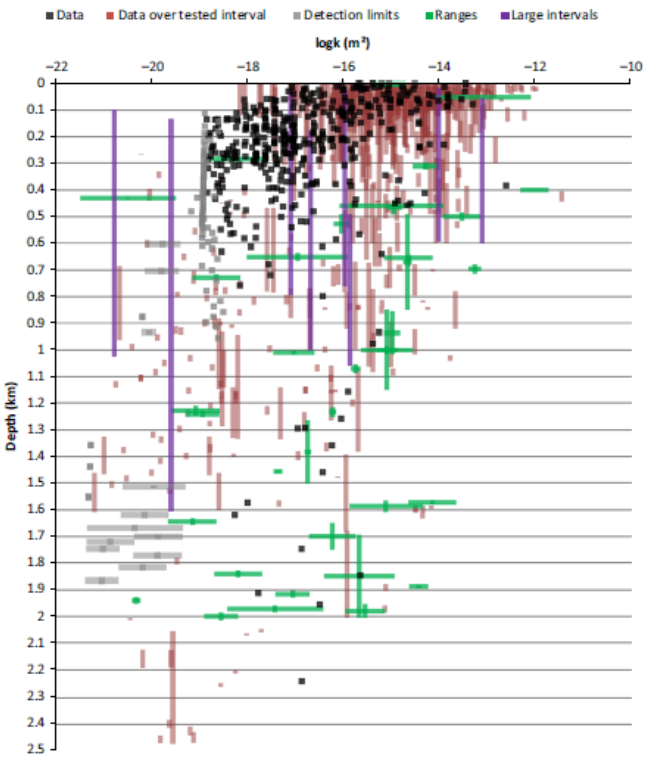

Figure 16: Permeability in crystalline rock (Ranjram 2015).

physically heterogeneous media.

1.2 Lixiviant selection; copper leaching with a HCl system

Hydrochloric acid is chosen as the leaching solution in this conceptual modelling study as it has proven to be effective and the chemistry is relatively simple compared to many other lixiviant sytems. Also, compared to other leaching systems relatively comprehensive information on the kinetic behaviour is readily available in the literature, which is a significant benefit in conjunction with the already complex and uncertain conditions of ISL in porphyry rock.

In-situ leaching is considered for depth of up to 2 km, with an approximate temperature of 60 ˚C and pressures of 20 MPa – 70 MPa (assuming a thermal gradient of 30 ˚C/km and hydrostatic – lithostatic pressure respectively). As oxygen is complicated and expensive to inject along with the lixiviant under these conditions (Hiskey 1994), chalcopyrite dissolution is assumed to occur in absence of oxygen (Kimball et al. 2010):

$$CuFeS_2 + 2H^+ = Cu^{+2} + Fe^{+2} + 2HS^- \quad (1)$$

1.3 Reactive transport model of fractured porphyry rock

Flow, transport and reaction processes and their interaction can be simultaneously assessed and quantified by reactive transport models (Steefel & Maher 2009; Geiger et al. 2002; Mangeret et al. 2012). However, significant challenges can arise from the large uncertainties of both physical and chemical parameters. This is particularly the case for modelling studies that investigate in-situ injection of lixiviants (Geiger et al. 2002) and the induced mineral leaching processes. Uncertainties can be ascribed to the great depth, for which generally sparse field data is available (relative to the degree of heterogeneity) and the spatial distribution of mineral assemblages and their spatial relation to features that control the rates of fluid flow. Techniques that approximate the dimensions and behaviour of hydraulic fractures are currently being developed, but to date the newly created fractures cannot be comprehensively characterised in-situ (Jeffrey et al. 2009). In terms of geochemical uncertainties a significant challenge is to understand and represent in detail the strong impact of hydrochloric acid on gangue minerals, which complicates the quantification of chalcopyrite dissolution due to a potentially large number of secondary reactions that need to be considered.

Previous applications of reactive transport modelling to ISL problems

Reactive transport models have previously been used for a wide range of subsurface problems to assess and quantify solute transport behaviour in both unconsolidated porous media and fractured hard rock. for the range of applications included, for example, the evaluation of hydrogeochemical conditions at contaminated sites, modelling of hydrothermal vein development, simulations that reconstructed porphyry alteration processes, long-term migration of radionuclides released from storage facilities and also simulations of uranium ISL processes (Bodin et al. 2003; De Windt et al. 2007; MacQuarrie & Mayer 2005; Cathles & Shannon 2007; Geiger et al. 2002).

Geiger et al. (2002), for example, modelled the hydrothermal alteration perpendicular to a vein. The application is relevant for ISL in the sense that it involves alterations in similar porphyry copper deposits (**Figure 2**). In their case a discrete high permeability fracture is bordered by a low permeability matrix. Solute transport in that system occurred by advection and dispersion in the fractures and by diffusion between the fracture and the matrix. Similarly, Cathles & Shannon (2007) used reactive transport models to reconstruct early potassium silicate alteration phase. The diffusion-controlled alteration of uniformly fractured rock was simulated to estimate the time-scale of the alteration process. Using a different matrix material but a similar type of set-up, De Windt et al. (2007) quantified the effect of different crack configurations to assess the potential for transport of

hazardous waste stored in cement. Diffusion and chemical processes were both considered in a coupled reactive transport model. The study illustrated how an interconnected crack network can cause a channelized circulation and therefore increased rates of waste element release. In this type of model application, the advection-driven transport of solutes is generally assumed to be negligible due to the low matrix permeability compared to the rate of diffusional transport. The assumption that solute transport in low permeability media (here, rock matrix) is described sufficiently accurate by 1D kinetic diffusion calculations was made for many studies (e.g., Steefel & Lichtner 1998; Brimhall 1979) (Figure 2).

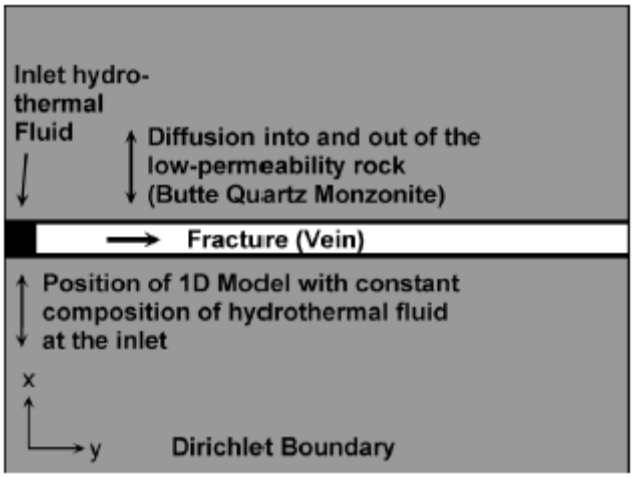

Figure 17: Schematic representation of the physical model for simulation of the hydrothermal alteration in Geiger (2002).

On a larger scale, reactive transport models in fractured media were, for example, used to investigate the interaction of groundwater with a fractured chalk aquifer (Mangeret et al. 2012). In their application a dual porosity approach was used to simulate fluid flow in an implicit network of interconnected fractures while mass exchange with the chalk matrix was assumed to occur through diffusion.

The model simulations, which accounted for considerable complexities such as secondary mineral reactions and (re-)precipitation resembled the field observations. Using a different approach a reactive hybrid transport model was developed by Spiessl et al. (2007) to account for the two different flow regimes, in a domain of a permeable matrix with highly conductive conduits. However, the hybrid transport principle would not be applicable to ISL schemes as the hydraulic fractures that will accommodate most of the fluid flow, will be too narrow to behave as conduits.

Numerical modelling approaches

Three types of numerical models are generally used to integrate chemical reactions with fluid flow and solute transport in porous media, depending on the scale of interest (Steefel et al. 2005):

- Continuum models: continuum equations using macro scale parameters are often derived intuitively by averaging over a representative elementary volume (REV) (Steefel & Maher 2009). In these models, the effective mineral surface area represented as reactive surface area, flow is described in terms of Darcy's law with velocity proportional to the pressure

gradient and fluid, solid and gas phases well mixed in the REV, respectively. Hence, uniform reaction rates occur within the control volume (Steefel 2009).

- Pore scale and pore network models: This type of models aims to capture pore scale behaviour through a set of rules governing mass transport and chemical/biological reactions within and between individual pores. Only recently such models are used to upscale transport and kinetic reactions from pore scale (Kang et al. 2007).
- Hybrid or multi-continuum models: These models combine pore scale and continuum scale behaviour. Since many of the physical, chemical, and biological processes take place at the pore scale, averaging approaches are required for these coupled processes at larger scales (Lichtner & Kang 2007). This type of model is most suitable for modelling fractured porous media with upscaled parameters on different scales, each represented by sets on continua which are hierarchically combined in a continuum formulation.

Flow transport and reactions are often described by macro-scale models where the employed continuum formulation was derived through up-scaling of the underlying micro-scale equations. The micro-scale processes governing ISL are not fully understood at this stage, although experience from analogue subsurface systems such as from aquifers affected by acid mine drainage is, at least to some extent, available.

In a previous modelling study with high relevance for the present study, Garzon (2009) accounted for heterogeneity by using a multiple continuum model that consisted of one mobile and multiple immobile domains, where all zones were connected through kinetic mass transfer processes. The definition of the domains was developed to mimic a discrete fracture network in which individual fractures, intersections and hydraulic parameters were considered according to their structural behaviour in hard rock. The model was used to examine a multicomponent system with a combination of equilibrium and kinetic reactions. The rate determining factors were found to be the mass transfer constant, kinetic rate reaction and distribution of reactants in the system. Lichtner (2000) compared Discrete Fracture Models (DFM) to Dual Continuum (dis-) Connected Matrix (DCM) models according to column leaching models on porphyry copper rock to illustrate the similarities and discrepancies among the different approaches (Figure 3). The DCCM model was identified as the most suitable model for small scale ISL testing.

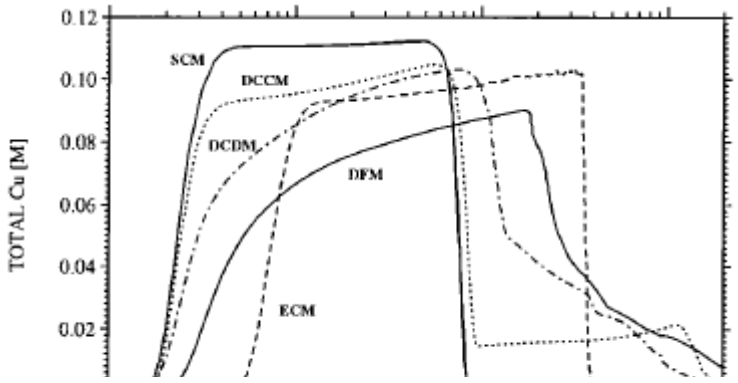

Figure 18: Copper breakthrough curves for SCM, ECM, DFM, DCCM and DCDM models (Lichtner 2000).

1.4 Objectives of this study

In-situ leaching is a technique which has the potential to become a significant economic contribution for the copper mining industry. To achieve this goal a wide range of research activities is still required. Although Lichtner and Garzon provided valuable insight in bladibla, it remains unclear… Also, …. Therefore, the aim of this study is to integrate currently available knowledge and data to illustrate, investigate and quantify the leaching processes and to explore the feasibility of extracting copper in fracture-stimulated systems at sufficiently high recovery rate. Based on the information compiled in the literature review that covers porphyry copper characteristics, the fracture stimulation of ore bodies and various previous applications of leaching agents (pt.1), this is achieved by defining a series of conceptual reactive transport model scenarios. The models are at the scale of a copper enriched vein, comprising a few centimetres; the model type is therefore referred to as vein-scale. The vein-scale results will be used to upscale rates and efficiencies and to obtain some first insights on the feasibility of the method at the industrial scale.

-

2. Vein-scale reactive transport modelling

To define realistic and representative model scenarios a multitude of chemical and physical parameters were extracted from the literature and to a smaller extent also through specific experiments. Key parameters include:

- The bulk rock composition that represents a typical porphyry copper deposit
- Relevant reaction rate expressions for mineral reactions in porphyry rock upon addition of a hydrochloric acid solution
- High-resolution physical parameter (conductivity, porosity) description that reflects the substantial small-scale heterogeneity of the porphyry rocks
- The expected structural behaviour of a hydraulic fracture in a copper ore deposit

2.1 Mineral maps

Chemical analysis of cm-size porphyry rock samples were made to obtain a representative small-scale characterisation of the chemical composition and physical structure. A QEMSCAN was used to create back-scattered electron brightness data and X-ray count rates provided the elemental composition at each point. These data were subsequently combined to map the spatial distribution of mineral phases. Chimage software was used for data analyses to combine element maps and hence to establish correlations between elements to identify minerals (Harrowfield et al. 1993). The resulting mineral maps are used to define both chemical and physical heterogeneities within the vein-scale reactive transport model. The bulk chemical composition determined by this characterisation was similar to other studies of porphyry rock (Christensen 1991; Lichtner 2000; Cathles & Shannon 2007; Geiger et al. 2002; Richards et al. 2001).

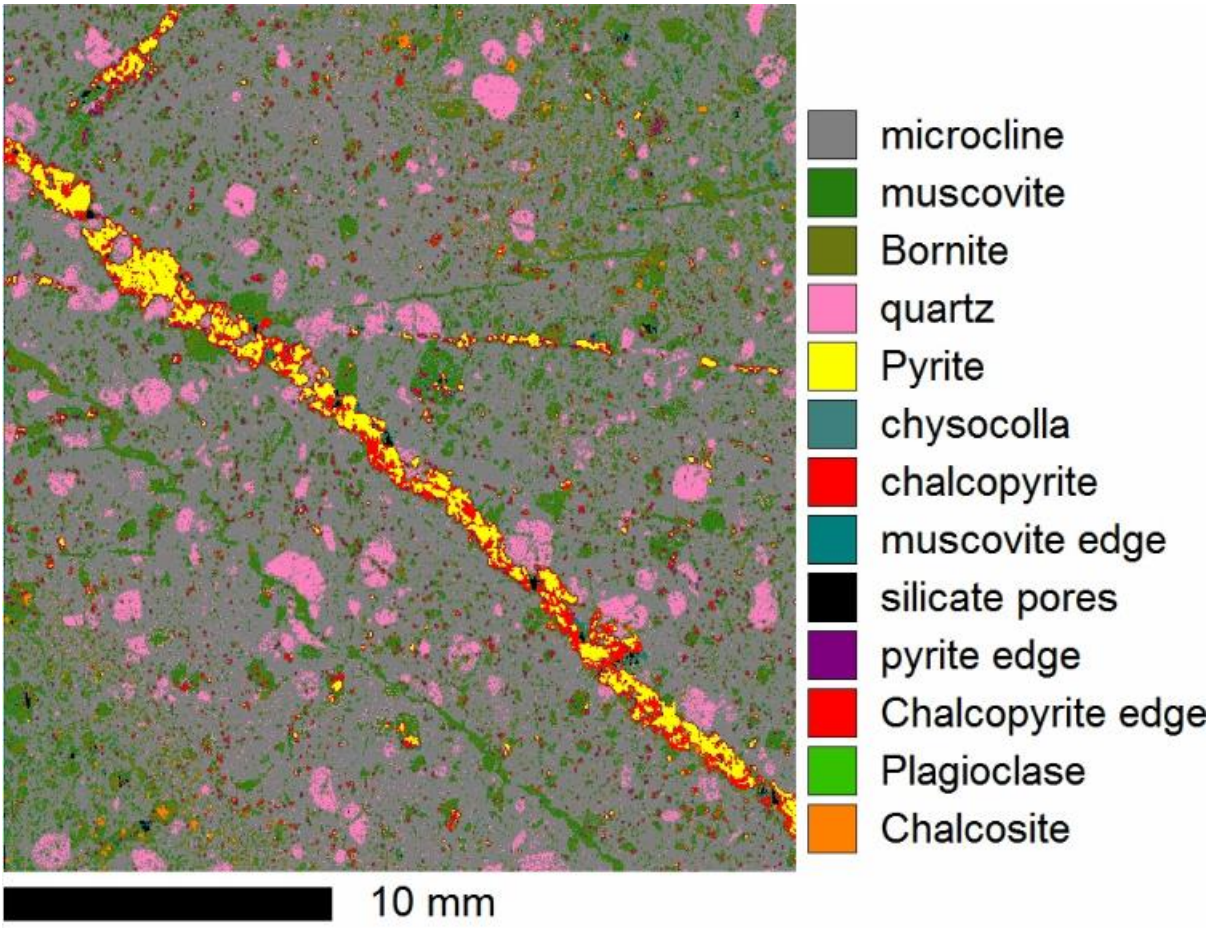

Figure 19: Mineral map resulting from Chimage analysis applied to Qemscan data on a porphyry rock sample.

2.1.1 Permeability and porosity structures / characteristics

The variations of mineral content on the mineral maps can be related to deformation and alteration phases. Veins and brecciated structures are interpreted based on mineral content, grainsize and orientation. Also basic assumptions can be made in terms of timing of their formation according to overprinting and cross-cutting relations (Pt.1). Based on these identifications and chemical assemblages (table 1), key parameters determining flow and solute transport behaviour could be defined using literature data and porosity experiments described in the following section.

2.1.2 Literature and porosity measurements

Experiments were performed to determine small-scale porosity variations. The samples that were mapped and used for the porosity analysis, were derived from Chile, where some of the largest porphyry copper deposits in the world are found, e.g., Los Bronces and Escondida (e.g. Christensen 1991; Sillitoe 2010). Three different samples were used for the porosity analysis. The results showed a significantly varying texture which can be related to differences in their respective crystallization processes. For example one sample from Les Bronces could be interpreted as a hydrothermal breccia due to its high tourmaline content and large clasts (Dill et al. 2012; Frikken 2003) and the MEL sample has characteristic of a late alteration veining event crosscutting a finely grained matrix. The samples thus represent some different parts of a porphyry ore system. Although characterization of the nature of the rock samples was not a key objective of this study, the samples give an impression of the variations in gangue and ore mineralogy and hence an initial understanding of the chemical components that should possibly be accounted for in the reactive transport model.

Table 2: Structures distinguished in the mineral map according to mineral compositions and structural relations.

Structure	Characteristic structures	Possible alteration phase	Orientation (angle of trend to top of sample)	Major components MEL-sample	Simplification
Matrix (M)	Large quartz and muscovite crystals fine grained microcline with finely scattered chalcopyrite.	1Potassic	-	Quartz Sericite Muscovite Oxyphlogopite	Chlorite Muscovite Quartz Calcium
Breccia (B)	Finely grained quartz and muscovite, scattered chalcocite replaced chalcopyrite.	4 Supergene enrichment (Chalcocite formed by weathered chalcopyrite and	Bands parallel to F?	Chalcocite Muscovite Quartz Sericite	Muscovite Quartz Chalcocite
Veins (V)	Continuous structure, cm scale, pyrite and chalcopyrite. Cut through matrix minerals.	3 Later alterations (not as deformed as F). P veins?	120 & 60	Chalcopyrite Pyrite Quartz	Chalcopyrite Quartz
Fracture	Thin (mm) cracks with predominantly	2 Early generation	90 & 135	Muscovite	Muscovite

(F)	muscovite, continuous but deformed / overprinted by microcline and quartz.	veins, potentially later enriched in chalcocite A-veins?		(Chalcocite)	Quartz

Plugs were drilled with a 1 cm diameter, distinguishing between vein, matrix and clast textures. The plugs were dried and weighted prior to being submerged in water. The wet-mass was subsequently measured after 5 minutes, 1 hour, 1 day, 7 days and 17 days, after which saturation was reached. Average values are calculated using porosity for the plugs taken in similar structures of the same rock type. (**Error! Reference source not found.**). Porosity was measured on a number of plugs for each structure so that statistical analysis could indicate the significance of the calculated average porosity per group appendix (B).

Table 3: Porosity values measured on plugs after being emerged 17 days. W, B and F refer to different rock samples; M, C and V refer to the structures matrix, clast and vein resp.

Groups	*Count*	*Average (%)*	*Variance*
WM	5	9.599147	2.98062
BM	2	4.384995	0.103776
FM	4	4.870102	5.430288
BC	2	5.665509	1.010412
WC	5	13.85815	36.62559
FV	3	3.693496	0.91277
BV	2	4.242022	1.763603
WV	4	6.965012	1.661089

2.2 Reactive transport model

Reactive transport models have been used in various ways and for a wide range of application to integrate physical and chemical processes. A simple form of the governing equation for coupled advective-dispersive hydrological transport and chemical reactions of aqueous species is (e.g., Prommer et al. 2003):

$$\frac{\delta C}{\delta t} = \frac{\delta}{\delta x}\left(D\frac{\delta C}{\delta x}\right) - \frac{\delta}{\delta x}(vC) + r \qquad (2)$$

The equation describes concentration (C) changes over time (t) and its dependence on pore water velocity (v), hydrodynamic dispersivity (D) and a source/sink rate due to chemical reactions (r). These are in turn determined according to the following relations using the parameters intrinsic permeability (k), acceleration due to gravity (g), viscosity (μ), density (ρ), effective porosity (ϕ_e), the hydraulic gradient (δh/δx), effective diffusion (D_e):

Main flow velocity: $$v = \frac{q}{\varphi_e} \qquad (3)$$

Darcy flux: $$q = -K\,\frac{\delta h}{\delta x} \qquad (4)$$

Hydraulic conductivity: $K = \frac{k\rho g}{\mu}$ (5)

Hydraulic dispersivity: $D_{T,L} = \alpha_{T,L} v + D_e$ (6)

Tortuosity: $T_L = (L/L_e)^2$ (7)

Effective diffusion: $D_e = D_a T_L$ (8)

In which D_a is the diffusion coefficient for a specific element in pure water and the tortuosity (T_L) is the ratio of the path length the solute would follow in water (L), relative to the tortuous path length in tortuous media (Steefel & Maher 2009).

2.2.1 Modelling Tools

Darcy-type flow was simulated with the USGS simulator MODFLOW (McDonald & Harbaugh 1988) and reactive transport was simulated with PHT3D (Prommer et al. 2003), which couples the multi-species solute transport model MT3DMS (Zheng & Wang 1999) with the geochemical model PHREEQC-2 (Parkhurst & Appelo 1999). iPHT3D (Atteia 2012) was used as the graphical interface for pre-processing of data, while python was used for processing of the model output data and visualisation of results.

2.2.2 Model setup – flow and conservative transport parameters

A two-dimensional (2D) model with a domain size10 cm × 10 cm was defined to simulate the reactive transport processes that occur at the vein-scale. The heterogeneous distribution of physical and chemical parameters that prevails at this scale was adopted from the mineral maps (discussed above in section 2). The structures that are resolved by these maps were used to define zones to which the different flow parameters and mineral assemblages were attributed (**Figure 5**). Heterogeneity of flow- and chemical parameters was defined according to the chemical variability defined by the mineral map (**Figure 4**). Darcy-type flow behaviour was assumed to be valid for these centimetre-scale simulations due to the small grainsize of the porphyry rock crystals and interlocked minerals.

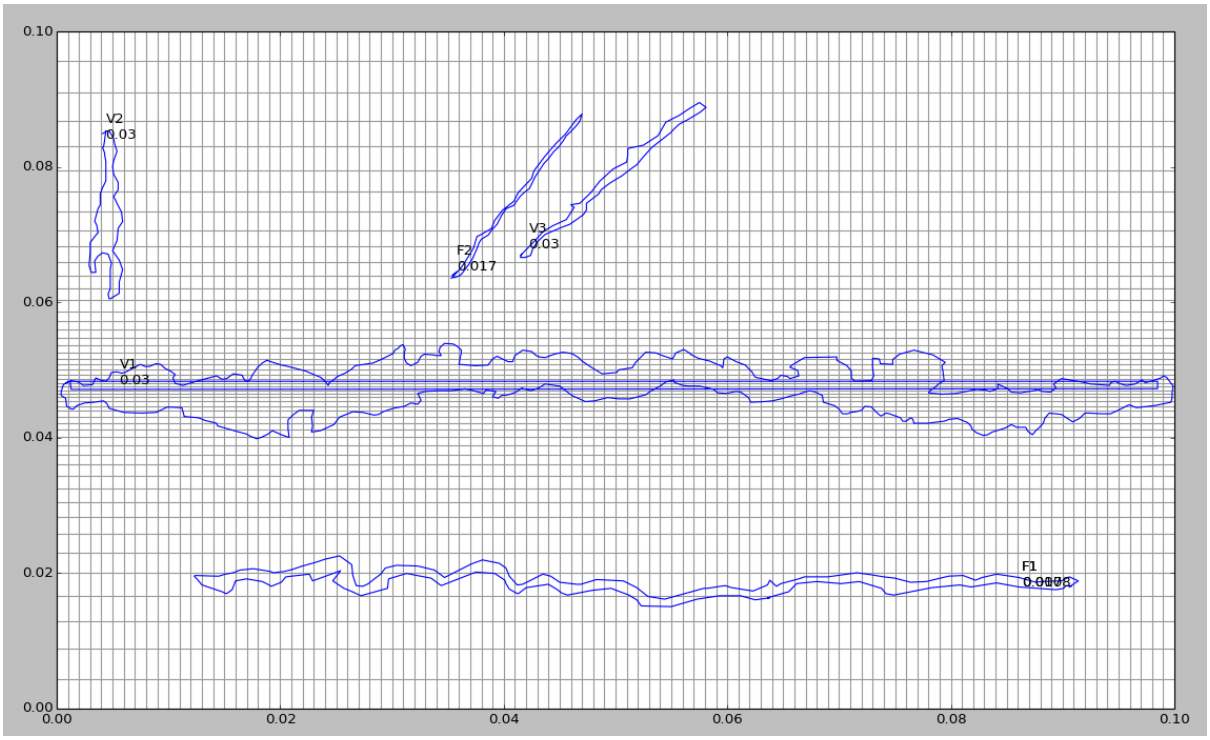

Figure 20: Grid domain showing the porosity variation according to structures defined from the mineral map x and y-axes in meters.

To simulate the lixiviant migration through the hydraulic fracture, a head difference of 0.02 m was applied over the distance between the model's influent and effluent end (10 cm), which resulted in flow velocities in the order of 10 m/day in the hydraulic fracture zone.

Porosity and hydraulic conductivity

Initially the assumption of a low porosity matrix (0.5 %) was applied according to earlier reported values for magmatic rock (Geiger et al. 2002; Bongiolo et al. 2007; Nick et al. 2009). Porosity values are in general mostly affected by the alteration stage, which can vary from unaltered, fairly altered to strongly altered and corresponding porosity ranges of 0.1-0.5, 0.4-1.0 and 1-5 percent respectively (Bongioli, 2007). A porosity increase of about one order of magnitude was reported by Sardini (2006) and Abelin (1991) and applied to veins and cracks in the model domain (**Error! Reference source not found.**). A variant of the base case reactive transport model was defined to investigate the sensitivity of copper dissolution to the measured porosity ranges, as applied to the different structures (V/M/F). No clasts were visible in the mineral map, therefore a slightly higher, i.e., above average matrix porosity was used to take these into account (**Error! Reference source not found.**). The effect of higher porosity on the effective diffusivity was accounted for according to equation**Error! Reference source not found.**), which results in an effective diffusion coefficient of 2×10^{-4} m^2/s.

Permeability values for crystalline rock matrix are commonly estimated to be in the range between 10^{-16} and 10^{-18} m^2 (**Error! Reference source not found.**). In crystalline rocks the permeability cannot be related to porosity by a general equation as the porosity is considered to be disconnected and the permeability relies on secondary structures like fractures and veins. The matrix is considered a very fine grained granular medium, therefore allowing to compute the permeability according to the Kozeny-Carman equation (Carman, 1956), e.g., grainsizes of 0.1-1 mm results in a matrix permeability of $10^{-15} - 10^{-17}$ m^2 (**Error! Reference source not found.**).

Table 4: Permeability (k) and related hydraulic conductivity (K) based on porosity derived from literature according to two different laws. In green Kozeny-Carman relation (Carman, 1956), in orange*** Empirical relation (Autio 2003) and for the hydraulic fracture (HF) using ** Cubic law (Snow, 1986). In red the values used in the reactive transport model are shown.*

Structure	Porosity (Literature)	k_{abs}* (m^2) K-C	K(m/day)	k (m^2) ***	K (m/day)	k (m^2) RT model	K (m/day)
Matrix	0.005	1.25×10^{-15}	0.0108	2.59×10^{-20}	2.24×10^{-7}	2.0×10^{-20}	1.73×10^{-6}
Vein	0.03	8×10^{-12}	1080	3.18×10^{-20}	2.75×10^{-7}	5.0×10^{-16}	4.32×10^{-3}
Crack	0.01	1×10^{-12}	8.64	2.64×10^{-20}	2.28×10^{-7}	1.0×10^{-16}	8.64×10^{-4}
HF**	1	1.04×10^{-8}	89856			5.0×10^{-12}	*50*

Hydraulic fracture

The width of the fracture created by hydraulic fracturing was assumed to be < 2 mm (Geiger 2002; Jeffrey 2009; Gazon 2009). For a width of 0.5 mm a fracture permeability of about 1.04×10^{-8} m^2 can be estimated (Snow 1968), 7 orders of magnitude higher than the matrix permeability which is estimated to be ~10^{-15} m^2 according to the porosity measurements. This corresponds well with the calculations reported by Geiger (2002) and Liedtke (2003). The structure is assumed to be planar on the scale of the model (Geiger 2002; Lichtner 1996). The behaviour in the porphyry rock structures is too complex to predict realistic fracture morphology. Given that further evaluation of mechanical interaction of fractures and mechanical heterogeneity goes beyond the scope of this study, the assumption was made that the fracture would most likely develop along a pre-existing fracture, which is now present as a vein. Copper sulphides tend to be concentrated in the vein, which makes this a favourable scenario for in situ leaching as it creates an exposed surface area of chalcopyrite minerals. To explore less favourable scenarios effective local-scale extraction rates were also assed for the case in which the hydraulic fracture is orientated perpendicular to the copper sulphide enriched main vein.

Dispersion factor

Hydraulic parameters for porphyry rock were gathered from the literature from cases considered to have similar characteristics of vein, matrix and fracture compositions (**Error! Reference source not found.**). The dispersivity was estimated to be very low (10^{-3} m) in the vein-scale model (Gonzalez-Garcia 2000; Odling 2007; Gelhar 1992). Transverse dispersivity was assumed to be 10% of the longitudinal dispersivity assuming alteration patterns result in preferential flow directions similar to what is commonly assumed in layered aquifers. However, although deformation causes altered structures to follow trends, these can still occur in random orientations. The ratio of transverse to longitudinal dispersivity in porphyry rock on this small scale therefore requires to be studied in more detail.

Solute transport

The hydraulic fracture was for simplicity represented in the model as a zone of high conductivity and porosity. While in reality the assumption of Darcy-type flow will not be valid within the vein, this approach is expected to be sufficiently accurate for this vein-scale study. Advection and to some extend also dispersion govern the transport of solutes within the fracture (Bodin et al. 2003). While explicitly modelled, solute concentrations of the major ionic constituents of the lixiviant can safely be assumed to remain more or less constant in the vein over the short travel distance due to the high flow rates. On the other hand solute transport from the fracture into the matrix and vice versa is expected to be controlled by diffusion.

Diffusion depends on the molecule size of the solute and rock properties including effective porosity and tortuosity (Bodin et al. 2003). These physical parameters can vary by one order of magnitude within a few tens of centimetres of crystalline rocks (Abelin et al. 1991) and can be calculated from the Stokes–Einstein relation for a given temperature and pressure (Cussler 1997). Local conditions that are found to affect diffusive properties are the alteration degree (increase by factor 20-200) and in-situ pressure conditions decrease diffusion coefficients (Bradbury & Green 1986). For simplicity, in this study a single molcular diffusion coefficient was applied throughout the model domain. This was assumed as copper dissolution relies on the transport of H^+ and Cu^{2+} of which the aqueous diffusion of Cu^{2+} is the slowest and therefore the rate limiting factor (Steefel & Maher 2009). Also, the diffusive transport perpendicular to the fracture into the matrix will be about four orders of magnitude slower than heat conduction, therefore isothermal conditions can be assumed for a lixiviant that enters in a fracture (Cussler 1997). The effects of increased in-situ temperatures at greater depth (e.g. >1000 m) on diffusion from and towards the fracture and the spatial and temporal variations that occur over the longer time-scales of field-scale ISL operations (months) during injection are neglected in this work. However, they should be further evaluated in future work.

A feedback mechanism results from the kinetic processes in the matrix, causing precipitation and dissolution to reduce or increase porosity, respectively. Pore diffusivity (D_p) is related to aqueous diffusivity (D_a) the following way (Geiger 2002):

$$D_p = D_{aq} 1.47 \phi^{0.72} \qquad (9)$$

Along fractures in igneous rocks, porosity values are in the range of 1-7% (Abelin 1991) decreasing to values below 0.5% in the unaltered rock (Bradbury and Green 1986). These gradients explain the limited extend (< 10 cm) of diffusion into igneous rock and therefore diffusion is mostly relevant in high porosity zones. An assumption of purely fractured rock is often made for the assessment of transport in crystalline rock, implying negligible permeability of the rock matrix compared to the fractures (Geiger 2002). This seems a valid assumption for modelling of hydrothermal alteration as transport will be controlled by natural fractures. However, in this case induced hydraulic fractures will interfere with all natural porosity variations, the solute diffusion into more distal high porosity zones parts should therefore not immediately be neglected.

2.2.3 Model setup - chemical parameters

The fracture and matrix were assumed to be occupied by groundwater that is in or close to geochemical equilibrium with the host rock. For simplicity, the groundwater was assumed to have a spatially constant chemical composition and that the inflowing lixiviant composition was not changing over time. Due to the assumed relatively high flow rates and the short domain length it could be assumed that the lixiviant would quickly spread along the fracture and that the lixiviant's major ion composition would barely change along the fracture, while copper concentrations would successively increase.

Rock composition

The mineral maps provided the mineral composition for the structural features that were defined on the images. For simplicity, these minerals grouped according to their reactivity and expected behaviour. The following set of minerals was considered:

- Chalcopyrite as the copper sulphide mineral is the main copper-containing mineral and expected to be the rate limiting factor for copper dissolution.
- Quartz, representing silicates that are assumed non-reactive over the time-scale simulated in this study, whereby feldspar minerals are included in this group.

- Calcite - as it typically is the most reactive acid consumer even though it is commonly found in small percentage in porphyry rock within the rock matrix.
- Muscovite and Chlorite representing micas (K and Al-phyllosilicates) and Mg-, Fe-, Ni-, Mn-phyllosilicates respectively, as their dissolution is highly acid consuming.

The maps were used to define estimates for the relative volume of the major minerals. According to these volumetric ratios the amount of mineral per litre was computed using rough estimates for density and molar mass. A theoretical experiment in PHREEQC-2 shows that with these concentrations, none of the minerals will be depleted after 34 pore flushes with the lixiviant. The set-up to test dissolution rates is obviously idealised compared to field scale and dissolution would be slower in realistic settings. None of the minerals will therefore become depleted, high initial mineral concentration can therefore be assumed.

For quartz and calcite the kinetic rate expression as provided in the standard PHREEQC-2 database was used according to the following expressions:

Quartz (Rimstidt & Barnes 1980):

$SiO_2 + 2\ H_2O = H_4SiO_4$:

$$r = V_{qtz}\gamma_{H_4SiO_4}\left(1.174 - 2.028 * 10^{-3}T - \frac{4158}{T}\right)a_{SiO_2}a_{H_2O}^2\ (1 - SR_{qtz})$$

Calcite (Plummer et al. 1978)*:*

$CaCO_3 = CO_3^{-2} + Ca^{+2}$

$$r = 10^{(0.198-\frac{444}{273.16+T})}a_{H^+} + 10^{(2.84-\frac{2177}{273.16+T})}a_{CO_2} + 10^{(-1.1-\frac{1737}{273.16+T})}a_{H_2O}$$

For muscovite, chalcopyrite and chlorite the dissolution reaction and kinetic rate expression is defined as follows:

Muscovite (Oelkers et al. 2008)*:*

$KAl_3Si_3O_{10}(OH)_2 + 10H^+ = K^+ + 3Al^{+3} + 3H_4SiO_4$

$$r = \left(10^{-6.53} - exp\left(\frac{-58.2}{RT}\right)\right)\left(\frac{a_{H^+}^3}{a_{Al^{3+}}}\right)^{0.5} \quad (10)$$

Chalcopyrite (Kimball et al. 2010)*:*

$CuFeS_2 + 2H^+ = Cu^{+2} + Fe^{+2} + 2HS^-$

$$r = 10^{-1.52}e^{-28200/RT}[H^+]^{1.68} \quad (11)$$

Chlorite (Lowson et al. 2007)*:*

$Mg_5Al_2Si_3O_{10}(OH)_8 + 16H^+ = 5Mg^{+2} + 2Al^{+3} + 3H_4SiO_4 + 6H_2O$

$$r = 10^{-10.46}\left(\frac{a_{H^+}^3}{a_{Al^{3+}}}\right)^{0.27} \quad (12)$$

In many porphyry veins pyrite occurs in conjunction with chalcopyrite. A significant detrimental effect is expected from the presence of pyrite as it consumes large amounts of ferric iron, but might also

increase the dissolution of chalcopyrite due to the protons produced and due to a galvanic effect of the minerals in contact (Senanayake 2009).

$$FeS_2 + 14\ Fe^{+3} + 8\ H_2O = 15\ Fe^{2+} + 16\ H^+ + 2\ SO_4^{-2} \quad (13)$$

For the simulation of pyrite, the groundwater was equilibrated with pyrite prior to the start of the simulation. This prevents reactions to occur when put in contact with the groundwater, similarly to the gangue minerals. As the mineral is rather reactive in any oxidizing condition, it was equilibrated using PHREEQC-2 allowing kinetic instead of equilibrium conditions reactions. As this is repeated 200 times to mimic the effect of a long period minerals exposed to the groundwater.

Secondary reactions

Secondary reactions will occur due to the strong effect of the highly acidic hydrochloric leaching solution. These side reactions are expected to reduce the chalcopyrite dissolution rate in two ways. Firstly, significant amounts of the leaching agent will be consumed by gangue minerals as these are commonly more reactive than copper sulphides. Therefore increased volumes of lixiviant are required to dissolve and preserve the mobility of the target minerals along the flow path. For example precipitation of gypsum is a common phenomenon in reservoirs rich in calcium (Brewer 1998). In this case, clay minerals form a major part of the bulk rock composition. Phyllosillicates exhibit different mineralogy and reactivity, two types that should be considered in this model are illites, hydrated potassium alumina silicates (muscovite and microcline), found as fibrous crystals that from bundles or break off, hence blocking pore throats. But also chlorite, a hydrated alumina-silicate, is very reactive with the injected lixiviant, from which dissolved iron could precipitate as $Fe(OH)_3$ (Saripalli et al. 2001). Precipitation of these ferric hydroxide minerals is described as:

$$Fe^{3+} + H_20 = Fe(OH)_3 + H^+ \quad (14)$$

Secondly, the precipitation of ferric iron sulphates on the mineral surface of chalcopyrite minerals, reducing its potential contact area with the lixiviant, which is referred to as passivation of chalcopyrite (Córdoba et al. 2009; Dutrizac 1989). As discussed above, precipitation of ferric iron sulphates is expected when the pH exceeds ~2, mainly in the form of jarosites (Córdoba et al. 2009). In saline groundwater conditions solid precipitation occurs predominantly in the form of jarosite in which M^+ is commonly K^+, Na^+ or H^+ (Watling et al. 2014) according to the following reaction:

$$3\ Fe^{3+} + M^+ + 2\ SO_4^{2-} + 6\ H_20 = MFe_3(SO_4)_2(OH)_6 + 6\ H^+ \quad (15)$$

Groundwater

Porphyry rock at depth will typically be saturated with highly saline groundwater, possibly at slightly basic pH (Leybourne 2006; Lichtner 2000). The composition of the groundwater used for this study was taken from (Leybourne 2006) as a representative water composition associated with porphyry copper deposits. Prior to the use in the reactive transport model this groundwater composition was equilibrated with the various bulkrock compositions, as discussed above. Some mixing of the injected lixiviant with the groundwater is expected at the fluid front, the extent of mixing will determine the fluid composition that actually reacts with the fractured rock. As the ratio of mixing is uncertain, initially a ratio of 10% groundwater is used in this study. A leaching solution with a pH of 2 was established by mixing the lixiviant in a ratio of 1:9 with ground water (**Error! Reference source not found.**).

An additional model variant was defined to investigate the impact of groundwater salinity on the copper leaching process. For this comparison a groundwater composition with significantly lower NaCl was adopted from (Lichtner 1996) (see **Error! Reference source not found.**).

At the larger scale copper extraction rates are expected to be sensitive to the flow velocities and thus the migration rate of the lixiviant. This is because proton consumption raises the pH of the leaching solution along the (main) flow path, which could eventually lead to precipitation the of iron sulphates. Although this would mostly be relevant on field scale, the effect of a lower flow rate will indirectly be tested in the vein-scale model by injection of a solution with a higher pH.

Table 5: Lixiviant compositions are equilibrated with the bulk rock composition at pH 1 and 2, adapted by mixing the lixiviant with the groundwater in ratios of 9:1 and 1:9 respectively. In addition of pyrite the lixivant-GW mix was put into kinetic equilibrium. **The 'neutral- groundwater' is equilibrated and mixed with the lixiviant. Saline groundwater according to Leybourne (2006), neutral groundwater and lixiviant according to Lichtner (1996).*

Component (mol/kgw)	lixiviant	GW saline	GW neutral	GW pyr-cpr*	lix pH1 saline	lix pH2 saline	lix neutral**
pe	1	0	12.601	-3.162	19.488	17.6	19.579
pH	19.601	6.81	8	7.75	1.047	2.04	1.036
Al	$2.50x10^{-2}$	$4.14x10^{-6}$	$2.04x10^{-8}$	$1.80x10^{-8}$	$2.25x10^{-2}$	$2.50×10^{-3}$	$2.25x10^{-2}$
Ba	-	$1.27x10^{-7}$	-	$1.27x10^{-8}$	$1.27x10^{-8}$	$1.14x10^{-7}$	$1.27x10^{-7}$
C	$3.40x10^{-4}$	$1.81x10^{-3}$	$1.74x10^{-3}$	$6.72x10^{-4}$	$3.62x10^{-4}$	$6.39x10^{-4}$	$4.54x10^{-4}$
Ca	$1.53x10^{-2}$	$1.51x10^{-2}$	$6.86\ x10^{-4}$	$1.37x10^{-2}$	$1.53x10^{-2}$	$1.38x10^{-2}$	$1.38x10^{-2}$
Cl	$5.00x10^{-3}$	$2.51x10^{-1}$	$3.67x10^{-3}$	$2.51x10^{-1}$	$2.98x10^{-2}$	$2.26x10^{-1}$	$4.87x10^{-3}$
Cu	$1.00x10^{-8}$	-	$3.23x10^{-8}$	$4.78x10^{-9}$	$9.49x10^{-9}$	$1.00x10^{-9}$	$6.76x10^{-6}$
Fe	$4.34x10^{-2}$	$5.69x10^{-7}$	$3.60x10^{-12}$	$5.73x10^{-7}$	$3.91x10^{-2}$	$4.35x10^{-3}$	$3.91x10^{-2}$
K	$1.26x10^{-4}$	$2.41x10^{-3}$	$2.58x10^{-5}$	$2.26x10^{-3}$	$3.56x10^{-4}$	$2.05x10^{-3}$	$1.14x10^{-4}$
Mg	-	$1.22x10^{-2}$	-	$1.33x10^{-2}$	$1.21x10^{-3}$	$1.19x10^{-2}$	$1.96x10^{-5}$
Mn	-	$1.15x10^{-5}$	-	$1.15x10^{-6}$	$1.15x10^{-6}$	$1.03x10^{-5}$	$1.15x10^{-5}$
Na	$5.00x10^{-3}$	$3.45x10^{-1}$	$5.00x10^{-3}$	$3.45x10^{-1}$	$3.90x10^{-2}$	$3.11x10^{-1}$	$5.00x10^{-3}$
S	$2.61x10^{-1}$	$7.497x10^{-2}$	$5.00x10^{-4}$	$7.50x10^{-2}$	$2.41x10^{-1}$	$9.35x10^{-2}$	$2.34x10^{-1}$
Si	$1.93x10^{-3}$	$1.142x10^{-4}$	$1.87x10^{-4}$	$1.41x10^{-4}$	$1.75x10^{-3}$	$3.20x10^{-4}$	$1.75x10^{-3}$

2.2.4 Initial and boundary conditions

Specified head boundaries were applied at discrete locations near the inflow and effluent end of the fracture. The injection of the lixiviant was modelled by a prescribed solution composition located at the upstream end of the fracture and flow into a hydraulic fracture was modelled by continuously applying a fixed head difference between the start and end of the domain. Tests with different boundary configurations showed that the vast majority fluid flow always remained focussed along the hydraulic fracture.

2.2.5 Conceptual model of the leaching process and translation into reaction network

The reactive transport model set up accounts for heterogeneities in the porphyry rock. The intrusion of the lixiviant triggers the dissolution of the minerals within the vein that is opened by the hydraulic fracture. The highly acidic lixiviant induces the dissolution of chalcopyrite which releases elemental copper into the aqueous phase. The concentration gradient between the fracture and the matrix was expected to drive diffusion of both Cu and H^+, which in turn enables dissolution in the immediate vicinity of the hydraulic fracture. Variations in physical and chemical parameters will either enhance or reduce the rate of chalcopyrite dissolution and (secondary) chemical reactions are expected to affect such parameters.

2.2.6 Investigated model scenarios

Selected scenarios that capture different plausible conceptual models and model parameters were investigated (Error! Reference source not found.). The efficiency, i.e., the effective vein-scale rate of copper dissolution was tested and compared among the investigated model scenarios by measuring the sensitivity of the Cu^{2+} mass flux at the effluent end of the model domain.

Table 6: Modelling scenarios.

Scenario	*Tested parameter*	*Description*
Physical parameters		
S1	Base case	Low matrix porosity (0.5%) with related conductivity (**Error! Reference source not found.**) applies and kinetic reactions of quartz, muscovite, chlorite, calcite and chalcopyrite are accounted for. The lixiviant is mixed in a ratio of 9:1 with the groundwater resulting a leaching solution with a pH of 1 (**Error! Reference source not found.**).
S2	High Porosity	The average porosity was applied for the different structures (M/F/V) in the porosity experiments (Attachment B and **Error! Reference source not found.**).
S3	Hydraulic Fracture orientation	The orientation of the hydraulic fracture (flow path) is oriented perpendicular (less favourable) compared to the chalcopyrite vein (attachment A).
S4	Scale	The model domain is extended to 20 m × 0.50 m (highly idealised industrial scale) to represent 1 straight ore-enriched vein cut by the hydraulic fracture (attachment A).
Chemical parameters		
S5	Dissolution rate of chalcopyrite	The dissolution rate constant of chalcopyrite is decreased by 50 %.
S6	Groundwater composition	The background solution (initial groundwater) has a more neutral composition according to table (**Error! Reference source not found.**).
S7	pH	The lixiviant is mixed in a ratio of 1:9 with the groundwater, resulting in a leaching solution with pH 2 (**Error! Reference source not found.**).
S8	+ Pyrite	Pyrite is included in the ore enriched vein, replacing 60 %of the chalcopyrite according to the mineral maps (Figure 4) and equation $FeS_2 + 14\ Fe^{+3} + 8\ H_2O = 15\ Fe^{2+} + 16\ H^+ + 2\ SO_4^{-2}$ (13).

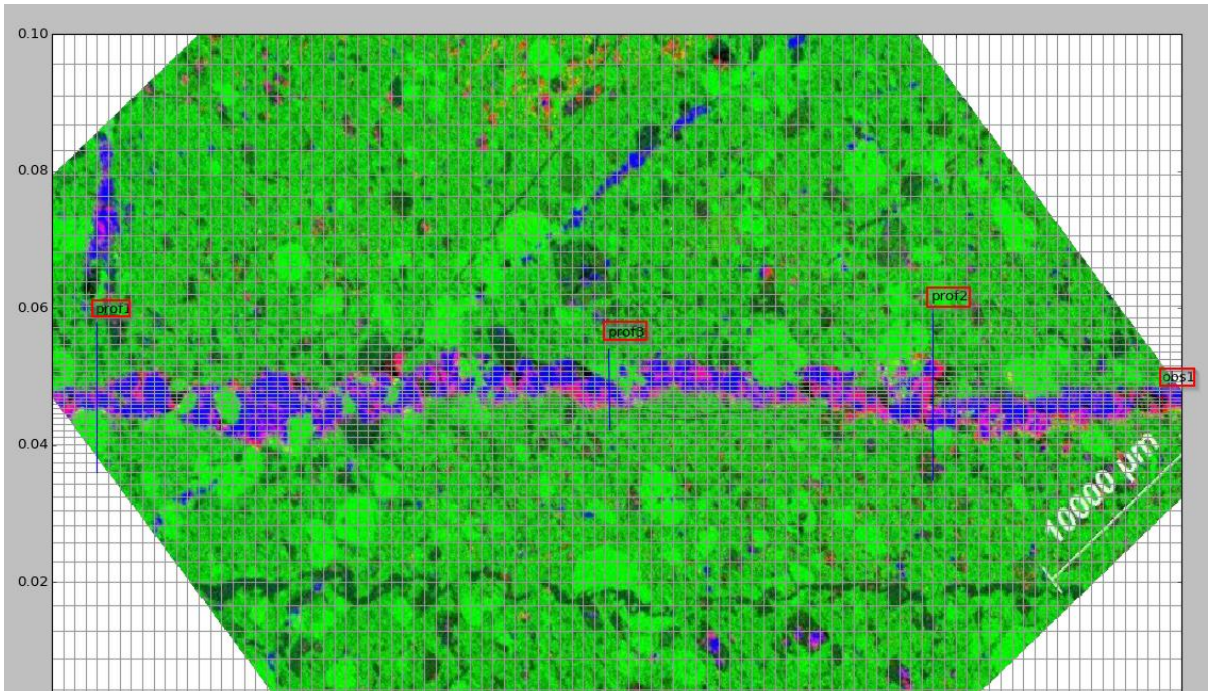

Figure 21: Domain set-up with refined grid (scale in meters), profile 1, 2 and 3 and observation point 1 (red marks) on the right hand side.

S9	+ Jarosite	Kinetic behaviour of jarosite is included according to equation ($3\ Fe^{3+} + M^{+} + 2\ SO_4^{2-} + 6\ H_20 = MFe_3(SO_4)_2(OH)_6 + 6\ H^{+}$ (15).
S10	+ Ferrihydrite	Kinetic behaviour of ferrihydrite is included according to equation (Fe3+ + $H_20 = Fe(OH)_3 + H^{+}$ (14).

The geochemical behaviour of the elements $Cu^{2+,}$ Fe^{3+}, S(6) and Cl, the latter acting as tracer), are plotted to show their behaviour upon injection of the lixiviant. Breakthrough curves (BTC), concentration profiles along profiles 1, 2, 3 (Figure 6) and contour maps of the concentrations were used for this purpose. Similarly, the distribution of the minerals chalcopyrite, chlorite, pyrite and precipitation of jarosite and ferrihydrite is shown via contour maps. Spatially integrated copper extraction rates are from the mass balance for copper for the model's effluent.

2.3 Results

The specific impact of processes and parameters was assessed by a sensitivity analysis that consisted of a range of model variants in which either physical or chemical processes were altered or appended. Results are generally compared to the 'base case model' S1, which uses the previously discussed hydraulic and chemical parameters (**Error! Reference source not found.**). In this section results on the effectivity of the vein-scale models will be shown. Additional results will be given throughout the discussion. Generally the units are meters, days and moles per litre.

2.3.1 Simulated leaching solution

In the base case S1 the lixiviant reaches the effluent end of the domain very rapidly, i.e., in 0.01 days (14 minutes). Within that time the major ion concentrations within the fracture switch from the ambient concentrations to the concentrations imposed by the lixiviant injection (**Figure 7**). Over the 10 day simulation time chloride concentrations in the proximity of the fracture (2-5 mm) are also reduced as a result of diffusion (**Figure 7Error! Reference source not found.**b). Similarly, the concentration of Fe^{3+} and S(6) gradually increases in the matrix over time (**Figure 7**b, c) and the pH is declines in the vicinity of the hydraulic fracture (**Figure 7**d).

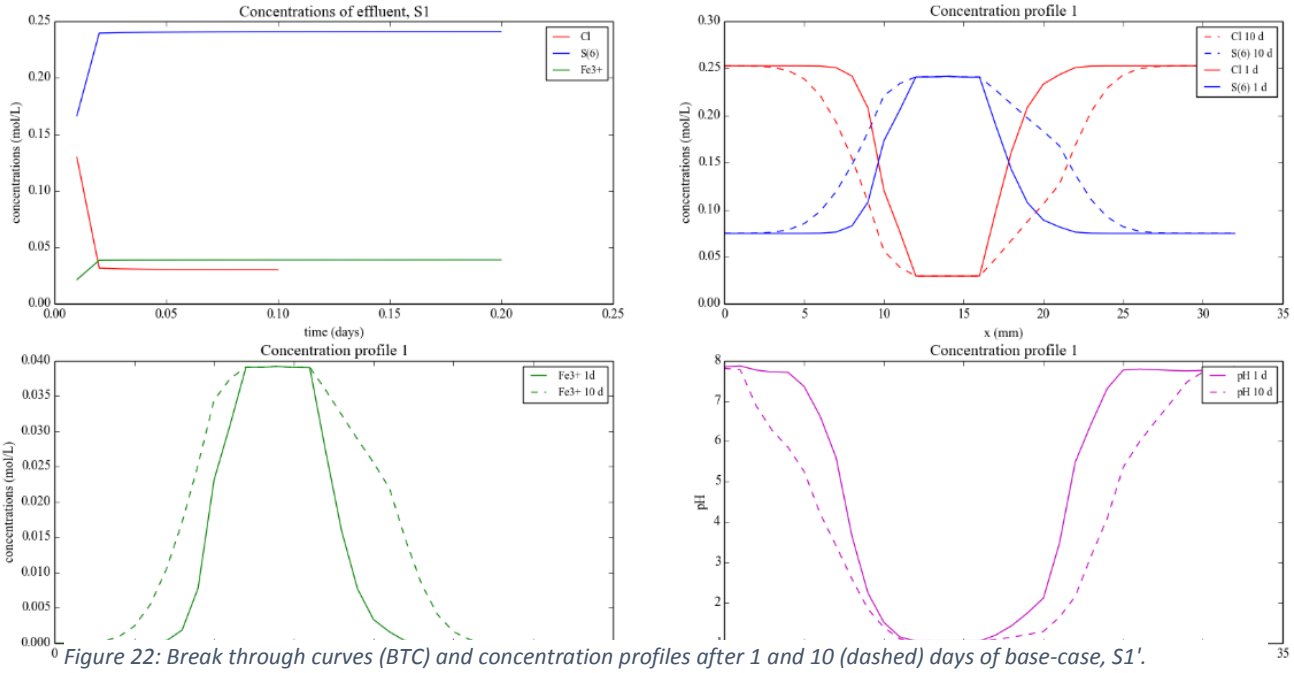

Figure 22: Break through curves (BTC) and concentration profiles after 1 and 10 (dashed) days of base-case, S1'.

2.3.2 Copper mass flux

Over the short time-scale of the model simulation only relatively small amounts of copper were dissolved. The mass flux of dissolved copper over time shows an initial rapid increase around the 0.01 days breakthrough time of the lixiviant and a successive, though slower further increase of the mass flux over the simulation period. The lixiviant flowrate 0.01 m^3/day results in a copper extraction rate of 10^{-5} g/day (S1) in the vein-scale model (**Figure 8**). On a field-scale (~20 m) this would imply $2x10^{-3}$ g/day assuming the strongly idealized behaviour of the small-scale models.

The availability of the leaching agent (H^+) at the interface between the fracture and the matrix was constant due to the constant lixiviant supply at the high flow rate. The effective dissolution rate inside the matrix depends on the availability of the leaching agent and on kinetic rate controls. This is demonstrated by a comparative model run with a decreased (50% of base case) kinetic rate constant (S5) and a comparative run with a higher pH (S7) (**Figure 8**). The 2 time decrease in the kinetic rate constant for chalcopyrite results in a copper mass flux reduction of 1 order magnitude and the injection of a lixiviant with an elevated pH of 2 (S7) results in a strong decrease of the copper

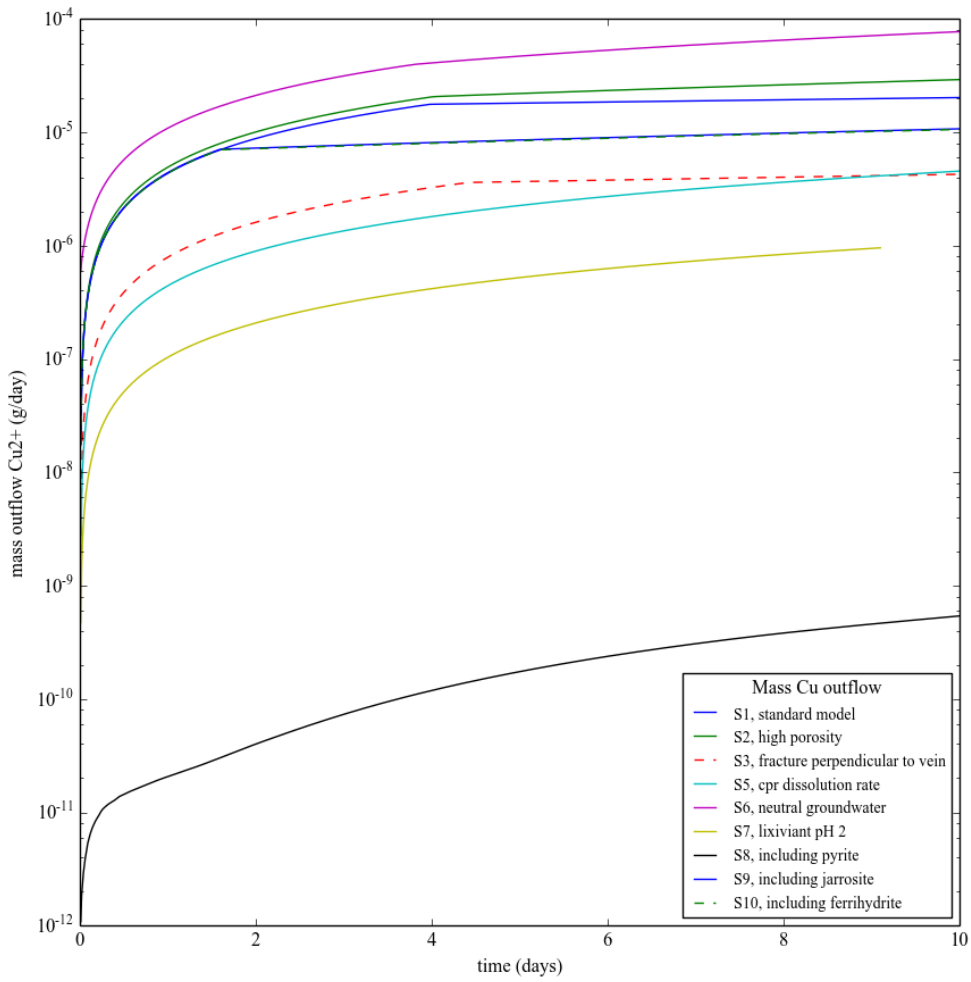

Figure 23: Dissolved copper mass outflow of hydraulic fracture for different model scenarios.

extraction rate (two orders of magnitude).

In contrast, a higher porosity (S2) slightly increases the amount of copper dissolved. This can be explained by the larger volumes of lixiviant that become available for the solid to dissolve. The high

copper concentrations in the lower salinity groundwater (S6) can be explained by the presence of copper in the initial groundwater composition (Error! Reference source not found.).

When the hydraulic fracture is oriented less favourable (S3), ea. perpendicular to the chalcopyrite enriched vein (Figure 8), the available contact area of the vein and lixiviant is significantly decreased

(~10% of base case, see *attachment A* for the domain set-up). The copper mass outflow is reduced by a similar factor, indicating the relation between available surface area of the chalcopyrite mineral and

the lixiviant. Accounting for the competitive lixiviant consumption by gangue minerals shows only clear effects on the dissolved copper mass outflow in the case of pyrite (S8) (Figure 8). In contrast

only small differences can be observed for the scenarios that included jarosite (S9) and ferryhydrite (S10). These results can be seen in more detail in Error! Reference source not found., indicating that

dissolved copper concentrations become slightly higher when taking jarosite into account (S9). Results for simulation scenarios that investigated the impact of secondary mineral precipitation are

shown in **Error! Reference source not found.** and **Error! Reference source not found.**. Precipitation occurred in the regions where ferric iron concentrations increased by diffusion and where the pH

increased or was above 2, allowing both jarosite and ferrihydrite to form under these conditions. As H^+ was produced in these reactions this resulted in a declining pH in the zones of precipitation.

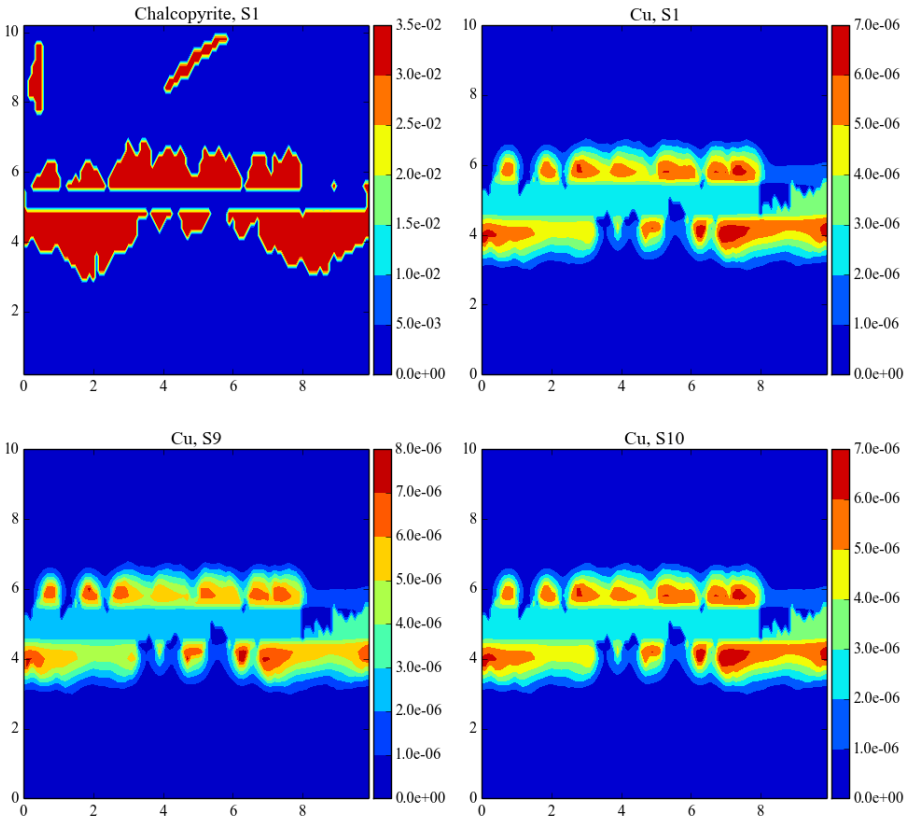

Figure 24: Chalcopyrite and dissolved copper concentrations after 10 days, comparing the base case - model (S1) with models accounting for the effect of jarosite (S9) and ferrihydrite (S10) precipitation respectively.

Jarosite precipitation results in a more pronounced pH change compared to ferrihydrite, as can be seen from the reaction stoichiometry (Fe3+ + $H_20 = Fe(OH)_3 + H^+$

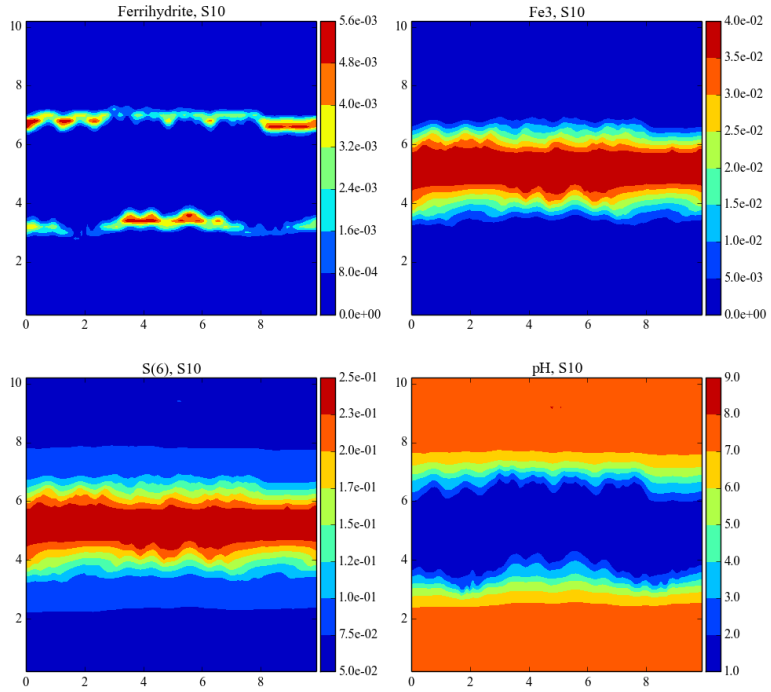

Figure 26: Ferrihydrite precipitation, related concentration of Fe(3), S(6) and pH in the solution.

(143 Fe3+ + $M^+ + 2\ SO_4^{2-} + 6\ H_20 = MFe_3(SO_4)_2(OH)_6 + 6\ H^+$

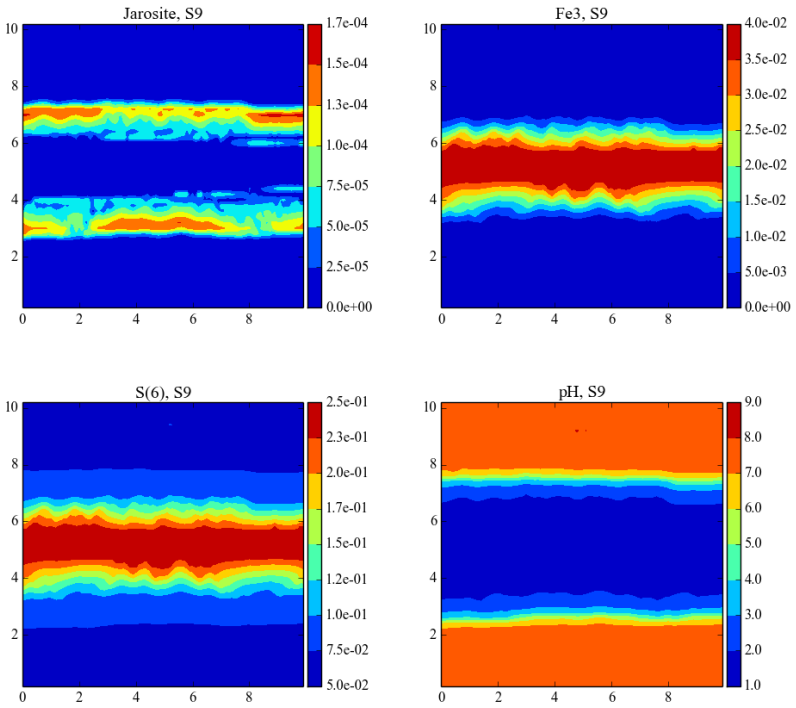

Figure 25: Jarosite precipitation, related concentration of Fe(3), S(6) and pH in the solution.

(15).

3. Field scale modelling

The application of ISL on industrial scale would be expected to involve the injection and production well at a distance of a few meters to a maximum of some, probably a few tens of meters (**Error! Reference source not found.**). The vein-scale models developed in this study therefore require upscaling to derive first estimates for achievable copper recovery rates. A limited number of field-scale experiments were previously performed for copper ISL, providing some indications on which physico-chemical processes should be accounted for in larger-scale simulations of ISL within porphyry copper deposits.

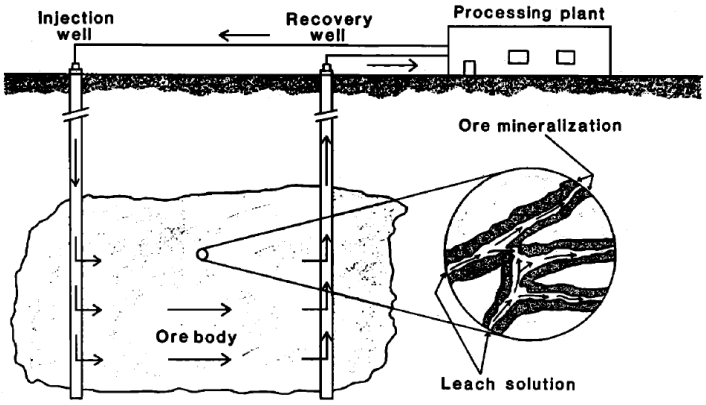

3.1 Model upscaling

Eventually any accurate field-scale modelling approach should mimic the chemical and physical response of the high resolution model. While the development of a scientifically correct and rigorous upscaling approach is beyond the scope of this thesis study, it is still of interest to derive some first approximations of potential larger-scale copper recovery rates. Using a simplified approach, a highly idealised field-scale model is proposed to capture the key processes that might occur at this scale. The larger-scale model accounts for the solute transport rates within the matrix similar to the diffusion rates observed in the small scale model, which showed only marginal effects at 5 cm distance from the hydraulic fracture after 10 days (**Figure 17**). The domain size of the larger-scale model was therefore selected to be 20 m x 50 cm. A 1 mm wide continuous hydraulic fracture was assumed to cut through a copper rich vein. Only one side of the vein is modelled as the problem is symmetric with respect to the centre of the vein.

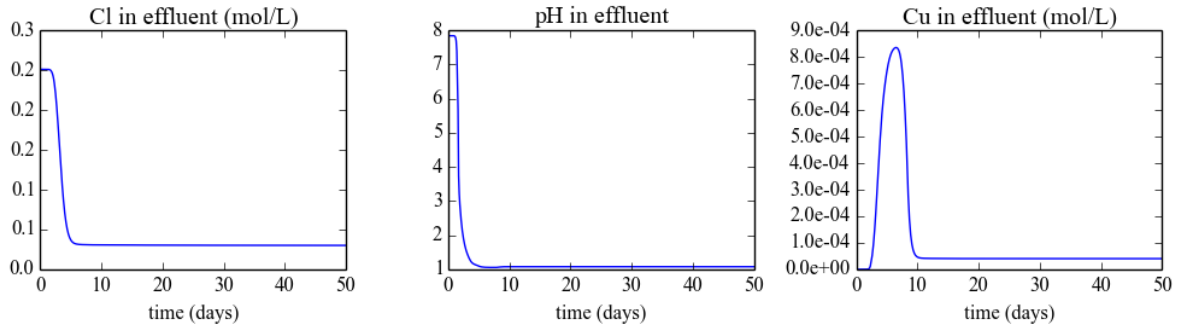

Figure 27: Concentrations at the effluent end of the domain over 50 days (for obs1 see Attachment A, figure 3).

The result of this simulation provide an illustration of the chemical response to lixiviant injection in the case of realistically achievable travel times (~ 2 days) (**Figure 13**). The simulation were run for 50 days.

This case can be considered as an optimal scenario in terms of ISL feasibility. Although complex, structural indicators on field-scale suggest leaching can be successful. Mineralized veins and cracks will show trends in their orientations according to the stress field during their formation. These structures in turn affect the orientation of newly formed hydraulic fractures. Hydraulic conductivity will mainly be determined by hydraulic fractures in the domain between the injection and extraction well. The present prevailing stress field determines the orientations of hydraulic fractures that are open for flow. Hence, pre-existing structures and newly stimulated fractures are most likely to coincide when the in-situ stress field resembles the stress field during formation of ore enriched veins (section 4.2.1 in pt.I). These phenomena regarding the extent and structure of ore concentrations, justify to develop future larger scale reactive transport models.

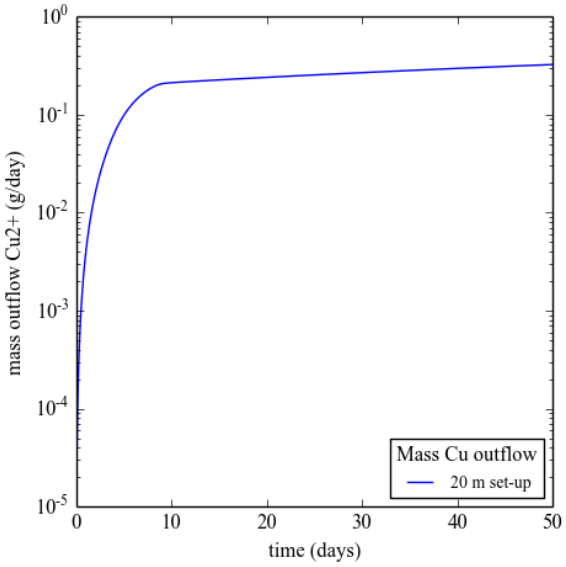

Figure 28: Dissolved copper flux at the effluent end of the domain.

3.2 Volume per hydraulic fracture considerations

The copper that could be dissolved along a hydraulic fracture depends on the surface area of chalcopyrite minerals exposed to the injected lixiviant. The dimensions of the copper enriched vein, the concentration of copper minerals in the vein and the probability of the vein to intersect with the

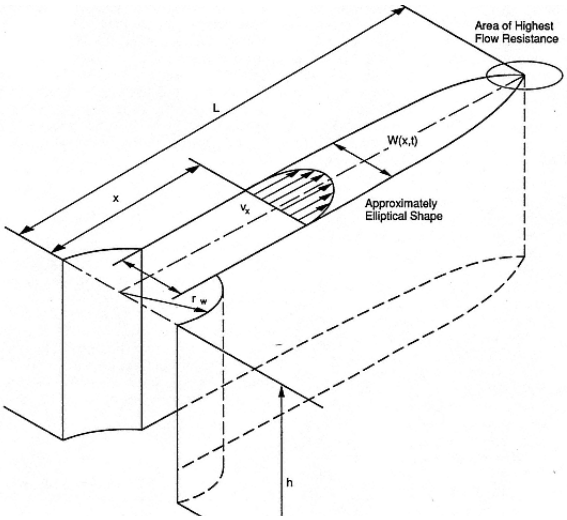

Figure 29: Hydraulic fracture progradation (Mechanics of materials, 2002) (As in pt1.).

hydraulic fracture should therefore be assessed. While it goes beyond the key objective of this study to determine these parameters precisely, some simple approximations can still be made with respect to the amount of lixiviant required to leach the available chalcopyrite along a hydraulic fracture. Hydro fractures are ellipse shaped structures, with an aperture (or width) commonly a few mm, and a length and height up to a few meters (Wong, 2013). They are therefore often modelled as planar features (Figure 15).

The minerals directly exposed to the lixiviant are the minerals cut by the hydraulic fracture. However, the total surface area of porphyry rock compared to that of the hydraulic fracture is significantly larger due to its low matrix permeability. The volume of the porphyry rock is in the order of magnitude of 1000 m^3 per hydraulic fracture. The loss of lixiviant into the rock matrix rather than the vein depends on the relative availability of surface, which can be expressed as A_{HF}/A_{rock} (Figure 31) and the permeability contrast between fracture and rock matrix..

In the vein-scale models the aperture of the hydraulic fractures was assumed to be 1 mm because in previous reactive transport studies the assumed range was 0.5-2 mm (e.g., Geilikman et al. 2013; Jeffrey et al. 2009; Steefel & Maher 2009; Geiger et al. 2002). On field scale, for a similar fracture width, larger injected volumes are required than in the vein-scale model. With increasing injection volumes, the relative permeability of the vein will decrease relative to that of the matrix. Anticipated injection volumes are in the order of magnitude of 10^3 m^3/day in porphyry rock according to pumping rates in previous field trials, i.e., 1000-2000 L/min (Morgan 1989; Metals 2014; Ahlness & Pojar 1983). Injection volumes of 1 gallon per minute per foot reservoir thickness are recommended after field trials (County et al. 2013), which converts to 1.6 m^3/day/meter reservoir thickness.

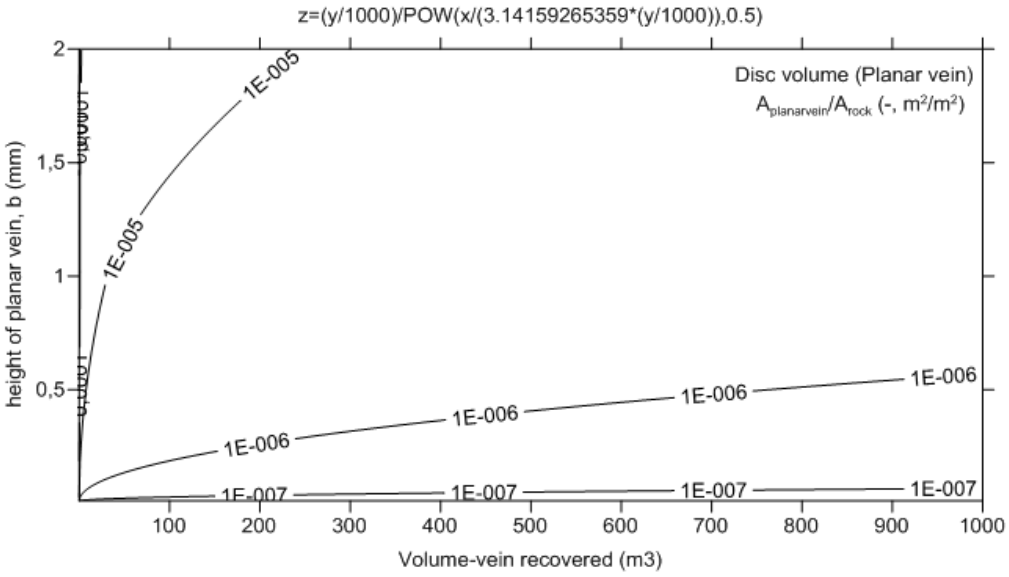

Figure 30: Surface area ratio of a planar vein (hydraulic fracture) to that of the rock according to the volume per vein (hydraulic fracture) (m3) and the aperture of the hydraulic fracture (mm).

For thin hydro fractures, the ratio of the surface area of the fracture to that of the rock decreases relatively fast with increasing injection volume, resulting in relatively low hydraulic fracture permeabilities (Figure 31). For an aperture of < 1 mm and recovered volume from the fracture of 10^3 m^3, the ratio of fracture to vein surface area is in the order of magnitude 10^{-6}. This would almost overcome the permeability difference of 10^{-7} as determined for the presented vein-scale reactive transport models, which could result in lixiviant loss in the matrix. The in-situ conditions require careful assessment of the injected volumes of lixiviant, fracture aperture and matrix permeability.

The aperture of hydraulic fractures will rely on proppants, as high lithostatic pressures prevent the fractures to naturally stay open in the in-situ pressure conditions. Proppants have a maximum size of a few mm (Treviranus 2013), which again points out that narrow fractures should be assumed. To prevent major fluid losses into the matrix, either flow rates should be reduced or fracture permeability should be increased. A higher number of hydraulic fractures per volume enhances the surface area of the vein and reduce the volume per fracture recovered (Figure 31) which could potentially prevent fluid losses to occur.

The dissolution of porphyry rock due to leaching over time caused rock matrix porosity to increase (e.g. Harpalani 2000; Brewer 1998), this leads to the rock matrix surface area to increase (Navarre-Sitchler et al. 2013), reducing surface area ratio (A_{HF}/A_{rock}). The increased porosity in altered vein structures, would imply a higher permeability and hence smaller permeability difference to overcome. The surface area of the matrix was determined to be 5.06×10^6 m^2 for a matrix porosity of 0.5% compared to 2 m^2 for the hydraulic fracture, increasing with a factor of 6 after weathering increased the porosity to up to 10% (Navarre-Sitchler et al. 2013).

3.3 Hydrodynamic consequences

Dispersion in porphyry rock on a larger scale is attributed to microfractures and variations in mineralization such as veins and cracks. The effect on the dispersion factor was tested on induced and naturally occurring microfractures in granites and found to be mostly dependent on length and connectivity, not on fracture density (Odling et al. 2007; Gonzalez- Garcia 2000). Veins and cracks show trends in orientation in the vein-scale model (Error! Reference source not found.), which is favourable for connected permeable structures to become connected on larger scale. In the matrix however, dispersivity will mostly be determined by micro-cracks and local-scale variations in porosity and permeability.

On industrial scale (up to a few tens of meters), channelling will occur in heterogeneous fractured rock as flow is concentrated along the flow paths with the lowest hydraulic resistance. Depending on the resolution of heterogeneity within a model on this scale, a much higher dispersion factor might be applied at those larger scale (Gelhar et al. 1992; Larsson et al. 2012), depending on the grid resolution and the resolution at which heterogeneity is resolved in the model.

Another effect of flow channelling is significant contact area reduction. Diffusion of the lixiviant into the rock matrix is controlled by the contact area between minerals and the lixiviant. High standard deviation of the hydraulic conductivity field increases channelization of the fluid flow in models that had an extension of some tens of meters (Larsson et al. 2012). Hydraulic fracturing in low permeability rock would result in a wide range of permeability and strong channelization accordingly. The consequence of reduced wetted area of the rock, would not only reduce contact area for diffusion into the rock matrix to occur, but also the relatively high porosity zones in the matrix could be passed. For future models of ISL on industrial scale, this implies the effect of other fractures and faults becomes important to consider, in contrast to the small porosity variations within the matrix.

As already briefly discussed above with respect to porosity changes at the vein-scale, dissolution of minerals after injection of the lixiviant can change hydrodynamic characteristics. Similarly, an increase of porosity and permeability by micro-scale observations from samples derived after field scale leaching experiments with sulphuric acid on a porphyry copper deposit (Harpalani & Williams 1999). The number, area and aperture of fractures increase due to the dissolution of copper minerals along the fractures. The porosity increase and the amount of copper recovered slowed down after several cycles of leaching in these experiments. A sharp decrease of permeability towards the end of the experiment (400 days) was attributed to clogging of fractures by precipitation of sulphates and

fracture wall rock breaking (Harpalani & Williams 1999). On another field scale in-situ leach test in the San Manuel porphyry copper deposits, permeability increased except near production wells where fractures were clogged by precipitation of secondary minerals (Brewer 1998).

On meter scale, increasing Cu^{2+} concentrations will develop in the fracture along the flow direction, as increasing amounts of chalcopyrite will be dissolved over time and in the vicinity of the extraction well. As a result the copper concentration gradient will be reduced and diffusion driven transport into the matrix will slow down. Additionally, the lixiviant will be increasingly neutralized due to extensive proton consumption by the matrix (clay) minerals along the hydraulic fracture. This effect decreases the effectivity of the lixiviant and increases the tendency of iron sulphate phases and ferrihydites to precipitate. For these reasons, for example the location of the ore body with respect to the injection and recovery well and lixiviant composition over time have to be considered on industrial scale.

The weathering of secondary minerals on field scale is an order of magnitude slower compared to experimental rates and two orders of magnitude slower than fresh granite weathering rates (White & Brantley 2003). The difference in element concentrations (Fe, Ca, Al) is assigned to precipitation of ferrihydrite, clay and calcite, which becomes increasingly important with increasing scale (Ganor et al. 2005). Fresh granite surfaces will consume higher amounts of protons as concluded form higher pH of the effluent. Flow rate variations affect the pH of the effluent, and hence affect the amount of clogging of pores over time caused by ferric oxide precipitation (White & Brantley 2003).

4. Discussion

4.1 Experiments and model setup

Reactive transport modelling was found to be suitable tool to integrate current process understanding and data to assess the potential of ISL in porphyry rock. However, at this stage only the relative sensitivity of copper dissolution to various physical and chemical parameters could be determined. Calibration of the models to results of experiments in realistic settings is required for future use of these models in a more qualitative manner. For example leaching of cores porphyry rock cores with a realistic bulk rock composition could provide better chemical (reaction rate) parameters. Field-scale experiments will provide essential data for the relevant physical effects, e.g., clogging and channelling, that have to be accounted for in reactive transport models.

In this study, the simulation time was limited to 10 days due to the high resolution heterogeneity, which required small time step sizes and therefore model run-times were often long (> 4 days). The time required to leach economical amounts of copper from chalcopyrite are on the scale of months up to years (e.g., Watling et al. 2010). The simulation time should be increased to several months to leach economical amounts of copper. Therefore the 10 day leaching tests simulated in the vein-scale models needs to be extended and therefore requires either reduced resolution heterogeneity or extended calculation times. For upscaling of the models to realistic (time-) scales a simplified heterogeneity would be preferable. The field-scale model that was proposed in this study gives an impression of the ability of reactive transport models to take the relevant parameters into account, however the favourable setup comprising continuous permeable and ore enriched structure, needs to be developed by including physical and chemical heterogeneity, for realistic predictions on copper dissolution form porphyry rock.

Heterogeneity can be reduced considering the transport mechanisms that dominate in the zones with different hydraulic properties. Due to low diffusion velocities, the lixiviant did have minor effects at a distance of 5 cm from the hydraulic fracture after 10 days (**Figure 17**). Consequently, even on longer time scales, a much smaller impact on, for example, the smaller veins at the top part of the mineral map (Figure 6) is expected, even though they have similar, favourable, flow and chemical characteristics as the main vein. As diffusion accommodates transport both from and back towards the hydraulic fracture, in order for copper to be removed from the rock via the hydraulic fracture, this process will take months to years. It seems legitimate to reduce the heterogeneity by only accounting for the detailed heterogeneity in case they occur in the immediate vicinity (~10 cm distance) from the modelled hydraulic fracture as only high porosity copper enriched veins near the expected fluid path

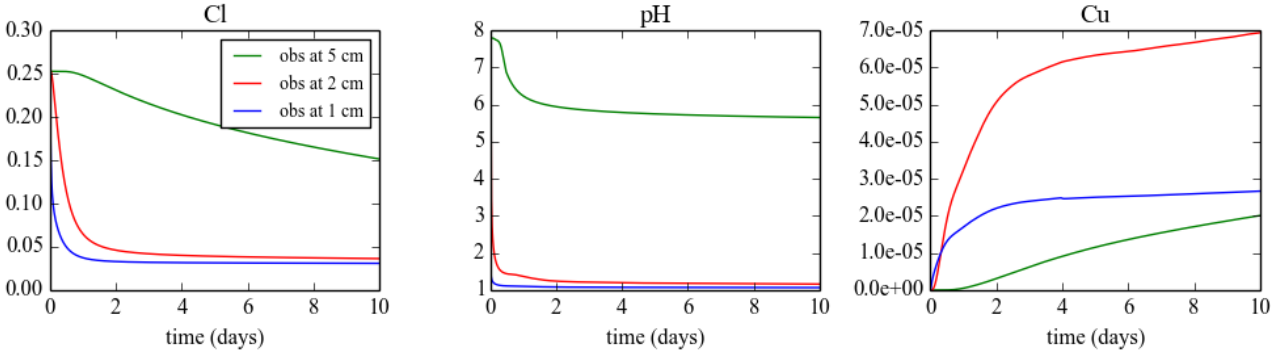

Figure 31: Concentrations after 10 days at 1, 2 and 5 cm from hydraulic fracture, S1.

way (hydraulic or natural fracture) will be affected be diffusion.

The model scenarios S8 - S10, account for kinetic behaviour of additional gangue and secondary minerals, to represent some of the complexity of the porphyry system. Some of these rate expressions have been well defined in the literature (equation 9, 10, 11), but the kinetic behaviour of jarosite and ferrihydrite is a function of their saturation index. More dissolution rate expressions should be derived from experiments on porphyry copper deposits, taking realistic bulk rock compositions into account. The increasing complexity mask the effects attributed to individual parameters. For example, the results show the ability of modelling bulk mineral dissolution and resulting (secondary) precipitation, but (high) pyrite concentrations could significantly decrease the pH preventing the precipitation of these minerals.

Not just simpler surrogates for the simulation of complex hydrodynamic patterns but also the reduction of chemical complexity could lead to more efficient models. The selection of minerals that was modelled to represent the bulk rock behaviour, i.e., the dissolution of gangue minerals and precipitation of secondary minerals were determined from the mineral maps of a specific deposit. A more extensive database with porphyry rock minerals and dissolution reaction rates, as determined using alternative leaching solutions, could lead to further simplifications of the considered chemical complexity. For example, according to the fast dissolution of chlorite compared to muscovite, chlorite consumes high amounts of protons and hence has a higher impact on the dissolution of chalcopyrite. However, before such conclusions can be made, rate constants of the kinetic reactions modelled should be improved by calibration of the rates with results of lab and field experiments.

4.2 Copper dissolution

The simulation time of 50 days results in higher mass flux compared to the vein-scale models due to much larger contact area for the lixiviant to react with chalcopyrite minerals and longer travel time in the vein (**Error! Reference source not found.**). The dissolution of copper according to the mass outflow plots of vein-scale models show linear relations with time of about $9*10^{-4}$ g/day (**Figure 14**), which converts to $8.22*10^{-8}$ mol m^{-2} s^{-1}, these compare well to the maximum copper dissolution rates of 6.5 – 5.3 * 10^{-8} mol m^{-2} s^{-1} resulting respectively from modelling (Senanayake 2007) and experimental data (Lazaro & Nicol 2003) in similar conditions. These linear relations are not expected to be realistic on industrial scale, as either the ore mineral depletes or secondary processes will affect the dissolution rate.

The simulations with the various model variants resulted overall in relatively small differences in the dissolution of chalcopyrite among the different models (**Error! Reference source not found.**). Some of the small differences between the scenarios can be attributed to the short simulation time (10 days) and the high initial chalcopyrite concentrations. The simulated dissolved copper concentrations along a selected profile give a better indication of the variations in dissolution rates (**Figure 19**). The elevated dissolved copper concentration observed for all scenarios can be explained by the presence of the copper enriched vein, and the dip in the centre coincides with the hydraulic vein cutting through. The copper concentrations however are also affected by the copper concentrations in the ambient groundwater and by how much copper is contained in the leaching solution, i.e., copper extracted further upstream in the vein. Taking this into account the high Cu^{2+} concentrations in S6 (**Figure 19**) can be entirely ascribed to the ambient groundwater composition applied in this model, and not to a faster dissolution of chalcopyrite (**Error! Reference source not found.**). Similarly, the lower chalcopyrite concentrations in the scenario with high porosity should be attributed to lower rock volume, not to slower chalcopyrite dissolution rate.

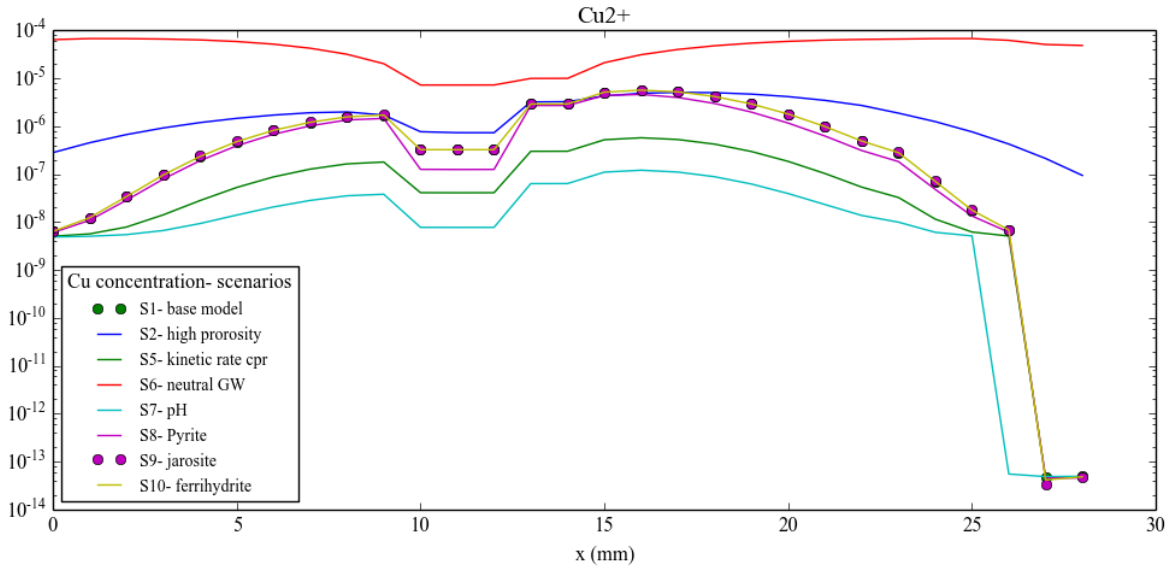

Figure 32: Cu^{2+} concentrations (mol/L), on log-scale, after 10 days in different scenarios along profile 2.

4.2.1. Flow properties

According to previous studies (e.g., Steefel & Maher 2009; Geiger et al. 2002) solute migration in the porphyry rock matrix is mainly controlled by diffusion, thus being the limiting factor for copper extraction. Local variations in porosity due to the presence of veins or other chemically altered features, enhances local diffusion rates as shown in **Error! Reference source not found.** by the spreading of Cl, pH and Fe^{3+}, which in turn triggers enhanced dissolution. Indeed the Cu^{2+} concentration profile exhibits higher concentrations along the profile compared to the lower porosity scenario (**Error! Reference source not found.**c). These differences seem significant, even as the diffusive properties of rocks in-situ can be a factor 2-2.5 lower than those of laboratory samples because of natural physical constraints (Skagius & Neretnieks 1986; Bradbury & Green 1986).

This figure also shows lower Cu^{2+} concentrations in the two peaks that correspond to the vein immediately next to the hydraulic fracture, corresponding to the slightly lower initial concentration of chalcopyrite due to the higher porosity as considered earlier. However, dissolved copper concentrations are relatively high at the rims of the vein in this scenario (S2), possibly due to the higher diffusion rate related to the increased pore space.

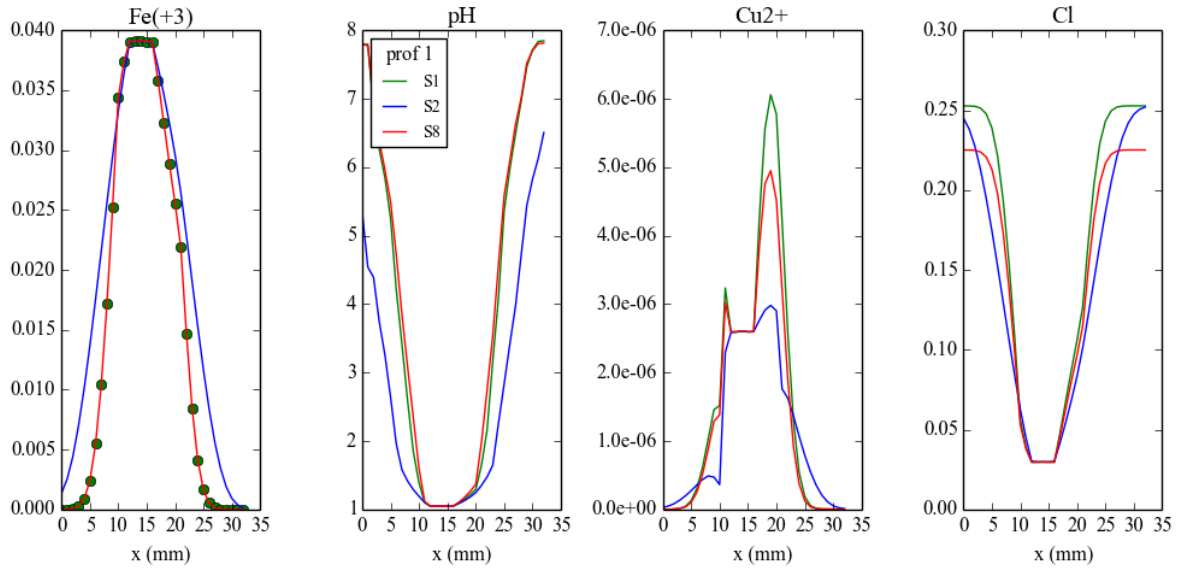

Figure 33: Concentrations (mol/L) for the base model (S1, green), higher porosity (S2, blue) and additional pyrite in the vein (S8, red), along profile 1 (see attachment A).

The measured porosity variations (**Error! Reference source not found.**) are considered significant taking into account that these results show solute spreading after 10 days, and extraction times in field applications would extend at least over several months. Porosities of up to 15 % were measured on the three different porphyry rock samples which is significantly higher than the porosity values generally encountered in the literature (< 1 %), even though these values might be overestimated in the small plugs (< 5 cm) as dead-end pores haven been artificially transformed into connected pores as the plugs were cut (Bradbury & Green 1986). Also, the results agree with porosity variations in altered rock (Bongiolo et al. 2007; Sardini 2006). These findings indicate that the observed altered structures could form preferential flow pathways. In this way the higher porosities could trigger a positive feedback mechanism in which dissolution and precipitation reactions can lead to progressive increase and decrease of porosity and hence affect the hydraulic conductivity (equation **Error! Reference source not found.**).

On the larger scale, the positive feedback mechanism could result from enhanced dissolution of high porosity (copper enriched) structures, resulting in channelizing fluid flow (Larsson 2012). A few studies indicate such mechanisms to occur on field-scale (Sainath & Harpalani 1993; Brewer 1998). The simplistic field-scale model (S4) accounts for 1-D diffusion as the concentration gradient is predominant perpendicular to the hydraulic fracture. Diffusion caused spreading of the lixiviant to be further developed closer to the injection point (**Figure 21**).

The effect of the injected lixiviant was already observed in Figure 13, in which the dissolved copper concentration increases after injection of the lixiviant. More detailed observations can be made from Figure 22, in which the grid cells of the 50 cm high domain (figure 3, attachment A), are all exaggerated up to a similar size, to be able to visualize chemical changes in the narrow (1 mm) vein at the bottom of the domain.

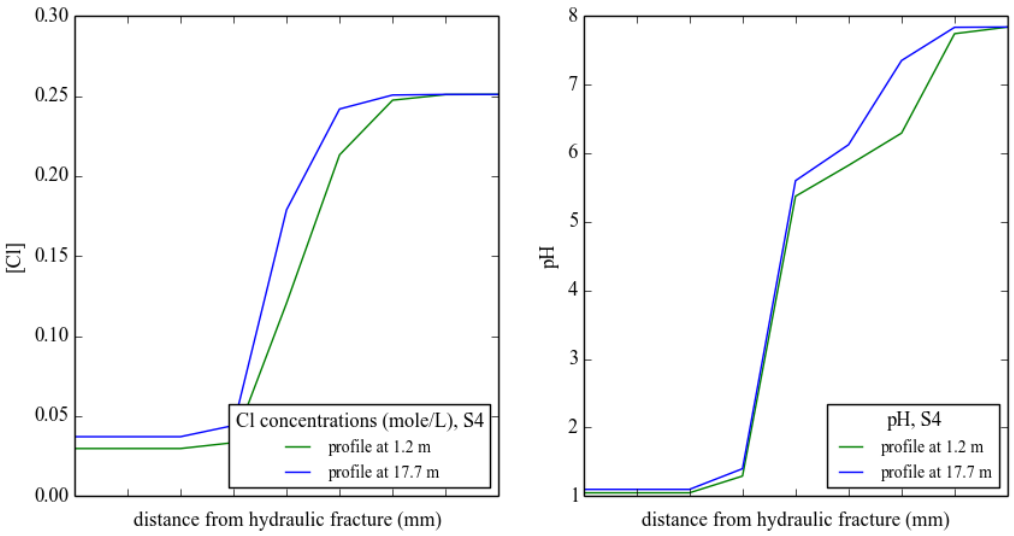

Figure 34: Change in concentration profile along the hydraulic fracture, with profile 1 (green) at 1.2 m, and profile 2 (blue) at 17.7 m from the injection point after 50 days. For location of profile 1 and 2, attachment A see figure 3.

The high flow velocity of the lixiviant assures a constant availability of protons that can act as a leaching agent along the hydraulic fracture. This indicates the dissolution of chalcopyrite is limited by the kinetic rate and copper ore availability in the hydraulic fracture. In contrast to the vein-scale model, chalcopyrite concentrations decrease significantly (Error! Reference source not found.c), but still do not deplete after 50 days of leaching. Kinetic rate and mineral availability were also found to be the main limiting factors modelling kinetic behaviour in discrete fracture models by Garzon (2009).

Copper concentrations increase where the pH is declining and triggers dissolution (Figure 22b). The concentration of dissolved copper increases and spread out over time (Figure 22b, note difference of copper concentration scaling after 20 and 50 days). The pH increase towards the end of the hydraulic fracture (Figure 22a) can be attributed to proton consumption along the flow path. Precipitation of secondary minerals increases accordingly towards the end of the fracture (Figure 22e).

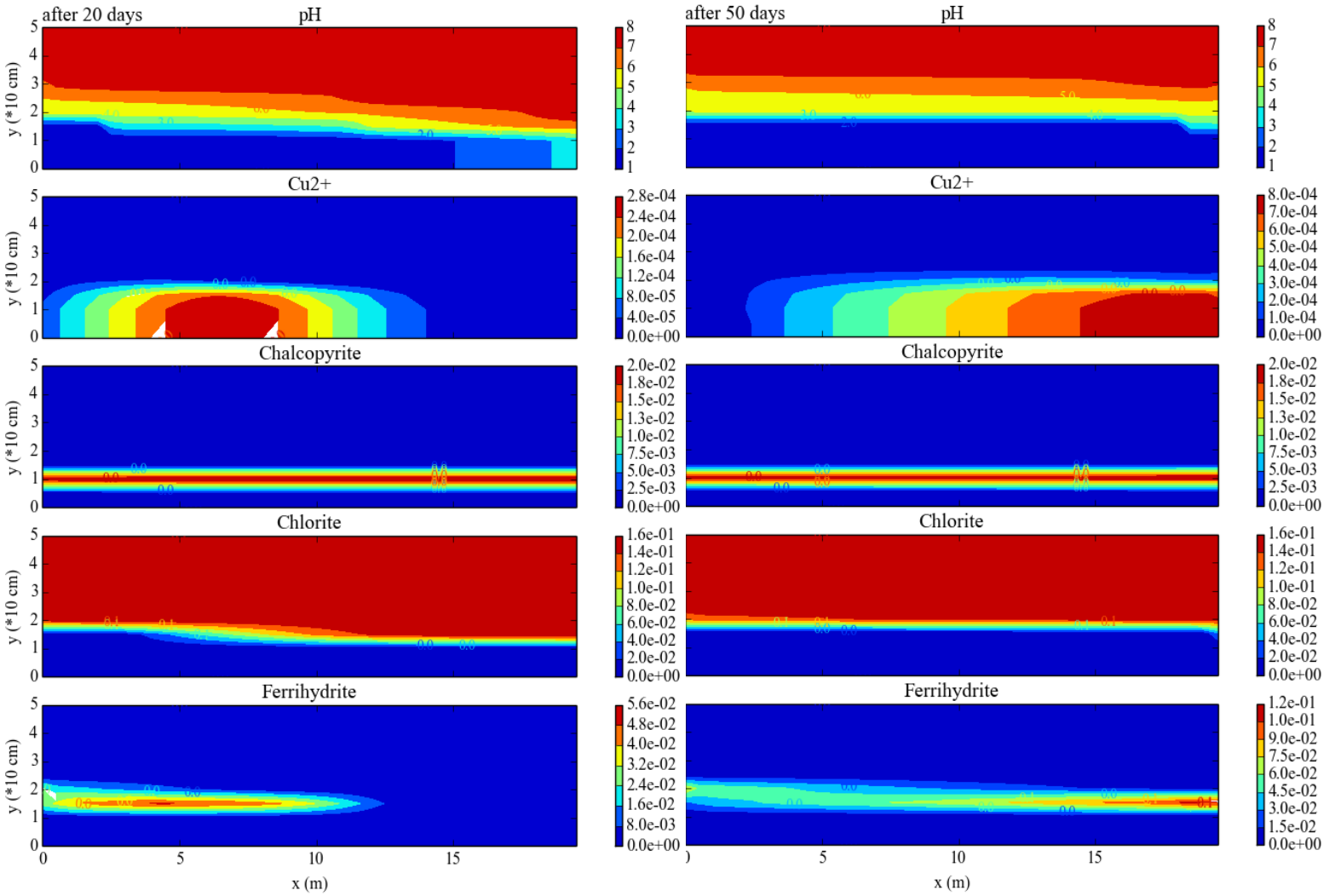

Figure 35: Concentrations (mol/L) after 20 days (left) and 50 days (right) in the 20 m domain. The y-axis is increasingly exaggerated towards the bottom, i.e. around the vein. Note the different concentration scales for ferrihydrite and Cu^{2+} on left and right.

Mineral surface availability is not just limited by the contact area with the hydraulic fracture, but could also be reduced by jarosite precipitation on the chalcopyrite surface. As ferrihydrite is shown to precipitate where pH decreases and ferric iron concentrations become sufficiently high due to chalcopyrite dissolution and spreading of the lixiviant (**Figure 22**e). Future modelling of this passivating effect requires to account for, i.e., explicitly model the available reactive surface area (A). Also future work may further investigate the scattered chalcocite crystals that were detected on the mineral map (**Figure 4**). These have a limited surface compared to their volume (V). A/V is the ratio of the total surface area to reaction solution volume (Herbert 1999). This changes over time, resulting in a factor $(m/m_0)^{2/3}$ which should be included in the kinetic rate expression.

Another rate determining factor for the reactions in the fracture is the mixing term of the dissolved elements in the fracture. Considering the in situ stress conditions, proppants will be required to keep the hydraulic fractures open for flow. Although the porosity will slightly decrease in the hydraulic

fracture, mixing of both the dissolved copper and leaching agents could be enhanced by the presence of proppants.

4.2.2 Chemical variables

For the chemical reactions occurring in an ISL system the chemical composition of the porphyry rock, lixiviant and groundwater were taken into account.

Groundwater

In the discussed vein-scale models, groundwater was considered stagnant at in-situ conditions (Krásný 2003). The groundwater was therefore equilibrated with the bulk mineralogy to account for their stability before interference of the lixiviant. The assumption of a homogeneous groundwater solution is a simplification, as in reality groundwater will be compartmentalized in relation to local mineral concentrations. Berger et al. (2001) distinguished between porphyry-, vein- and unmineralized rock-waters according to field study data. The local equilibria of the groundwater with surrounding minerals will be disturbed by hydraulic fracturing and pumping, this will be moving the local groundwater patches and hence triggering reactions with an adjacent mineralization area even before injection of the lixiviant.

The effect of different background concentrations (**Error! Reference source not found.**) is clearly visible in **Figure 19**, as the salinity starts to decrease when the lixiviant is injected in the saline groundwater, opposed to the more neutral groundwater scenario. The salinity of the groundwater is found to accelerate oxidation of chalcopyrite and bornite (Watling 2013b). The pH behaves almost similar over time for the different groundwater compositions, but a slightly higher pH can be observed at the lower part of the fracture after injection in the saline groundwater (S1) (**Figure 23**). Higher Cu^{2+} concentrations in the groundwater than in the lixiviant are observed for S6 (in neutral groundwater), these concentrations will even counteract the diffusion gradient driving copper

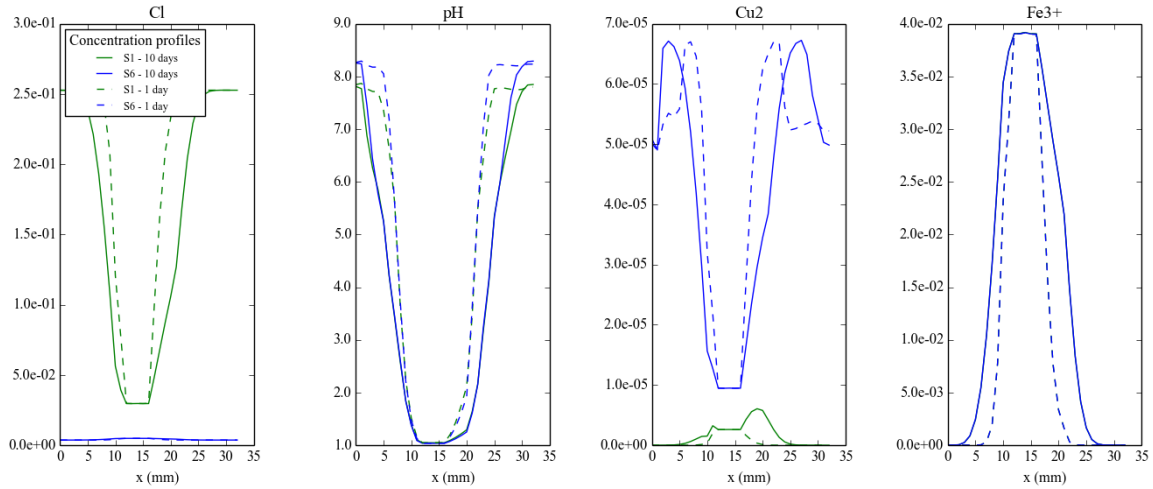

Figure 36: Concentration profiles after 1 day and 10 days of lixiviant injection in strongly saline groundwater (SW, green) and more neutral groundwater (blue) along profile 1.

transport from the matrix to the hydraulic fracture (**Figure 19**c and **Figure 23**).

The presented models do not account for the effect of in-situ conditions on the density and viscosity of the groundwater and in turn hydraulic conductivity, as salinity, pressure and temperature increase with depth. Brine viscosity increases with pressure and salinity, but decreases with increasing temperature (Driesner 2007). This results in a density of 989 kg/m^3 and dynamic viscosity of 0.475

×10-^{3} kg/m^{3} s (Niepelt 2009) which could result in a significant increase of hydraulic conductivity

Hydraulic conductivity: $K = \frac{k\rho g}{\mu}$ (5)

.

Lixiviant composition

The leaching solution mixed with groundwater that was simulated to flow into the fracture has a pH of 1.047 (**Error! Reference source not found.**) and established a strong concentration gradient from the hydraulic fracture to the matrix due the continuous flow through the fracture. This gradient drives diffusion of the leaching agents (H^{+} and Fe^{3+}).Therefore injection of a leaching solution with an elevated pH of 2 results in slower solution spreading (.

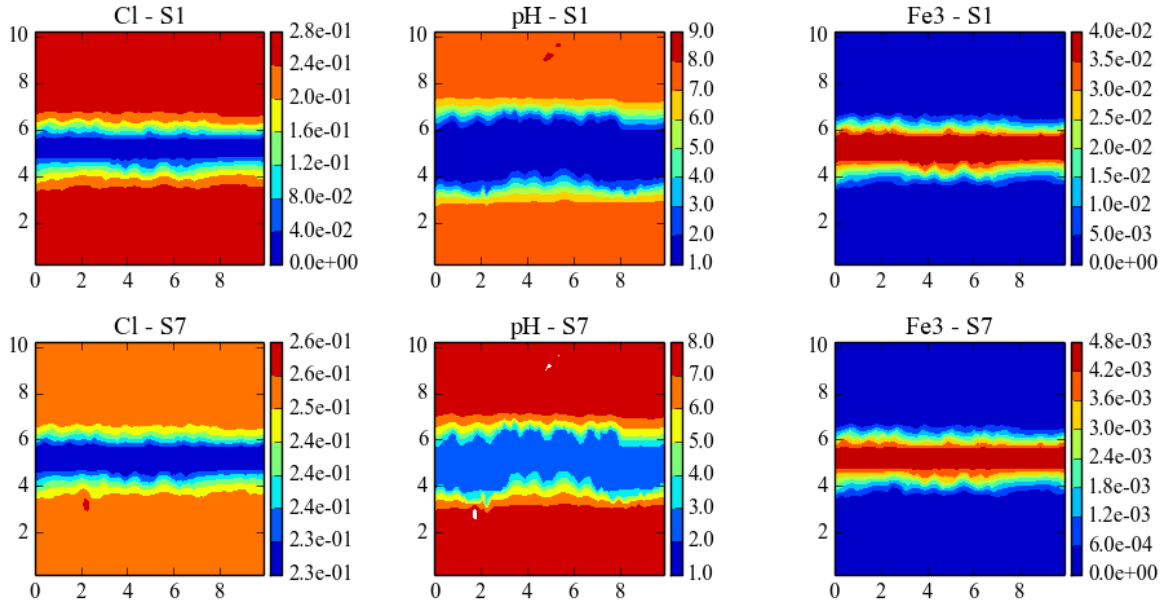

Figure 37).

Figure 37: Solute concentrations after 10 days of injection of lixiviant with pH 1 (upper row) and pH 2 (lower row).

The effect on mineral dissolution of injection of the lixiviant at a pH of 2 is tested for the base case and its strongly saline water (**Figure 25**). The chlorite dissolves significantly slower at higher pH, which might explain the high availability of protons for the dissolution of chalcopyrite and in turn the slightly lower chalcopyrite concentrations in the pH 2 scenario.

Relatively high concentrations of Fe^{3+} were used in the lixiviant in this study (**Table 5**), compared to other studies (3.58 x 10^{-5} mol/L, Miki 2011). However, the dissolution rate of chalcopyrite depends only on pH in the presented models ($CuFeS2 + 2H^{+} = Cu^{+2} + Fe^{+2} + 2HS^{-}$ **(1)**), so the concentration of this oxidizing agent will not affect the result. Still, in leaching solutions with ferric iron as the major oxidizing agent, the dissolution of chalcopyrite is strongly dependent on pH (e.g. Córdoba et al. 2009; Senanayake 2009; Yevenes 2010).

Dialnet (2009) finds small concentration increase of dissolved copper mainly in the first 20 days at a pH 1 compared to pH 2. In the same study, larger effects are measured for dissolved iron concentrations, which roughly double when increasing the pH from 1 to 2. To take these effects into account, similar models should be made with kinetic rate expressions in which dissolutions depends (partially) on Fe^{3+} concentrations.

For other copper sulphides like covellite, dissolution is shown to increase up to a pH of 2 (Miki 2011) as a result of the formation of $CuCl_2^-$ complex ions (Cheng and Lawson, 1991). In presence of these complexes the redox couples Cu(II)/Cu(I) (fast) or Fe(III)/Fe(II) (slow) can oxidize sulfide minerals (Nicol and Lazaro 2003; Miki and Nicol 2008).

More modelling in the range of pH 1-2 is required on field scale, as optimal leaching rates are found at a pH of 1.5 (Senanayake 2009; Yevenes 2010) but also highest rates of Fe^{3+} precipitation was found at this pH in high salinity groundwater (Watling 2014). Testing different leaching solutions is required as

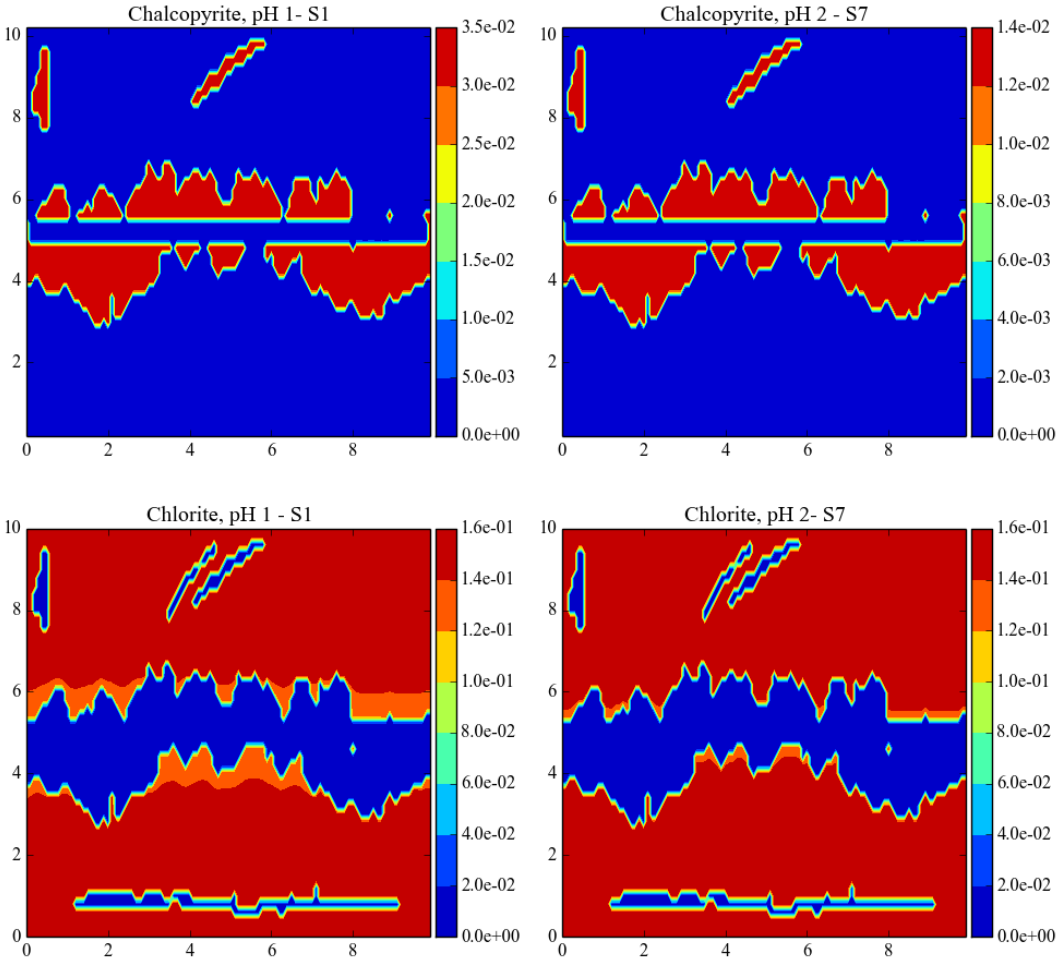

Figure 38: Chalcopyrite and chlorite dissolution after 10 days injection of a lixiviant with pH 1 and 2 respectively.

for an example the solubility of Cu and Fe^{3+} increases in HSO_4 solutions compared to HCl solutions.

Secondary reactions

The presence of pyrite results in slightly lower chalcopyrite concentrations after 10 days (**Figure 26**). Partially these results can be attributed to the lower initial chalcopyrite concentrations, but this only

accounts for about 10 percent of the reduction whereas the vein concentrations are about half the value of the result of the base case model. According to previous studies, pyrite is expected to increase the dissolution of chalcopyrite due to a galvanic effect. The effect of pyrite on the leaching of chalcopyrite has been investigated mostly under oxidizing conditions and high temperature (Abraitis et al. 2004; Al-Harahsheh et al. 2006; Dutrizac 1989; Li et al. 2010; Parker & Khodakovskii 1995). Especially finely disseminated pyrite in a ratio of 4:1 to chalcopyrite is found to accelerate dissolution in the case of covellite (Miki & Nicol 2011). When chalcopyrite and pyrite are in close contact the galvanic effect is enhanced as chalcopyrite behaves like and anode and dissolves more rapidly (Nicol et al. 2010).

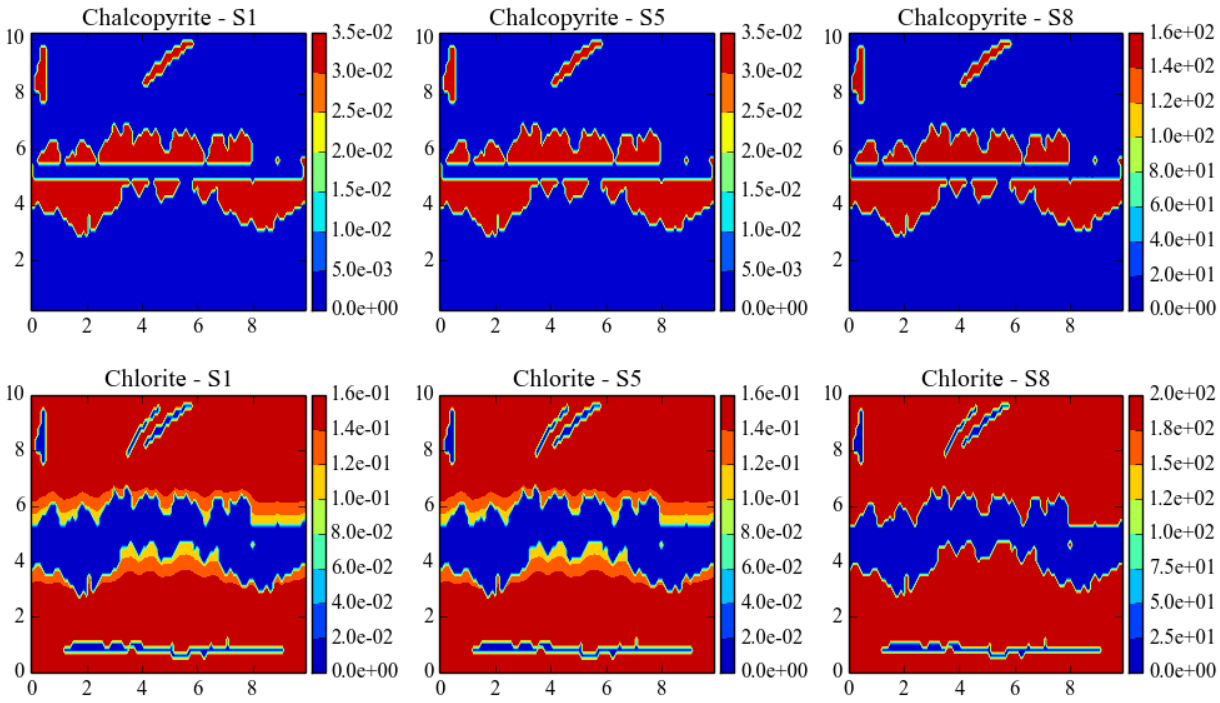

Figure 39: Chalcopyrite (upper row) and chlorite (lower row) dissolution after 10 days, showing the base model (S1) compared to lower chalcopyrite dissolution rate (S5) and in presence of pyrite (S8) from left to right.

When including ferrihydrite and jarosite precipitation, the chalcopyrite is dissolved faster (**Figure 19**) potentially due to proton production (Fe3+ + H20 = $Fe(OH)_3 + H^+$

(14)3 $Fe^{3+} + M^+ + 2\ SO_4^{2-} + 6\ H_20 = MFe_3(SO_4)_2(OH)_6 + 6\ H^+$

(15). However, this effect will be reduced as chalcopyrite dissolution in reality not only relies on pH (section 2.2.1). Precipitation of ferrihydrites and sulphur is expected at a pH > 2 (e.g. Velásquez Yévenes 2009; Dutrizac 1989), and therefore occurs in the matrix adjacent to and not in the hydraulic fracture (**Error! Reference source not found.** and **Error! Reference source not found.**). As the most effective pH for chalcopyrite dissolution would be just below pH 2 (Velásquez Yévenes 2009; Miki & Nicol 2011; Watling et al. 2014), it would be worth wile to test the effect of pH in the range of 1-2 to find the optimum between these mechanisms.

The precipitation of ferrihydrites at increased pH (**Error! Reference source not found.**) could cause clogging of pore throats and thus reduced lixiviant flow. Slower chalcopyrite dissolution is also expected due to the precipitation of jarosite as observed in **Error! Reference source not found.**. In

sulphuric acid leaching systems, direct oxidation by Fe^{3+} also cause elemental sulphur to precipitate, this way blocking the mineral surface (Senanayake 2009; Miki & Nicol 2011). Iron will be released to solution preferentially over copper and sulphur, consequently the chalcopyrite surface will be enriched with these elements over time (Acero et al. 2009). The formation of elemental sulphur on intermediate products (chalcocite and covellite) and formation of iron hydroxides was suggested to be responsible for the slow leaching kinetics of chalcopyrite (Saripalli et al. 2001; Bouffard & Dixon 2004). The reaction was found to be faster after addition of chloride for temperatures higher than 50 ˚ C due to the greater oxidizing power (Dutrizac 1971; Yevenes 2010) and would therefore be relevant for in-situ conditions. However, on the long term, the sulphur surface layer will not have a passivating effect according to (Acero et al. 2009).

Other copper sulphides

The copper sulphides that are encountered in porphyry rock were represented by chalcopyrite in this study. However, some bornite and chalcocite was present on the mineral maps. Bornite is not expected to affect the copper dissolution from the ore body as it reacts very slowly (time spans of years) (Watling 2013b) and forms a passivation layer (Velásquez Yévenes 2009). Contrarily, the significant amount of chalcocite (Cu_2S) (Figure 4), is known to be more reactive than chalcopyrite (Miki, 2011; Watling, 2013). This copper sulphide requires days to months to dissolve, compared to months to years for chalcopyrite. As it is a major copper sulphide in many supergene enriched deposits (Ingebritsen & Appold 2012; Richards 2011) it is the second most abundant copper sulphide and contains 79,9 % copper, chalcocite could potentially affect the copper dissolution rate.

Chalcocite dissolution occurs in two steps in reaction with ferric iron with covellite (FeS) as an intermediate reaction product. The first step is the fastest of which the reaction rate is mostly effected by temperature (Gupta & Mukherhee 1990) and the availability of ferric iron. Dissolution of this mineral could thus be favourable in in-situ conditions and seems significant to take the presence of chalcocite into account in future modelling, using a leaching system with ferric iron as an oxidizing agent.

5. Conclusions and suggestions for future work

Reactive transport modelling is considered feasible of as a future predictive tool for ISL, even though in this stage models give a rather qualitative impression of mineral behaviour. Calibration of the models is required according to experimental data, to make valid quantitative estimations of dissolution rates. To calibrate the reactive transport models data should be obtained from column or field experiments, primarily performed on supergene rock deposits or stockworks of copper enriched vein deposits as these are mostly expected to be economical copper deposits.

The extension of the presented high resolution 'vein-scale' models to field scale and time scale of months, will either require suitable upscaling techniques for key parameters and processes and/or substantial computational power. Key parameters should be represented by generalized values according to data obtained in a high resolution reactive model. Chemical parameters would involve mineral and lixiviant composition and representative values for hydrodynamic parameters of the rock matrix and copper enriched vein must be determined. This would involve reduction of the heterogeneities in flow parameters which can be done by only taking into account altered structures within 10 cm from the expected flow path as these will be reached by diffusion. Further generalizations could be made for gangue minerals rates involved for example by defining the average proton consumption of the matrix mineralogy.

The contact area of the hydraulic fracture with the chalcopyrite enriched structures has significant effect on the extracted copper rate. However, more extensive research to porosity in ore bearing veins and more importantly their interconnectivity, should be integrated to make predictions on the development of their flow properties over time. Behaviour of hydraulic fractures can be monitored using e.g. micro seismic sensors. This way fracture closure due to the in-situ stress field and interaction with existing veining structures can be studied.

- The kinetic behaviour of a limited amount of minerals was involved in this study, mostly based on the chemical analysis porphyry rock samples and verified by literature. Rock compositions of other copper ore deposits could point out other important minerals to affect the overall reactive behaviour.
- Local variation in porosity due to the presence of veins or other chemically altered features, could enhance local diffusion and hence reaction rates. Higher porosity coincides with copper enriched structures according to porosity measurements performed in this study. The related enhanced effective diffusion coefficient indicates favourable settings for ISL as these show to enhance transport of protons and Cu.
- Leaching experiments on samples (similar to) in-situ porphyry rock should be carried out to quantify dissolution effect of HCL as a lixiviant and the changes of the hydrodynamic structure in the samples. These experiments should preferably be performed on decimetre-scale as the scale of veins (commonly mm-cm) creates a relatively large surface area by creating the plug, affecting flow behaviour though a vein both mechanically and hydro dynamically.
- The injected HCl solution should be tested in the range of pH of 1-2 in more detail to find optimal acidity for dissolution of chalcopyrite and preventing the precipitation of ferryhydrites on field scale. Testing different leaching solutions is required as for example the solubility of Cu and Fe^{3+} increases in HSO_4 solutions compared HCl.
- The vein-scale models in this study show the ability to account for precipitation of these minerals in the matrix, but do not simulate potential clogging of the hydraulic fracture

itself as the pH is kept constant on this scale. The presence of proppants in the hydraulic fracture is required to keep fractures open at in-situ conditions, as a consequence mixing of the lixiviant within the fracture might result in faster reactions.

- Chalcocite is a common and copper rich mineral that should be accounted for in ISL because of its faster dissolution kinetics compared to chalcopyrite. It is commonly distributed in supergene deposits and dissolves in presence of ferric iron as an oxidizing agent.

6. Acknowledgements

I would like to express my gratitude to Henning Prommer for the useful comments, support and input through the learning process of this master thesis and for organizing the funding provided for the project by CSIRO Land and Water. Furthermore I would like to thank Angus McFarlane for the useful discussions, his effort to provide chemical analyses and guidance in the experiments we performed and my supervisors Niels Hartog and Majid Hassanizadeh at Utrecht University. Finally, I would like to thank my parents for their encouragement and support.

7. References

Abelin, H. et al., 1991. A large-scale flow and tracer experiment in granite 1. Experimental design and flow distribution. *Water Resources Research*, 27(12), pp.3107–3117.

Abraitis, P.K. et al., 2004. Acid leaching and dissolution of major sulphide ore minerals: processes and galvanic effects in complex systems. *Mineralogical Magazine*, 68(2), pp.343–351.

Acero, P. et al., 2009. Chalcopyrite dissolution rate law from pH 1 to 3. *Geologica Acta*, 7(3), pp.389–397.

Ahlness, J. & Pojar, M., 1983. In situ copper leaching in the United States : case histories of operations. *United States Bureau of Mines*.

Al-Harahsheh, M. et al., 2006. ToF-SIMS and SEM study on the preferential oxidation of chalcopyrite. *International Journal of Mineral Processing*, 80(2-4), pp.205–214.

Aylmore, M.. & Muir, D.., 2001. Thiosulfate leaching of gold—A review. *Minerals Engineering*, 14(2), pp.135–174.

Azadi, M., Mirmohammadi, M. & Rasekh, P., 2014. Geometric-Genetic and Mineralogic Classification of veinlets and breccias in Kahang Porphyry Copper Deposit, Northern East Isfahani. *Symposium of Crystallography and Mineralogy of Iran*, Miner Deposits.

Baria, R. et al., 1999. European HDR research programme at Soultz-sous-Forêts (France) 1987–1996. *Geothermics*, 28(4-5), pp.655–669.

Bell, S.L., Welch, G.D. & Bennett, P.G., 1995. Development of ammoniacal lixiviants for the in-situ leaching of chalcopyrite. *Hydrometallurgy*, 39(1-3), pp.11–23.

Berger, B.R., Wanty, R.B. & Tuttle, M.L., 2001. Scale versus detail in water-rock investigations 2: Field-scale models of fracture networks in mineral deposits. *Geology*.

BGS, C., 2010. Definition, mineralogy and deposits. *British Geological Survey, Copper, Minerals UK*, (March).

Bierlein, F.P. et al., 2006. Distribution of orogenic gold deposits in relation to fault zones and gravity gradients : targeting tools applied to the Eastern.

Bodin, J., Delay, F. & de Marsily, G., 2003. Solute transport in a single fracture with negligible matrix permeability: 1. Fundamental mechanisms. *Hydrogeology Journal*, 11(4), pp.418–433.

Bongiolo, E.M. et al., 2007. Quantification of porosity evolution from unaltered to propylitic-altered granites: The14C-PMMA method applied on the hydrothermal system of Lavras do Sul, Brazil. *Anais da Academia Brasileira de Ciencias*, 79(3), pp.503–517.

Bouffard, S.C. & Dixon, D.G., 2004. *Heap Biooxidation of Refractory Gold Ores: Current State of the Art*,

Bradbury, M.H. & Green, A., 1986. Investigations into the factors influencing long range matrix diffusion rates and pore space accessibility at depth in granite. *Journal of Hydrology*, 89(1-2), pp.123–139.

Brenner, S.L. & Gudmundsson, a, 2002. Permeability development during hydrofracture propagation in layered reservoi rs. *Norges geologiske undersokelse Bulletin*, 439, pp.71–77.

Brewer, M.D., 1998. Column leaching experiments and mass balance modelin simulation in-situ leaching within the oxide zone.

Brimhall, G.H., 1979. Lithologic determination of mass transfer mechanisms of multiple-stage porphyry copper mineralization at Butte, Montana; vein formation by hypogene leaching and enrichment of potassium-silicate protore. *Economic Geology*, 74(3), pp.556–589.

Britt, L.K. et al., 2013. Waterfracs: We Do Need Proppant After All. In *SPE Annual Technical Conference and Exhibition*. Society of Petroleum Engineers.

Camus, F., 2003. Geología de los sistemas porfíricos en los Andes de Chile: Santiago. *Servicio Nacional de Geología y Minería*, p.267.

Cathles, L.M. & Shannon, R., 2007. How potassium silicate alteration suggests the formation of porphyry ore deposits begins with the nearly explosive but barren expulsion of large volumes of magmatic water. *Earth and Planetary Science Letters*, 262(1-2), pp.92–108.

Christensen, R.J., 1991. In situ mining with oilfield technology. *Oilfield Review*, pp.8–17.

Chuprakov, D. et al., 2011. Hydraulic-Fracture Propagation in a Naturally Fractured Reservoir. *SPE Production & Operations*, 26(1).

Clark, A.H., 1993. Are outsize porphyry copper deposits either anatomically or environmentally distinctive? *Society of Economic Geologists Special Publication*, 2, pp.213–282.

Cooke, D.R., Hollings, P. & Walshe, J.L., 2005. Giant porphyry deposits: Characteristics, distribution, and tectonic controls. *Economic Geology*, 100(5), pp.801–818.

Cooke, D.R., Hollings, P. & Walshe, J.L., 2006. Giant Porphyry Deposits: Characteristics, Distribution, and Tectonic Controls. *Economic Geology*, 100(5), pp.801–818.

Corbett, G., 2009. Anatomy of porphyry-related Au-Cu-Ag-Mo mineralised systems : Some exploration implications. *Australian Institute of Geoscientists North Queensland Exploration Conference*, (June), pp.1–13.

Córdoba, E.M. et al., 2008a. Leaching of chalcopyrite with ferric ion. Part I: General aspects. *Hydrometallurgy*, 93(3-4), pp.81–87.

Córdoba, E.M. et al., 2008b. Leaching of chalcopyrite with ferric ion. Part IV: The role of redox potential in the presence of mesophilic and thermophilic bacteria. *Hydrometallurgy*, 93(3-4), pp.106–115.

Córdoba, E.M. et al., 2009. Passivation of chalcopyrite during its chemical leaching with ferric ion at 68 °C. *Minerals Engineering*, 22(3), pp.229–235.

County, P. et al., 2013. Florence Copper Project NI 43-101 Technical Report Pre-Feasibility Study.

Cox, S.F., Knackstedt, M.A. & Braun, J., 2001. Principles of structural control on permeability and fluid flow in hydrothermal systems. *Society of Economic Geologists Rev*, 14, pp.1–24.

Cussler, E.L., 1997. *Diffusion: Mass Transfer in Fluid Systems*, Third Edition, Cambridge University Press.

Dershowitz, B., 2011. of in situ leach mining. , (November), pp.19286–19288.

Dill, H.G. et al., 2012. Depth-related variation of tourmaline in the breccia pipe of the San Jorge porphyry copper deposit, Mendoza, Argentina. *Ore Geology Reviews*, 48(October 2011), pp.271–277.

Dong, Y.B. et al., 2013. Effects of quartz addition on chalcopyrite bioleaching in shaking flasks. *Minerals Engineering*, 46-47, pp.177–179.

Dreisinger, D., 2006. Copper leaching from primary sulfides: options for biological and chemical extraction of copper. *Hydrometallurgy*, 83(10-20).

Driesner, T., 2007. The system H2O-NaCl. Part II: Correlations for molar volume, enthalpy, and isobaric heat capacity from 0 to 1000 C, 1 to 5000 bar, and 0 to 1 XNaCl. *Geochimica et Cosmochimica Acta*, 71(20), pp.4902–4919.

Dutrizac, J.E., 1990. Elemental sulfur formation during the ferricchloride leaching of chalcopyrite. *Hydrometallurgy*, 23, pp.153–176.

Dutrizac, J.E., 1989. Elemental Sulphur Formation During the Ferric Sulphate Leaching of Chalcopyrite. *Canadian Metallurgical Quarterly*, 28(4), pp.337–344.

Dutrizac, J.E., 1974. The kinetics of dissolution of chalcopyrite in ferric ion media. *Metallurgical Transactions B*, 9b, pp.431–439.

Economides, M.J. & Boney, C., 2000. Chapter 2 Formation Characterization : Well and Reservoir Testing.

Ehrig, K., 2014. Using Mineralogy to Identify Opportunities and Solve Operational Issues at Mine Sites. In *AUSIMM – Adelaide Branch*.

Einaudi, M.T., Hedenquist, J.W. & Inan, E.E., 2003. Porphyry to Epithermal Environments. *Society*, (February), pp.1–50.

Faleiros, A.M. et al., 2014. Fluid regimes, fault-valve behavior and formation of gold-quartz veins - The Morro do Ouro Mine, Ribeira Belt, Brazil. *Ore Geology Reviews*, 56, pp.442–456.

Flett, D.S., 2002. Chloride hydrometallurgy for complex sulphides: A review. *CIM Bulletin*, 95(1056).

Fournier, R.O., 1999. No Title. *Economic Geology*, 94(1193).

Fredd, C.N. et al., 2000. Experimentastudy of hydraulic fracture conductivity demonstrates the benefits of using proppants. *SPE Journal*, 60326.

Frikken, P.H., 2003. *Breccia-hosted copper molybdenum mineralisation at Rio Blanco, Chile*.

G, O. et al., 2001. Geology of the Chuquicamata Mine: A progress report. *Economic Geology*, (96).

Ganor, J. et al., 2005. The dissolution kinetics of a granite and its minerals - Implications for comparison between laboratory and field dissolution rates. *Geochimica et Cosmochimica Acta*, 69(3), pp.607–621.

Garwin, S., 2002. The geologic setting of intrusion-related hydrothermal systems near the Batu Hijau porphyry copper-gold deposit, Sumbawa, Indonesia, in Goldfarb. *Society of Economic Geologists, Special Publication*, (9), pp.333–366.

Garzon, L.D.D., 2009. *On multicomponent reactive transport in porous media: from teh natural complexity to analytical solutions*.

Geiger, S. et al., 2002. New insights from reactive transport modelling: The formation of the sericitic vein envelopes during early hydrothermal alteration at Butte, Montana. *Geofluids*, 2(3), pp.185–201.

Geilikman, M., Xu, G. & Wong, S., 2013. Interaction of Multiple Hydraulic Fractures in Horizontal Wells. *SPE Unconventional Gas*

Gelhar, L.W., Welty, C. & Rehfeldt, K.R., 1992. A critical review of data on field-scale dipsersion in aquifers. *Water*, 28(7), pp.1955–1974.

Groves, D.I., 1993. The crustal continuum model for late Archaean lode-gold deposits of the Yilgarn Block, Western Australia. *Miner. Deposita*, 28, pp.366–374.

Gupta, C.K. & Mukherhee, T.K., 1990. *Hydrometallurgy in Extration Processes*,

Gustafson, L.B., 1978. Some major factors of porphyry copper genesis. *Economic Geology*, 73(5), pp.600–607.

Habache, N. et al., 2005. Leaching of copper oxide with different acid solutions. *Chemical Engineering Journal*, 152, pp.1334–1336.

Harpalani, S., 2000. Effect of leaching on microstructure and flow in an in situ mining operation. *Mineral Resources Engineering*, 9(2), pp.193–204.

Harpalani, S. & Williams, J.R., 1999. Effect of leaching on microstructure and flow in an in situ mining operation. *Rock M chanics for Industry*.

Harrowfield, I.R., MacRae, C.M. & Wilson, N.C., 1993. Chemical Imaging in Electron Microprobes. In *Proceedings of the 27th Microbeam Analysis Society Annual MAS Meeting, New York, NY, USA*. pp. 547–548.

Hedenquist, J.W. & Henley, R.W., 1985. Hydrothermal eruptions in the Waiotapu geothermal system, New Zealand: Their origin, associated breccias, and relation to precious metal mineralization. *Economic Geology*, 80, p.640−1668.

Helle, S. et al., 2005. Improvement of mineralogical and chemical characterization to predict the acid leaching of geometallurgical units from Mina Sur, Chuquicamata, Chile. *Minerals Engineering*, 18(13-14), pp.1334–1336.

Herbert, R.B., 1999. *MiMi - Sulfide oxidation in mine waste deposits- A review with emphasis on dysoxic weathering*,

Hiroyoshi, N. et al., 2001. Enhancement of chalcopyrite leaching by ferrous ions in acidic ferric sulfate solutions. *Hydrometallurgy*, 60(3), pp.185–197.

Hiskey, J.B., 1994. In-situ leaching recovery of copper: what's next? *Hydrometallurgy*.

Hiskey, J.B., 1AD. leaching recovery of copper : what ' s next ?

IAEA, I.A.E.A., 2001. Manual of acid in situ leach uranium mingin technology. In *IAE-TECDOC-1239, Vienna, Austria*.

Ingebritsen, S.E. & Appold, M.S., 2012. The physical hydrogeology of ore deposits. *Economic Geology*, 107(4), pp.559–584.

Jansen, M. & Taylor, A., 2003. Overview of gangue mineralogy issues in oxide copper heap leaching. *ALTA conference, May 19-. 24*, p.32.

Jansen, M and Taylor, a, 2003. Overview of gangue mineralogy issues in oxide copper heap leaching. *ALTA conference, May 19-. 24*, p.32.

Jeffrey, R.G. et al., 2009. Measuring Hydraulic Fracture Growth in Naturally Fractured Rock. *SPE Annual Technical Conference and Exhibition*, pp.1–19.

Kang, Q., Lichtner, P.C. & Zhang, D., 2007. An improved lattice Boltzmann model for multicomponent reactive transport in porous media at the pore scale. *Water Resources Research*, 43(12).

Khashgerel, B., 2006. Geology and reconnaissance stable isotope study of the Oyu Tolgoi porphyry Cu-Au system, South Gobi, Mongolia. *Economic Geology*, 101, pp.503–522.

Kimball, B.E., Rimstidt, J.D. & Brantley, S.L., 2010. Chalcopyrite dissolution rate laws. *Applied Geochemistry*, 25(7), pp.972–983.

Kinnunen, P.H.M. & Puhakka, J. a., 2004. Chloride-promoted leaching of chalcopyrite concentrate by biologically-produced ferric sulfate. *Journal of Chemical Technology and Biotechnology*, 79(8), pp.830–834.

Klauber, C., 2003. Fracture-induced reconstruction of a chalcopyrite (CuFeS2) surface. *Surface and Interface Analysis*, 35(5), pp.415–428.

Krásný, J., 2003. Important role of deep-seated hard rocks in a global groundwater flow: possible consequences. In *In: Krásný J., Hrkal Z. and Bruthans J. (eds.), Proceedings – IAH Internat. Conference on "Groundwater in fractured rocks" Prague, IHP-VI, Series on Groundwater 7. UNESCO*. pp. 147–148.

Lang, J.R. et al., 2014. Geology and Magmatic-Hydrothermal Evolution of the Giant Pebble Porphyry Copper-Gold-Molybdenum Deposit, Southwest Alaska. *Economic Geology*, V.108, pp.437–462.

Larsson, M., Niemi, A. & Tsang, C.F., 2012. A study of flow-wetted surface area in a single fracture as a function of its hydraulic conductivity distribution. *Water Resources Research*, 48(1), pp.1–9.

Lazaro, I. & Nicol, M.J., 2003. The role of non oxidative processes in the leaching of chalcopyrite. , pp.367–381.

Van der Lee, J., 2008. Mining of valuable metals: in situ and heap leaching. , p.Technical Report Nr. R080929JVDL.

Leybourne, M.I. & Cameron, E.M., 2006. Composition of groundwaters associated with porphyry-Cu deposits, Atacama Desert, Chile: Elemental and isotopic constraints on water sources and water-rock reactions. *Geochimica et Cosmochimica Acta*, 70(7), pp.1616–1635.

Li, J. et al., 2010. Chalcopyrite leaching: The rate controlling factors. *Geochimica et Cosmochimica Acta*, 74(10), pp.2881–2893.

Li, J.W. et al., 2008. Origin of the Tongshankou porphyry-skarn Cu-Mo deposit, eastern Yangtze craton, Eastern China: Geochronological, geochemical, and Sr-Nd-Hf isotopic constraints. *Mineralium Deposita*, 43(3), pp.315–336.

Lichtner, P.C., 2000. Critique of dual continuum formulations of multicomponent reactive transport in fractured porous media. , 122, pp.281–298.

Lichtner, P.C. & Kang, Q., 2007. Upscaling pore-scale reactive transport equations using a multiscale continuum formulation. *Water Resources Research*, 43(12).

Lowson, R.T. et al., 2007. The kinetics of chlorite dissolution. *Geochimica et Cosmochimica Acta*, 71(6), pp.1431–1447.

Lu, Z.., Jeffrey, M.. & Lawson, F., 2000. An electrochemical study of the effect of chloride ions on the dissolution of chalcopyrite in acidic solutions. *Hydrometallurgy*, 56(2), pp.145–155.

MacQuarrie, K.T.B. & Mayer, K.U., 2005. Reactive transport modeling in fractured rock: A state-of-the-science review. *Earth-Science Reviews*, 72(3-4), pp.189–227.

Mangeret, a., De Windt, L. & Crançon, P., 2012. Reactive transport modelling of groundwater chemistry in a chalk aquifer at the watershed scale. *Journal of Contaminant Hydrology*, 138-139, pp.60–74.

Maréchal, J.C., Dewandel, B. & Subrahmanyam, K., 2004. Use of hydraulic tests at different scales to characterize fracture network properties in the weathered-fractured layer of a hard rock aquifer. *Water Resources Research*, 40(11), pp.1–17.

Martens, E. et al., 2012. In situ recovery of gold: Column leaching experiments and reactive transport modeling. *Hydrometallurgy*, 125-126, pp.16–23.

McDonald, J.M. & Harbaugh, A.W., 1988. *MODFLOW, A Modular 3D Finite Diference Ground Water Flow Model; Open-file report 83-375; U.S. Geological Survey*,

McQueen, K.G., 2005. Ore deposit types and their primary expressions. *Regolith Expression of Australian Ore Systems.* pp.1–14.

Meinert, L.D., Dipple, G.M. & Nicolescu, S., 2005. World Skarn Deposits. , pp.299–336.

Metals, C.F., 2014. Overview of the Van Dyke Project.

Miki, H. & Nicol, M., 2011. The dissolution of chalcopyrite in chloride solutions. IV. the kinetics of the auto-oxidation of copper(I). *Hydrometallurgy*, 105(3-4), pp.246–250.

Millenacker, D.J., 1989. In Situ Mining: Research by U.S. Bureau of Mines May Lead to Innovative and Low-cost Copper Mining Methods. *Eng. and Min. J.*, pp.56–58.

Morgan, J., 1989. Mining 1988. *Mining Engineering*, pp.1–11.

Mudd, G.M., 2002. Critical review of acid in situ leach uranium mining: 1. USA and Australia. *Environmental Geology*, 41(3-4), pp.390–403.

Navarre-Sitchler, A.K. et al., 2013. Porosity and surface area evolution during weathering of two igneous rocks. *Geochimica et Cosmochimica Acta*, 109, pp.400–413.

Nazari, G. & Asselin, E., 2009. Morphology of chalcopyrite leaching in acidic ferric sulfate media. *Hydrometallurgy*, 96(3), pp.183–188.

Nick, H.M. et al., 2009. Modeling transverse dispersion and variable density flow in porous media. *Transport in Porous Media*, 78(1), pp.11–35.

Nicol, M., Miki, H. & Velásquez-Yévenes, L., 2010. The dissolution of chalcopyrite in chloride solutions: Part 3. Mechanisms. *Hydrometallurgy*, 103(1-4), pp.86–95.

Nordstrom, D.K. & Alpers, C.N., 1998. Geochemistry of acid mine waters, part A - processes, techniques and health. *Society of Economic Geologists*, 6a.

Odling, N.W. a et al., 2007. Laboratory measurement of hydrodynamic saline dispersion within a micro-fracture network induced in granite. *Earth and Planetary Science Letters*, 260(3-4), pp.407–418.

Oelkers, E.H. et al., 2008. An experimental study of the dissolution mechanism and rates of muscovite. *Geochimica et Cosmochimica Acta*, 72(20), pp.4948–4961.

Olvera, O.G. et al., 2014. Electrochemical dissolution of fresh and passivated chalcopyrite electrodes. Effect of pyrite on the reduction of Fe3+ ions and transport processes within the passive film. *Electrochimica Acta*, 127, pp.7–19.

Oraby, E.A. & Eksteen, J.J., 2014. A NEW PROCESS FOR COPPER LEACHING FROM COPPER AND COPPER-GOLD RESOURCES. *Journal of Engineering Sciences*, 42(6), pp.1440 – 1449.

Parker, V.B. & Khodakovskii, I.L., 1995. Thermodynamic Properties of the Aqueous Ions (2+ and 3+) of Iron and the Key Compounds of Iron. *Journal of Physics and Chemistry Reference data*, 24(5), pp.1701–1745.

Parkhurst, D.L. & Appelo, C.A.J., 1999. User's guide to PHREEQC (Version 2) : a computer program for speciation, batch-reaction, one-dimensional transport, and inverse geochemical calculations. *U.S. Geological Survey : Earth Science Information Center, Open-File Reports Section. Water-Resources Investigations Report*, pp.99–4259.

Plummer, L.N., Wigley, T.M.L. & Parkhurst, D.L., 1978. The kinetics of calcite dissolution in CO2 - water systems at 5°C to 60°C and 0.0 to 1.0 atm CO2. *American Journal of Science*, (278), pp.179–216.

Prommer, H., Barry, D.A. & Zheng, C., 2003. MODFLOW/MT3DMS-Based reactive Transport Modeling. *Groundwater*, 41(2), pp.247–257.

Rabeau, O. et al., 2013. Log-uniform distribution of gold deposits along major Archean fault zones. *Mineralium Deposita*, 48(7), pp.817–824.

Rahman, M.M. & Rahman, S.S., 2013. Studies of Hydraulic Fracture-Propagation Behavior in Presence of Natural Fractures : Fully Coupled Fractured-Reservoir Modeling in Poroelastic Environments. *International Journal of Geomechanics*, 13(December), pp.809–826.

Ranjram, M., Gleeson, T. & Luijendijk, E., 2015. Is the permeability of crystalline rock in the shallow crust related to depth, lithology or tectonic setting? *Geofluids*, 15(1-2), pp.106–119.

Redmond, P.B. & Einaudi, M.T., 2010. The Bingham Canyon porphyry Cu-Mo-Au deposit. I. Sequence of intrusions, vein formation, and sulfide deposition. *Economic Geology*, 105(1), pp.43–65.

Reinicke, A. et al., 2010. Hydraulic fracturing stimulation techniques and formation damage mechanisms-Implications from laboratory testing of tight sandstone-proppant systems. *Chemie der Erde - Geochemistry*, 70(SUPPL. 3), pp.107–117.

Richards, J., Boyce, A. & Pringle, M., 2001. Geological Evolution of the Escondida Area, Northern Chile: A Model for Spatial and Temporal Localization or Pophyry Cu Mineralization. *Economic Geology*, 96, pp.271–305 ST – Geological Evolution of the Escondid.

Richards, J.P., 2011. Magmatic to hydrothermal metal fluxes in convergent and collided margins. *Ore Geology Reviews*, 40(1), pp.1–26.

Richards, J.P., 2003. Tectono-Magmatic Precursors for Porphyry Cu- (Mo-Au) Deposit Formation. *Economic Geology*, 98, pp.1515–1533.

Rimstidt, J.D. & Barnes, H.L., 1980. The kinetics of silica-water reactions. *Geochimica et Cosmochimica Acta*, 44(11), pp.1683–1699.

Riveros, K. et al., 2014. Magnetic properties related to hydrothermal alteration processes at the Escondida porphyry copper deposit, northern Chile. *Mineralium Deposita*, pp.693–707.

Rushing, J.A. & Sullivan, R.B., 2003. Evaluation of hybrid water-frac stimulation technology in the bossier tight gas sand play. *SPE*, (84394.).

Rusk, B.G., Miller, B.J. & Reed, M.H., 2008. Fluid-inclusion evidence for the formation of Main Stage polymetallic base-metal veins, Butte, Montana. *Arizona Geological Society Digest*, p.573–581.

Sainath, N.R. & Harpalani, S., 1993. Effect of leaching on permeaility of drill cores from a copper ore body. *Mining Engineering*, (1305).

Sardini, P., 2006. On the connected porosity of mineral aggregates in crystalline rocks. *American Mineralogist*, 91(7), pp.1069–1080.

Saripalli, K.P. et al., 2001. Changes in Hydrologic Properties of Aquifer Media Due to Chemical Reactions: A Review. *Critical Reviews in Environmental Science and Technology*, 31(4), pp.311–349.

Seedorff, E. & Einaudi, M.T., 2004. Henderson porphyry molybdenum system, Colorado: I. Sequence and abundance of hydrothermal mineral assemblages flow paths of evolving fluids, and evolutionary style. *Economic Geology*, 99(1), pp.3–37.

Seedorff, E. et al., 2008. Root zones of porphyry systems: Extending the porphyry model to depth. *ECONOMIC GEOLOGY*, 103, p.939–956.

Senanayake, G., 2009. A review of chloride assisted copper sulfide leaching by oxygenated sulfuric acid and mechanistic considerations. *Hydrometallurgy*, 98(1-2), pp.21–32.

Senanayake, G., 2007. Chloride assisted leaching of chalcocite by oxygenated sulphuric acid via Cu(II)-OH-Cl. *Minerals Engineering*, 20(11), pp.1075–1088.

Sibson, R.H., 2000. Fluid involvement in normal faulting. *Journal of Geodynamics*, 29(3-5), pp.469–499.

Sillitoe, R.H., 2010. Porphyry Copper Systems, Sillitoe, 2010.pdf. , pp.3–41.

Sinclair, W.D., 2007. Porphyry Deposits. *Mineral deposits of Canada, Special Publication*, No. 5, pp.223–243.

Skagius, K. & Neretnieks, I., 1986. Porosities and diffusivities of some nonsorbing species in crystalline rocks. *Water Resources Research*, 22(389).

Snow, D.T., 1968. Rock fracture spacings, opening, and porosities. *Proceedings American Society of Civil Engineers.*, 94, pp.73–91.

Sparrow, G.J. & Woodcock, J.T., 1995. Cyanide and Other Lixiviant Leaching Systems for Gold with Some Practical Applications. *Mineral Processing and Extractive Metallurgy Review*, 14(3-4), pp.193–247.

Spiessl, S.M. et al., 2007. A process-based reactive hybrid transport model for coupled discrete conduit-continuum systems. *Journal of Hydrology*, 347(1-2), pp.23–34.

Steefel, C., Depaolo, D. & Lichtner, P., 2005. Reactive transport modeling: An essential tool and a new research approach for the Earth sciences. *Earth and Planetary Science Letters*, 240(3-4), pp.539–558.

Steefel, C.I. & Lichtner, P.C., 1998. Multicomponent reactive transport in discrete fractures: I. Controls on reaction front geometry. *Journal of Hydrology*, 209(1-4), pp.186–199.

Steefel, C.I. & Maher, K., 2009. Fluid-Rock Interaction: A Reactive Transport Approach. *Reviews in Mineralogy and Geochemistry*, 70(1), pp.485–532.

Tosdal, R. & Richards, J., 2001. Magmatic and structural controls on the development of porphyry Cu±Mo±Au deposits. *Reviews in Economic Geology*, 14, pp.157–181.

Treviranus, I., 2013. Importance of size & shape for proppants quality. ASTM D18.26.

Velásquez Yévenes, L., 2009. The kinetics of the dissolution of chalcopyrite in chloride media. , (March), p.290.

Wang, S., 2009. Aqueous Lixiviants : Principle , Types and Applications. Journal of Materials, pp.37–42.

Watling, H.R., 2013a. Chalcopyrite hydrometallurgy at atmospheric pressure: 1. Review of acidic sulfate, sulfate-chloride and sulfate-nitrate process options. *Hydrometallurgy*, 140, pp.163–180.

Watling, H.R., 2013b. Chalcopyrite hydrometallurgy at atmospheric pressure: 1. Review of acidic sulfate, sulfate-chloride and sulfate-nitrate process options. *Hydrometallurgy*, 140, pp.163–180.

Watling, H.R. et al., 2014. Effect of water quality on the leaching of a low-grade copper sulfide ore. *Minerals Engineering*, 58, pp.39–51.

Watling, H.R., 2006. The bioleaching of sulphide minerals with emphasis on copper sulphides - A review. *Hydrometallurgy*, 84(1-2), pp.81–108.

Watling, H.R. et al., 2010. XXV International Mineral Processing Congress (IMPC 2010) Process options for difficult arid-region nickel laterites Process options for difficult arid-region nickel laterites. , (Impc), pp.1–22.

Weis, P., Driesner, T. & Heinrich, C. a, 2012. Porphyry-copper ore shells form at stable pressure-temperature fronts within dynamic fluid plumes. *Science (New York, N.Y.)*, 338(6114), pp.1613–6.

White, A.F. & Brantley, S.L., 2003. The effect of time on the weathering of silicate minerals: Why do weathering rates differ in the laboratory and field? *Chemical Geology*, 202(3-4), pp.479–506.

De Windt, L., Badreddine, R. & Lagneau, V., 2007. Long-term reactive transport modelling of stabilized/solidified waste: from dynamic leaching tests to disposal scenarios. *Journal of Hazardous Materials*, 139(3), pp.529–536.

Zhang, X. & Jeffrey, R.G., 2013. Development of Fracture Networks Through Hydraulic Fracture Growth in Naturally Fractured Reservoirs. *Intech*, p.18.

Zhang, Y., Robinson, J. & Schaubs, P.M., 2011. Numerical modelling of structural controls on fluid flow and mineralization. *Geoscience Frontiers*, 2(3), pp.449–461.

Zheng, C. & Wang, P.P., 1999. MT3DMS: A modular three-dimensional multispecies model for simulation of advection, dispersion and chemical reactions of contaminants in groundwater

systems: Documentation and user's guide. *Army Engineer Research and Development Center. Contract Report SERDP-99-1*.

Attachment A

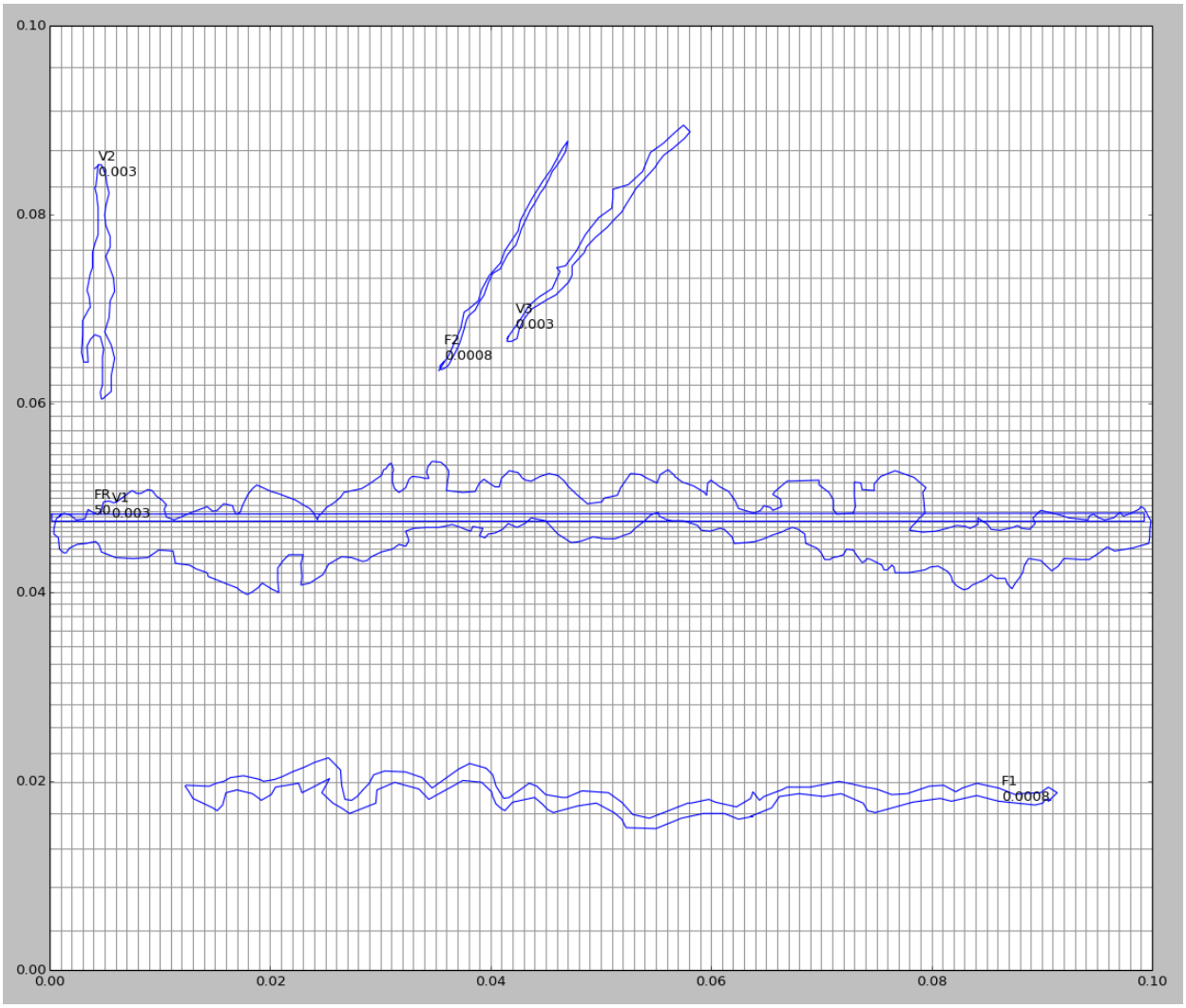

Figure 40: Model setup showing permeability values for the various structures defined from the mineral map. The straight horizontal structure simulates the hydraulic fracture. X and Y axis are given in meters. This structure is used for all vein-scale scenarios (S1-S10) except for S3.

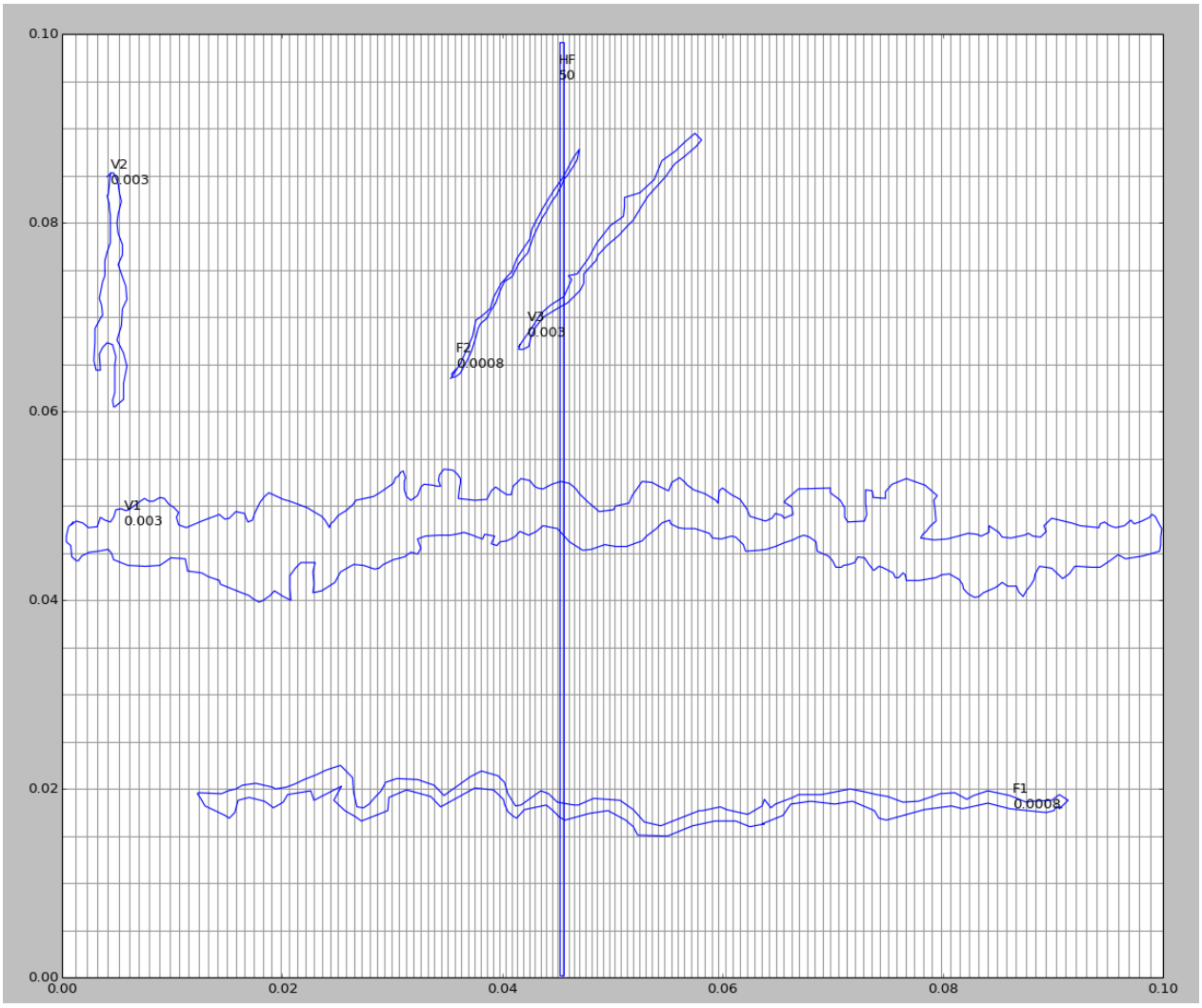

Figure 41: Model setup as in figure 1, but with the hydraulic fracture oriented perpendicular to the chalcopyrite enriched vein (S3).

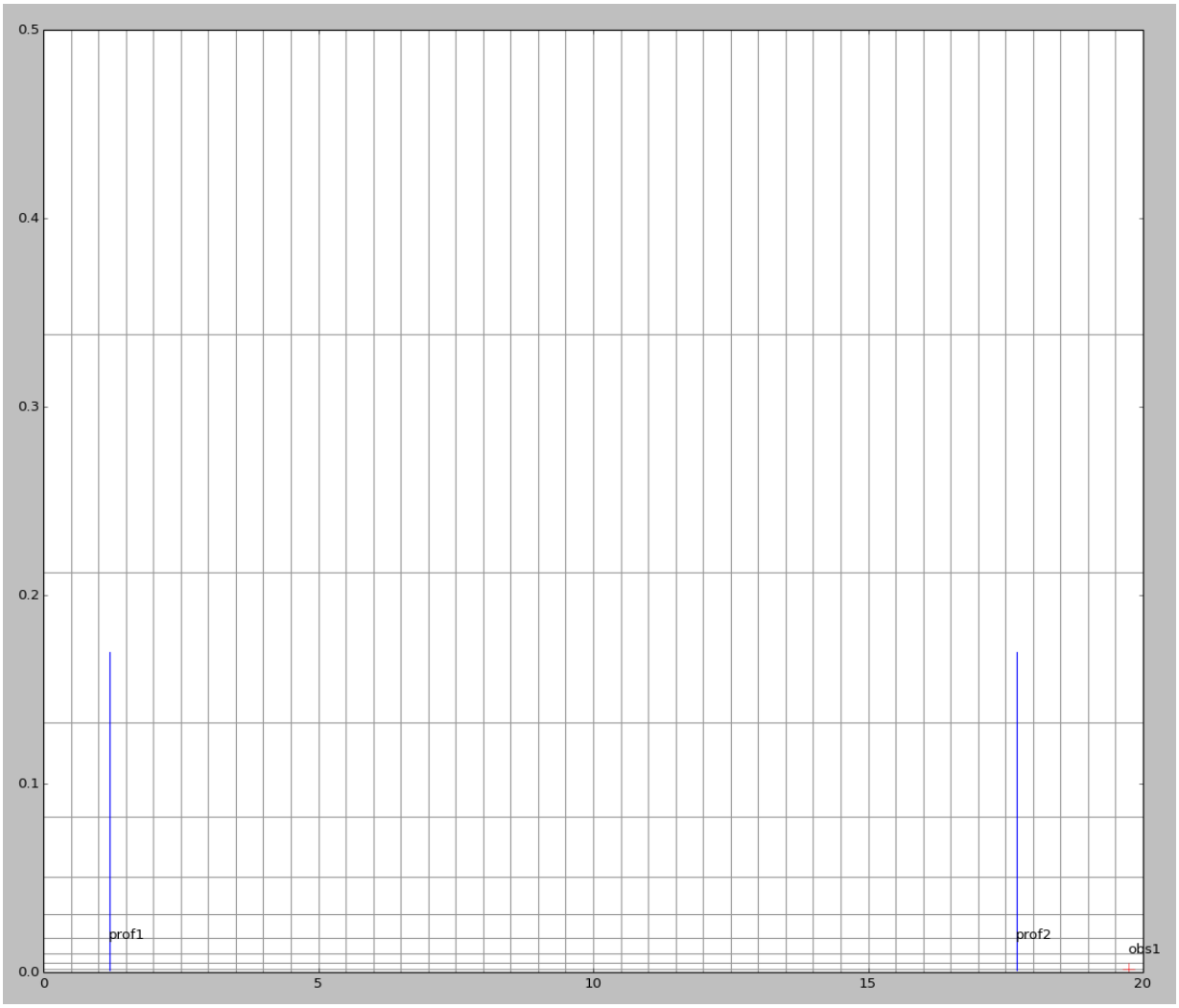

Figure 42: Domain setup for the 'field-scale' model, showing the location of the profiles and observation point used in figure 21.

Attachment B

Figure 43: 'F'-sample.

Figure 44: 'B'-sample

Figure 45: 'W'-sample.

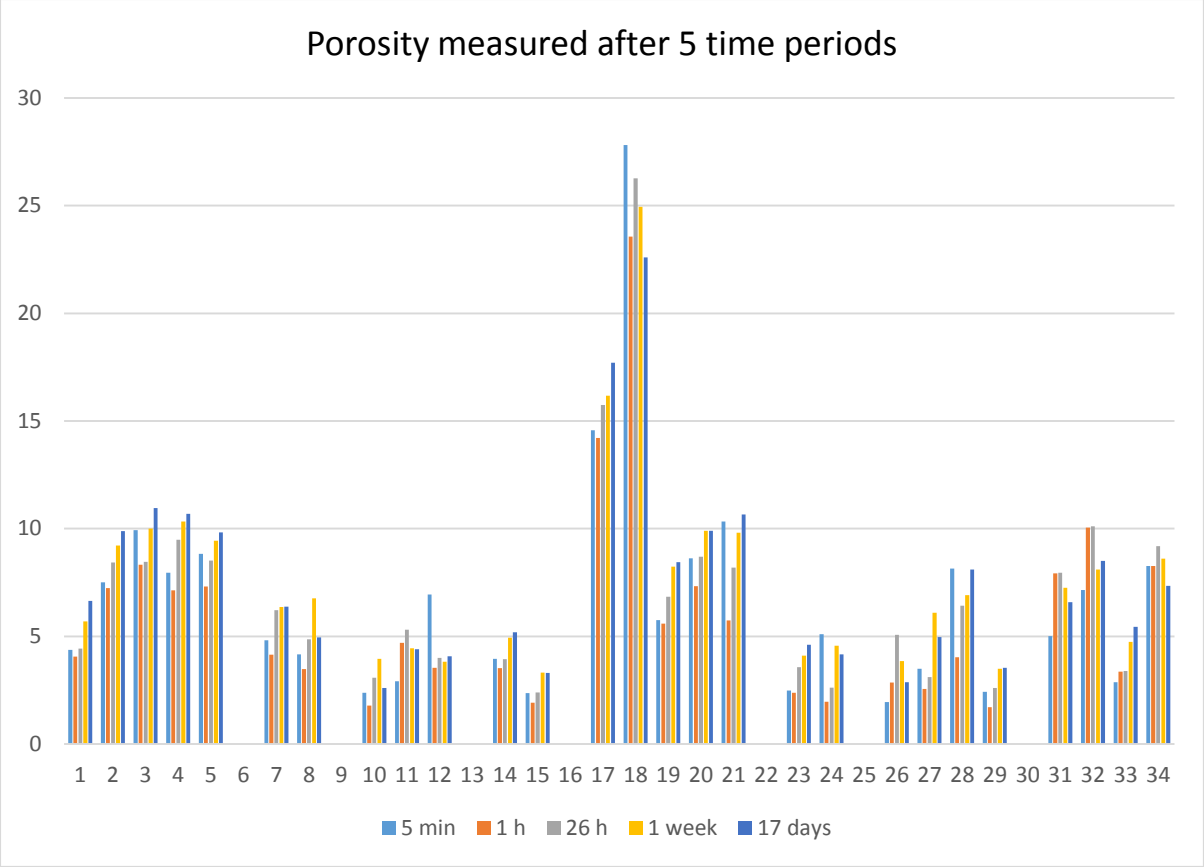

Figure 46: Sample 12, 18, 21 and 28 consist (partially) of loose clast material that broke off when submerged in water. The General trend shows that measured porosity increases over time according to expected further perculation of water in to the samples.

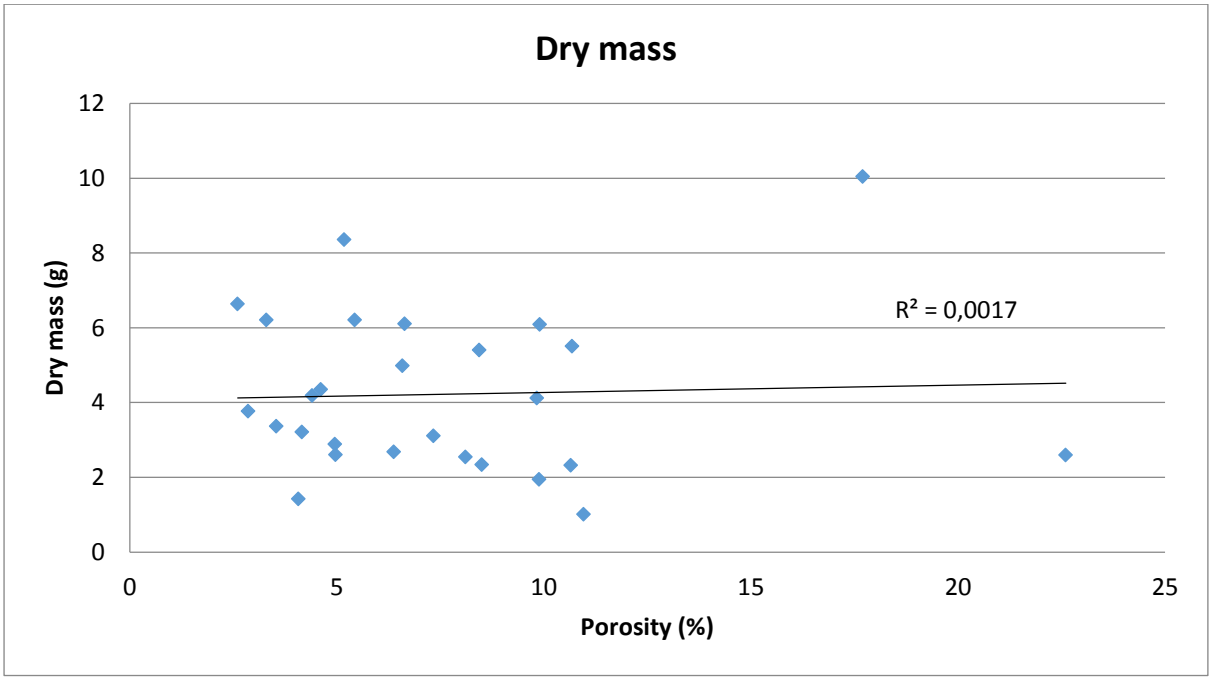

Figure 47: No relation between measured porosity and dry mass indicates the size (and surface) of the samples did not affect the porosity values e.g. by the sample containing water on the surface when measured.

Table 7: (Like table 2 in Pt.2): Porosity values measured on plugs after being emerged 17 days. W, B and F refer to different rock samples; M, C and V refer to the structures matrix, clast and vein respectively.

Groups	*Count*	*Average*	*Variance*
WM	5	9.599147	2.98062
BC	2	5.665509	1.010412
FV	3	3.693496	0.91277
BV	2	4.242022	1.763603
WC	5	13.85815	36.62559
BM	2	4.384995	0.103776
FM	4	4.870102	5.430288
WV	4	6.965012	1.661089

The variance is < 3 for most of the groups. Mostly the clast structures in the 'White' (W) samples show great variation. Porosity > 25% (Figure 46) was measured in this group and explains the high average and variance. This average value was not applied as a representative for clasts in porphyry rock as the plugs taken for this group mostly contained significant amounts of what is considered matrix-material and were of very loose consistency causing the plugs to partially fall apart.

Table 8: Average values of different samples.

Groups	***Count***	***Average***	***Variance***
W	14	10.36761	21.04546
B	6	4.764175	1.067088
F	7	4.365842	3.414944

Variance exhibits high values for the F and W samples. As the F-plugs comprise only two structures (V and M) which are clearly identifiable hence causing variance to be significant. Basic uncertainty within rock types is higher, i.e. C/V/M categories contribute to variability.

Table 9: Average values of different structures.

Groups	***Count***	***Average***	***Variance***
M	11	6.931467	9.386566
C	7	11.5174	40.56628
V	9	5.269398	3.704281

Basic uncertainty within these groups is higher and contributes more variability. Again, M and V could be tested further.